Electrochemical Studies of Pyrite and Galena

by

Yanqing Li

Thesis submitted to the Faculty of the

Virginia Polytechnic Institute and State University

in partial fulfillment of the requirements for the degree of

MASTER OF SCIENCE

in

Mining and Minerals Engineering

APPROVED:

Roe-Hoan Yoon, Chairman	Paul E. Richardson, Co-Chairman
Gregory T. Adel	Gerald H. Luttrell

May, 1994

Blacksburg, Virginia

Electrochemical Studies of Pyrite and Galena

by

Yanqing Li

Dr. Roe-Hoan Yoon, Chairman

Dr. Paul E. Richardson, Co-Chairman

Mining and Minerals Engineering

(ABSTRACT)

The major objective of this work was to investigate the initial oxidation behavior of pyrite in order to better understand how mine wastes containing pyrite generate acid water. It was found that a unique potential exists at which a fresh surface of pyrite undergoes neither oxidation nor reduction. This potential is pH dependent and is referred to as the "stable" potential. The stable potential was found to be 0 V at pH 4.6 and -0.3 V at pH 9.2. Fresh, unoxidized pyrite surfaces were obtained by fracturing under the electrolyte while holding at the stable potentials. The initial oxidation behavior of pure pyrite was investigated using cyclic voltammetry technique by beginning potential sweeps from the stable potential and sweeping in the positive-going or negative-going direction.

The effects of semiconducting properties of pyrite on its electrochemical behavior were studied by photocurrent measurement. The results indicate that pyrite samples from Peru and Spain are all highly n-type. A spontaneous depletion layer is formed on the fresh surfaces of n-type pyrite. The depletion layer is attributed to an intrinsic, acceptor-

like surface state. Charge storage in this surface state pins the band edge over a wide potential range, accounting for the metallic-like electrochemical behavior that has been reported for pyrite. Electrochemical and photocurrent measurements were also conducted on galena for comparison with pyrite. The results indicate that galena samples from the same cluster have varying semiconducting properties, ranging from nearly intrinsic to highly n-type. Abrasion introduces defects in the surface of pyrite and galena, which strongly decrease the magnitude of photocurrent.

Acknowledgments

Sincere appreciation is extended to Dr. Roe-Hoan Yoon and Dr. Paul E. Richardson for their guidance and support throughout the course of this investigation. The author is thankful for Dr. Gregory T. Adel and Dr. Gerald H. Luttrell for their helpful suggestions and advice. Appreciation is also extended to Keith B. Kutz and Wayne Slusser for their technical assistance. Thanks are also given to the staff and fellow graduate students at the Center for Coal and Minerals Processing.

The financial supports from the U.S. Department of Energy (grant No. DE-FG22-92PC92547) and the Bureau of Mines (allotment No. G1125232, subagreement #92-16) are greatly appreciated.

Finally, the author wishes to express his special appreciation to his family, and especially to his wife, Jing Lan, for their continued encouragement.

Table of Contents

List of Figures

List of Tables

Chapter 1. Introduction

1.1. General

This thesis represents a study of the oxidation behavior of pyrite and galena. It was undertaken to better understand the initial oxidation of these minerals and to determine if the source or semiconducting properties influence their initial oxidation behavior. Pyrite was chosen because it is present in nearly all ore bodies and causes considerable technological and environmental problems. Galena was chosen for study because it exhibits well-characterized semiconducting properties.

Current interest in the electrochemical behavior of pyrite is stimulated by: the need to desulfurize coal (Meyers, 1977), flotation separation with other sulfide minerals (Majima, 1969; Janetski, Woodburn and Woods, 1977; Leppinen, Basilio and Yoon, 1988), to prevent its oxidation to minimize acid mine drainage (Singer and Stumm, 1970; Doyle and Mirza, 1990), to treat low grade and complex sulfide ores by direct leaching (Peters and Majima, 1968), the possibility of electrowinning of metals directly from sulfide ores (Everett, 1982), and the need to develop effective solar energy conversion materials (Jaegermann and Tributsch, 1983; Ennaoui, Fiechter, Goslowsky and Tributsch, 1985; Ennaoui, Fiechter, Jaegermann and Tributsch, 1986).

Pyrite is a major ash-forming mineral in coal. The two major reasons for the poor sulfur rejection during coal flotation are superficial oxidation of pyrite and

incomplete liberation (Yoon, Lagno, Luttrell and Mielczarski, 1991; Luttrell and Yoon, 1992). Superficial oxidation of pyrite and other sulfide minerals leads to self-induced flotation, due to the presence of a sulfur-rich surface (Trahar, 1984; Luttrell and Yoon, 1984a and b). When pyrite is present in coal, its combustion leads to the production of sulfur dioxide which is considered a major contributor to acid rain. The environmental consequences of burning coals containing pyrite have stimulated a search to find a low-cost, physical beneficiation process to remove the pyritic sulfur before combustion.

Pyrite is also a common constituent of base-metal ore deposits. Its flotation and depression is important in the extraction of valuable mineral components. Pyrite is often depressed in the separation process, however the self-induced flotation caused by superficial oxidation worsens the separation process (Ball and Richard, 1976; Buckley and Riley, 1991). Aqueous oxidation of pyrite produces acid water and leads to acid mine drainage (AMD) which causes severe water contamination. Although the initial oxidation of pyrite is relatively slow, once the pH drops below 5, *Thiobacillus ferrooxidans* greatly accelerates its oxidation and the rate of acid formation (Singer and Stumm, 1970; Byerly, 1990; Doyle, 1990). A better understanding of pyrite oxidation processes will aid in controlling acid mine drainage and in rejecting pyrite in coal and mineral flotation.

Galena is a major source of lead. Its concentration is usually accomplished by froth flotation using xanthates as collectors. The interaction of galena with xanthates is electrochemical, involving the anodic oxidation of the collector and cathodic reduction

of oxygen (Woods, 1976). Thus oxygen is necessary for its flotation. However, slight oxidation induces galena flotation in the absence of collector (Trahar, 1984), while, excessive oxidation is known to hinder its flotation (Sutherland and Wark, 1955). The effect of the semiconducting properties of galena on its oxidation and flotation has drawn the attention of some researchers (Guarnaschelli, 1970; Richardson and Maust, 1976; Richardson and Edelstein, 1978; Grandke and Cardona, 1980; Richardson and O'Dell, 1985; Fletcher and Horne, 1991). A further study is needed in order to have a better understanding of the effect of the semiconducting properties of galena on its oxidation behavior.

1.2. Literature Review

Oxidation reactions at semiconducting electrode surfaces are considerably different than those at metal electrode surfaces. The difference arises from the low and variable concentrations of electronic carriers and the two energetically different pathways for charge transfer. There are two major techniques that can be used to elucidate the significance and the role of semiconducting properties in oxidation/reduction reactions. These are determination of the photoresponse to light that is highly absorbed by the semiconducting minerals and measurement of the interfacial impedance.

In semiconductors, the electron and hole concentration can be readily varied by light. Since electrons and holes are reactants in oxidation/reduction reactions, their concentrations can directly affect the kinetics. Also, because of the low and variable

electron and hole concentrations, a space charge layer exists just beneath the surface of semiconducting electrodes. This space charge layer responds to changes in electrode potential and its properties can be measured by electrochemical impedance techniques.

In this section, the structure of the electrode-solution interface, electrode potential, the energy band model, photoeffects at the semiconductor-solution interfaces, and electrochemical impedance spectroscopy are discussed. The electrochemistry of pyrite and galena is also reviewed.

1.2.1. Solid-Solution Interface

a. Structure of electrode-solution interface

When a solid is put in an electrolyte solution, excess negative or positive charges will concentrate on the solid surface. The solution side develops the same amount of excess charge with the opposite sign (counter ions) to keep charge neutrality. This charge separation process represents the electrical double layer that is formed between the solid surface and the solution. Modern theory (Bockris and Reddy, 1970; Bard and Faulkner, 1980; Adamson, 1990) considers that the solution side of the double layer is made up of several layers (Figure 1.1). The inner layer contains solvent molecules and sometimes some specifically adsorbed species. The specifically adsorbed species can be neutral molecules, anions, and sometimes cations. The specifically adsorbed ions are generally considered to be unsolvated, and the locus of their centers defines the position of the inner Helmholtz plane (IHP). The distance from the IHP to the solid surface is of a few (about 3-5) angstroms. The dielectric constant ϵ of the water molecules within

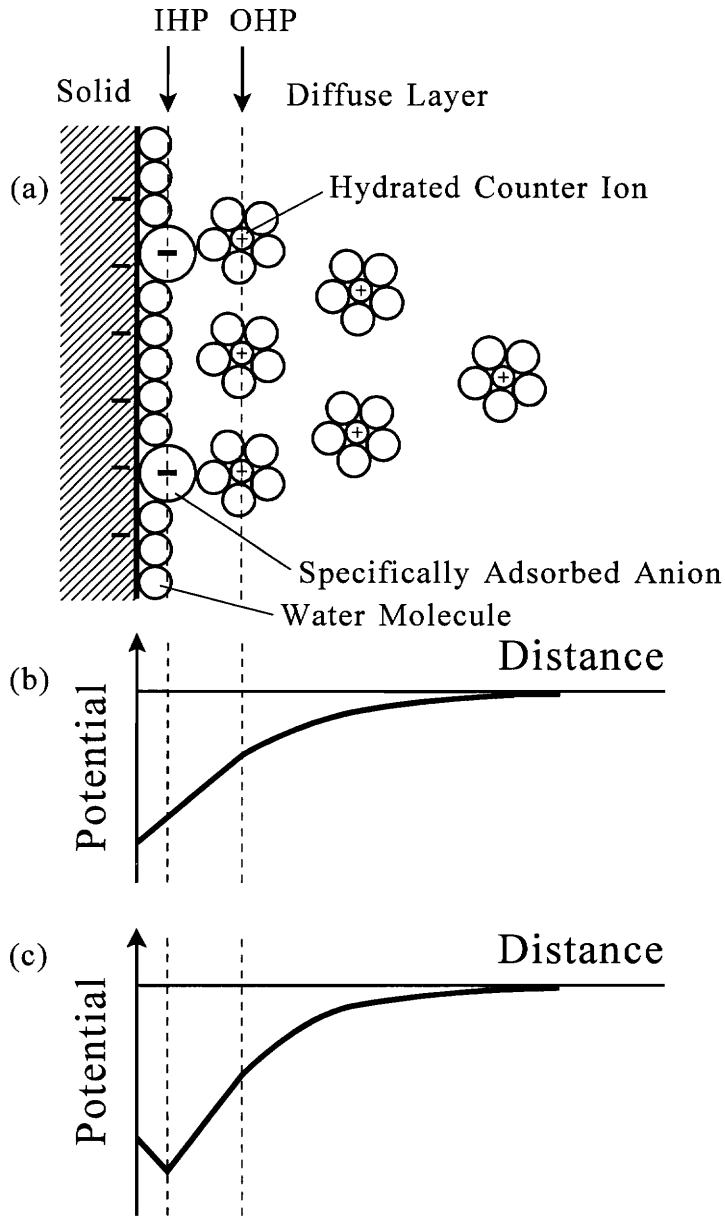

Figure 1.1. Structure of the electrical double layer at the solid-solution interface with anion specific adsorption (a) and the potential distribution across the double layer in the cases of no specific adsorption (b), and anion specific adsorption (c) (adapted from Bockris and Reddy, 1970; Bard and Faulkner, 1980).

the IHP is about 5 (Adamson, 1990). The inside of the IHP consists mostly water molecules. According to a rough calculation (Bockris and Reddy, 1970, page 739), at least 70% of the metal surface must be covered with water molecules. Next to the IHP are solvated counter ions, which are equilibrated by the thermal motion and the electrostatic interaction with the solid surface. This plane is called the outer Helmholtz plane (OHP). Beyond the OHP, the excess solvated counter ion concentration decreases progressively to the bulk solution values. Figure 1.1 shows the ions and potential distribution across the double layer for non-specific adsorption and anion specific adsorption. In the solution side of the double layer, only excess counter ions are shown.

One method of studying the electrical double layer is to examine its charge storage capacity. The total capacitance of the electrical double layer, C_{dl}, in the metal-solution interface can be considered as the Helmholtz (OHP), C_H, and diffuse layer, C_D, capacitances in series (Bockris and Reddy, 1970):

$$\frac{1}{C_{dl}} = \frac{1}{C_H} + \frac{1}{C_D} \qquad \textbf{(1.1)}$$

The capacitance of the Helmholtz layer, C_H, is nearly a constant, about 17 μF/cm^2 (Bockris and Reddy, 1970), while the capacitance of the diffuse layer is dependent on the electrolyte concentration. For strong electrolyte solution, $C_D \gg C_H$ over certain range of potential, and $C_{dl} \approx C_H$.

b. Electrode potential

Electrode potential is defined as the electromotive force (emf) value for a

reduction half-cell reaction (Bard and Faulkner, 1980).

For a general reversible reduction reaction,

$$O + ne^- \rightleftharpoons R \tag{1.2}$$

when it is coupled with a hydrogen electrode,

$$2H^+(aq) + 2e^- \rightleftharpoons H_2(g) \tag{1.3}$$

The cell reaction is

$$R + nH^+(aq) \rightleftharpoons O + \frac{n}{2}H_2(g) \tag{1.4}$$

and its free energy change (Bard and Faulkner, 1980) is

$$\Delta G = \Delta G^0 + RT \ln \frac{[O][H_2]^{\frac{n}{2}}}{[R][H^+]^n} \tag{1.5}$$

The cell emf, V, is defined by,

$$\Delta G = -nFV \tag{1.6}$$

and in standard state,

$$\Delta G^0 = -nFV^0 \tag{1.7}$$

therefore,

$$V = V^0 - \frac{RT}{nF} \ln \frac{[O][H_2]^{\frac{n}{2}}}{[R][H^+]^n} \quad (1.8)$$

which is the Nernst equation.

For a standard hydrogen electrode (SHE), $[H^+(aq)] = 1$ M, and $[H_2(g)] = 1$ atm,

$$V = V^0 - \frac{RT}{nF} \ln \frac{[O]}{[R]} \quad (1.9)$$

This equation defines the reduction potential for the half cell reaction 1.1 relative to the SHE.

1.2.2. Semiconductor-Solution Interface

a. Energy band model

According to molecular orbital theory, electronic energy levels can ensemble into energy bands. The highest filled band is the valence band, E_v, and the lowest empty band the conduction band, E_c (Kittel, 1968). The energy difference between these two bands is the band gap, E_{bg}. For a metal, the two bands overlap, $E_{bg}=0$; or the energy gap is small, and only a small amount of energy is needed for the electron to move from one level to another. For a semiconductor, E_{bg} is usually less than a few electron volts (eV), and for small band gap semiconductor, such as galena, electrons in the valence band may be excited into the conduction band by thermal motions at room temperature. For an insulator, E_{bg} is large compared with the thermal energy kT of the electrons, and electrons in the valence band cannot be significantly excited into the conduction band.

However, light adsorption can be used to generate electron-hole pairs for both semiconductors and insulators.

The Fermi level, E_F, represents the energy level where the probability of occupancy by an electron is 1/2 (Kittel, 1968; Finklea, 1988). The Fermi level is approximately in the middle of E_c and E_v for an intrinsic semiconductor. For an n-type semiconductor, the Fermi level is closer to the conduction band edge, while for a p-type semiconductor, the Fermi level is closer to the valence band edge.

b. Effect of applied potential

If a potential is applied to a semiconductor electrode, in addition to the potential change in the solution side of the electrical double layer, there is also a potential change from the surface to the bulk within the electrode. This causes band bending at the semiconductor surface due to the space charge layer. Figure 1.2 illustrates band bending and the potential distribution between the space charge layer, Helmholtz layer and the diffuse layer at a semiconducting electrode surface.

The charge storage capacity of the semiconductor-solution interface can be considered as the capacitances of three layers in series (Bockris and Reddy, 1970):

$$\frac{1}{C} = \frac{1}{C_{SC}} + \frac{1}{C_H} + \frac{1}{C_D} \qquad \textbf{(1.10)}$$

The last two terms are the same as that of metal electrodes (equation 1.1). The observed capacitance depends upon the electron concentration in the semiconductor and the ionic concentration in solution. As mentioned previously, the Helmholtz capacitance is about

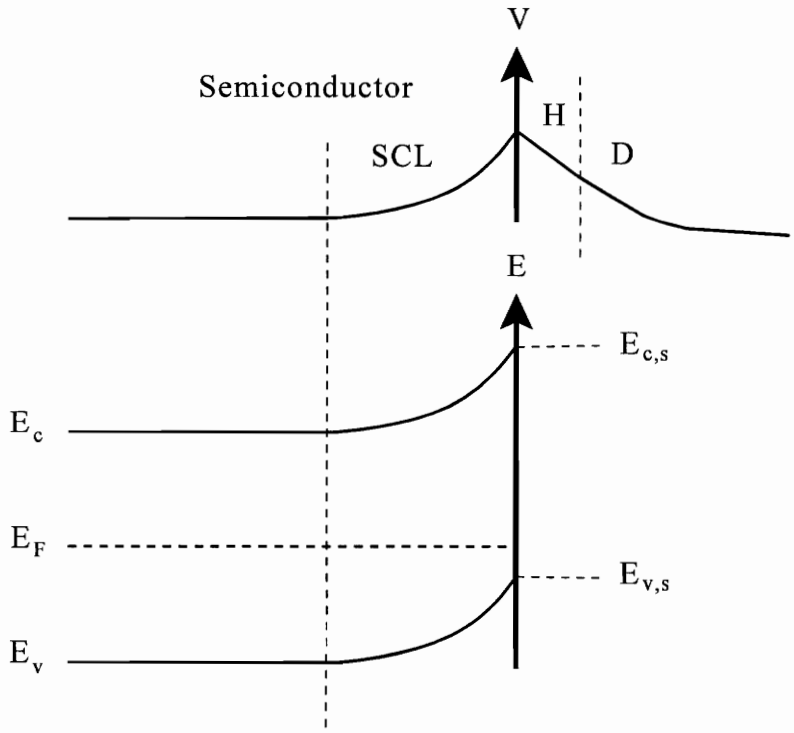

Figure 1.2. Band-bending and electrical potential distribution across semiconductor-solution interface. SCL=space charge layer; H=Helmholtz layer; D=diffuse layer. The relative thickness of these layers are not shown to scale. $E_{c,s}$ and $E_{v,s}$ mark the surface energies of the conduction and valence band edges respectively. The semiconductor is intrinsic, with positive band-bending (after Finklea, 1988).

17 $\mu F/cm^2$, and $C_D \gg C_H$ in strong electrolyte solution. For many semiconductors, the space charge layer capacitance is relatively small, about 0.01-1 $\mu F/cm^2$. Therefore, in concentrated electrolyte solution, the measured capacitance is given by: $C \approx C_{SC}$.

The band bending is the result of the relatively low concentrations of electrons and holes in the semiconductor and the difference in their mobility. Thus, the application of an electric field or the adsorption of a charge on the surface causes a redistribution of electrons and holes just beneath the surface in the space charge layer. As discussed by Finklea (1988), the band bending can be positive or upwards, with E_c and E_v higher at the surface than in the bulk, or the band bending can be negative or downwards, with E_c and E_v lower at the surface than in the bulk. The magnitude of the band bending is equal to the total potential drop across the space charge layer. For a given semiconductor and electrolyte, there exists a unique potential at which the potential drop across the space charge layer is zero, this potential is called the flat band potential (V_{fb}). Figure 1.3 illustrates the band-bending as a function of applied potential.

For an intrinsic semiconductor in a strong electrolyte solution, all of the potential change relative to V_{fb} appears in the space charge layer, and the magnitude of band bending in eV equals the change in applied potential with respect to V_{fb}:

$$E_{c,s} - E_{c,b} = q\,(V - V_{fb}) \qquad \textbf{(1.11)}$$

where q is the electron charge (Figure 1.3). This is also true for n- and p-type semiconductors, provided that the applied potential moves the nearer band edge away

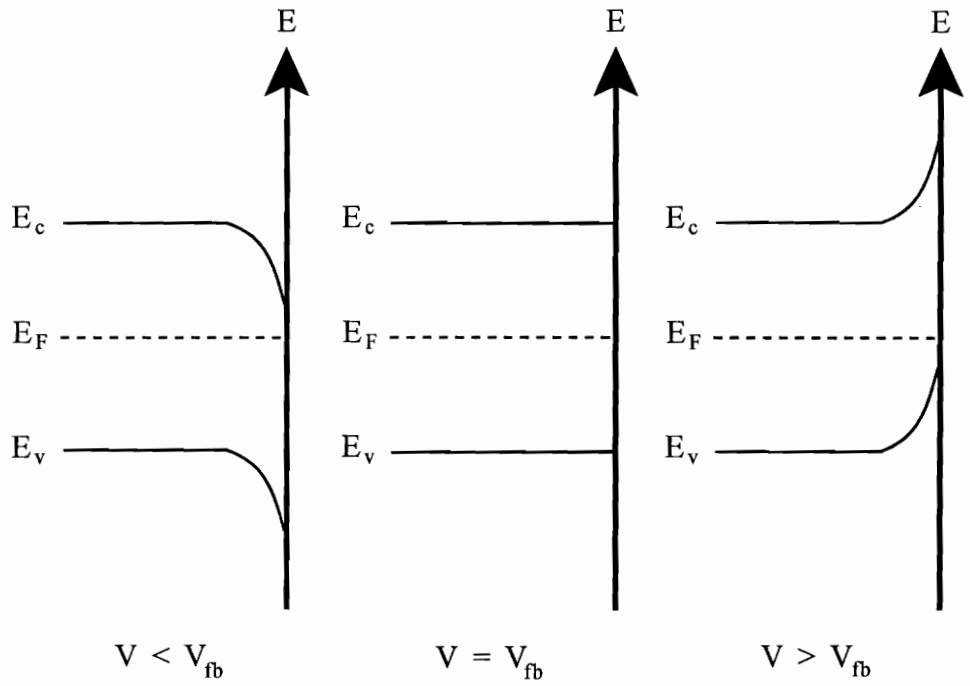

Figure 1.3. Band-bending as a function of the applied potential for an intrinsic semiconductor. V=applied potential; V_{fb}=flatband potential (after Finklea, 1988).

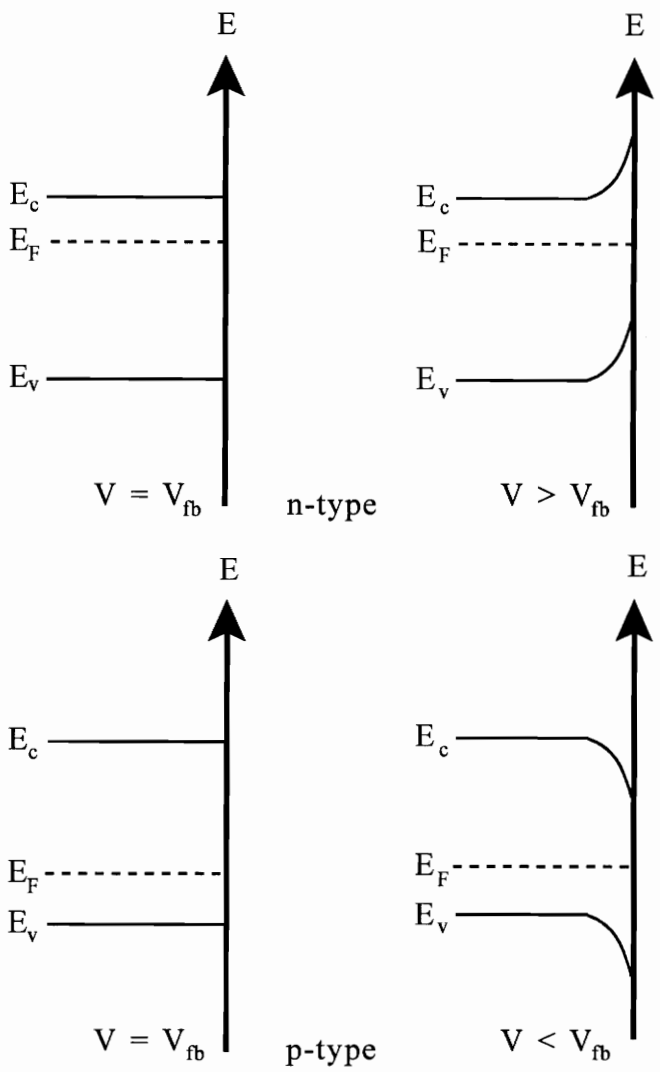

Figure 1.4. Band-bending for n- and p-type semiconductors. All of the potential change occurs in the space charge layer (after Finklea, 1988).

from the Fermi level at the surface (Figure 1.4), i.e., n-type semiconductors must be biased positive of V_{fb} and p-type semiconductors negative of V_{fb} (Finklea, 1988).

V_{fb} varies with electrolyte composition, depending on the redox potential of the solution and the adsorption/desorption equilibria of ions on the semiconductor surface. If only H^+ and OH^- determine the surface charge, then the flat band potential changes with pH according to equation 1.12:

$$V_{fb} = V_{fb}(pzc) - \frac{2.3RT}{F}(pH - pH(pzc)) \qquad (1.12)$$

The pzc is the condition of zero net surface charge. For a metal sulfide, the specific adsorption of sulfide ion, HS^- or S^{2-}, or the formation of oxidation layers, can shift V_{fb}.

Figure 1.5 illustrates several different types of space charge layers for an n-type semiconductor. An accumulation layer is formed at potentials negative of V_{fb}. The majority carriers (electrons) move towards the electrode surface and holes to the interior. The Fermi level at the surface shifts towards the conduction band. With the application of a negative potential, the surface concentration of electrons approaches that of metal, and the semiconductor surface is degenerate (Figure 1.5 (a)). When the applied potential moves positive of V_{fb}, holes are accumulated at the surface, electrons repelled from the surface and a depletion layer is created (Figure 1.5 (b)). When the potential becomes still more positive, the Fermi level at the surface approaches the valence band edge. The concentration of holes exceeds that of electrons, and the surface becomes p-type (Figure 1.5 (c)).

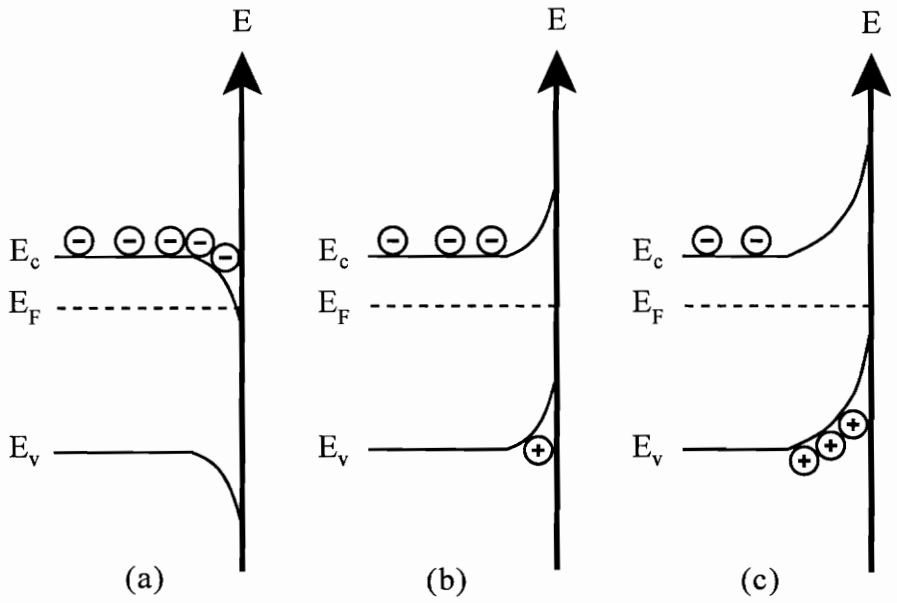

Figure 1.5. Types of space charge layers in an n-type semiconductor surface. (a). Accumulation layer; (b). Depletion layer; and (c). Inversion layer (adapted from Finklea, 1988).

c. Photoeffects at the semiconductor-solution interface

A photon of light with energy greater than the band gap can excite an electron from the valence band to the conduction band. The maximum wavelength (λ_{bg}) of the light that can be used to excite an electron from a semiconductor with band gap E_{bg} can be expressed (Finklea, 1988) by:

$$\lambda_{bg} = \frac{1240}{E_{bg}} \qquad (1.13)$$

where λ_{bg} is in nanometer, and E_{bg} in electron volts. Photogeneration of electrons and holes are especially significant when the wavelength of incident light decreases below λ_{bg}.

When an electron-hole pair is generated by light, the electric field in the space charge layer separates the two charge carriers. Figure 1.6 illustrates this separation process for a depletion layer at an n-type electrode. Here, the photogenerated holes move towards the surface and the photogenerated electrons towards the bulk. The holes have an oxidizing power roughly equivalent to the potential of the valence band edge at the surface, and are capable of oxidizing a molecule whose formal potential is more negative than $V_{v,s}$ (Finklea, 1988). This gives rise to the photocurrent. The excited hole and electron can also recombine one another with the evolution of heat or a photon. Recombination reduces the net concentration of photogenerated electrons and holes and also reduces the magnitude of photoeffects at the semiconducting electrodes.

The photocurrent depends on the energy distribution of the incident photons, the absorption coefficient of the semiconductor, the diffusion distance of the excited hole and

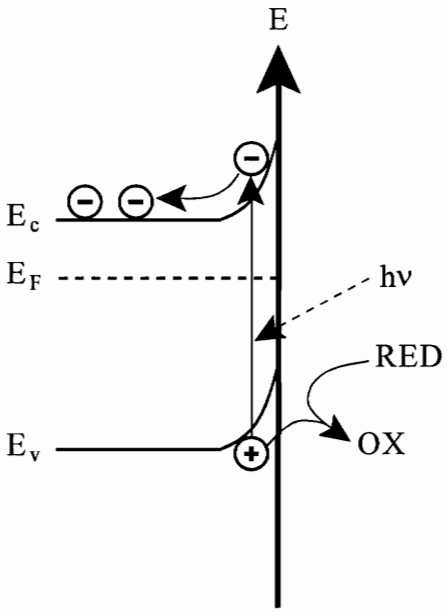

Figure 1.6. Photocurrent generation at an n-type semiconductor surface. $V > V_{fb}$, a depletion layer is formed. Photogenerated holes move to the surface and oxidize solution reductant (after Finklea, 1988).

electron, and the recombination rate of photogenerated carriers.

Information of the potential drop across the space charge layer of a semiconducting electrode can also be obtained from its photoresponse. The fastest process that occurs when a semiconducting electrode is illuminated is an instantaneous increase in the concentration of charge carriers. The separation of photogenerated electrons and holes causes a sudden relaxation for the potential drop across the space charge layer. This shows up as an equivalent change in electrode potential. Slower processes involve rearrangement of ions at the interfaces. Measurement of the instantaneous or fast photoresponse is a good method of determining the flat band potential. At flat bands, there is no space charge to separate the electrons and holes and no photoresponse is observed. There may be a small Dember potential (Many, Goldstein and Grover, 1971) due to different mobilities of electrons and holes.

1.2.3. Electrochemical Impedance Spectroscopy

a. Electrochemical impedance theory

An electrochemical cell can be represented by a pure electronic circuit (Southampton Electrochemistry Group, 1985). An electrode interface during an electrochemical reaction is analogous to an electronic circuit consisting of an array of resistors and capacitors. The impedance of the interface can be used to characterize the electrochemical system in terms of its equivalent electronic circuit based on ac circuit theory.

A simple system could be represented by the circuit shown in Figure 1.7

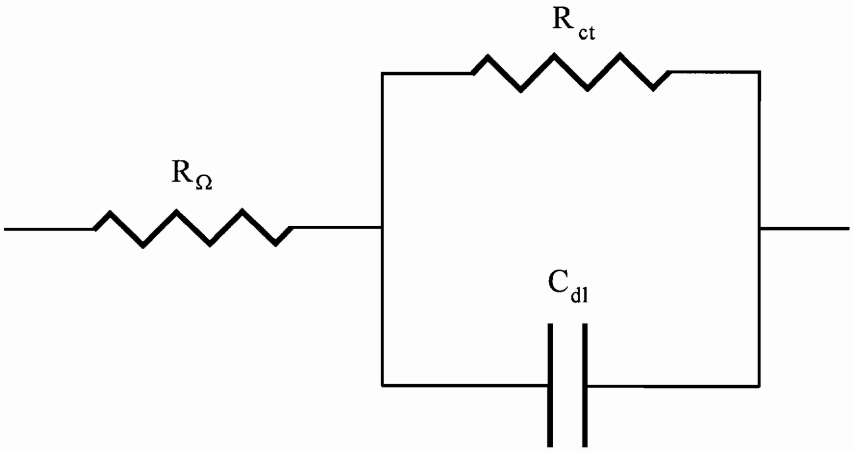

Figure 1.7. Equivalent electronic circuit for a simple electrochemical cell (after Southampton Electrochemistry Group, 1985).

(Southampton Electrochemistry Group, 1985). R_Ω is the uncompensated resistance between the working electrode and the reference electrode. R_{ct} is the charge transfer resistance (or polarization resistance) at the electrode/solution interface. C_{dl} is the double layer capacitance at this interface (see Section 1.2.1 (a)). The electrochemical reaction rates can be calculated from R_{ct}. Double layer capacitance measurements can provide information on adsorption and desorption phenomena, film formation processes at the electrode, and the integrity of organic coatings.

For a resistor, R, the impedance equals its resistance. For a capacitor, C, its impedance equals $-j/\omega C$ (ω is the angular frequency of the ac voltage). For the series circuit of a resistor, R, and a capacitor, C, the impedance can be expressed by $Z=R-j/\omega C$. For a parallel RC circuit,

$$\frac{1}{Z} = \frac{1}{R} + \frac{1}{-\frac{j}{\omega C}} \qquad \textbf{(1.14)}$$

then,

$$Z = \frac{R}{1 + j\omega CR} \qquad \textbf{(1.15)}$$

multiplying the numerator and the denominator by $(1-j\omega CR)$, separating the real and the imaginary components,

$$Z = \frac{R}{1 + \omega^2 C^2 R^2} - \frac{j\omega C R^2}{1 + \omega^2 C^2 R^2} \qquad (1.16)$$

For the circuit shown in Figure 1.7,

$$Z = R_\Omega + \frac{R_{ct}}{1 + \omega^2 C_{dl}^2 R_{ct}^2} - \frac{j\omega C_{dl} R_{ct}^2}{1 + \omega^2 C_{dl}^2 R_{ct}^2} \qquad (1.17)$$

where the real and the imaginary components are as follows:

$$Z_r = R_\Omega + \frac{R_{ct}}{1 + \omega^2 C_{dl}^2 R_{ct}^2} \qquad (1.18)$$

$$Z_i = - \frac{\omega C_{dl} R_{ct}^2}{1 + \omega^2 C_{dl}^2 R_{ct}^2} \qquad (1.19)$$

Elimination of ω from this pair of equations yields (Southampton Electrochemistry Group, 1985):

$$(Z_r - R_\Omega - \frac{R_{ct}}{2})^2 + Z_i^2 = (\frac{R_{ct}}{2})^2 \qquad (1.20)$$

Hence $-Z_i$ vs. Z_r should give a circular plot centered at $Z_r = R_\Omega + R_{ct}/2$ and $-Z_i = 0$, and having a radius of $R_{ct}/2$. Figure 1.8 depicts the result. From this figure, R_Ω, R_{ct} and C_{dl} can be obtained.

Figure 1.9 gives the impedance complex plane plot for various simple electronic circuits.

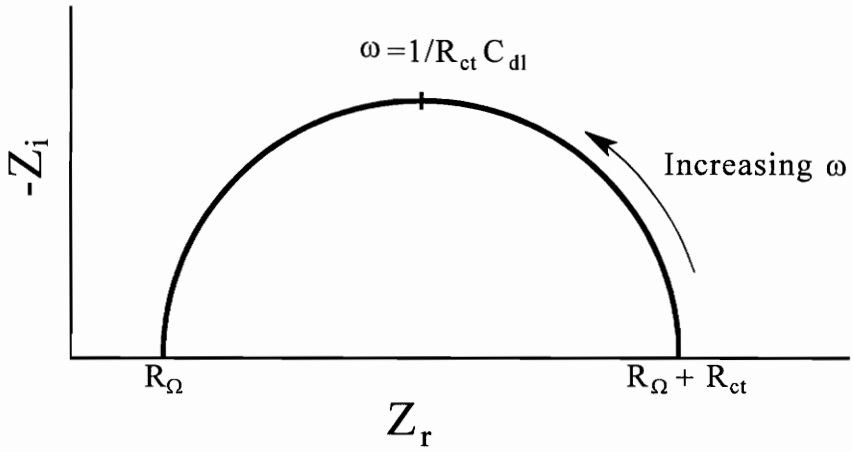

Figure 1.8. Impedance complex plan plot for the equivalent circuit of Figure 1.7 (after Southampton Electrochemistry Group, 1985).

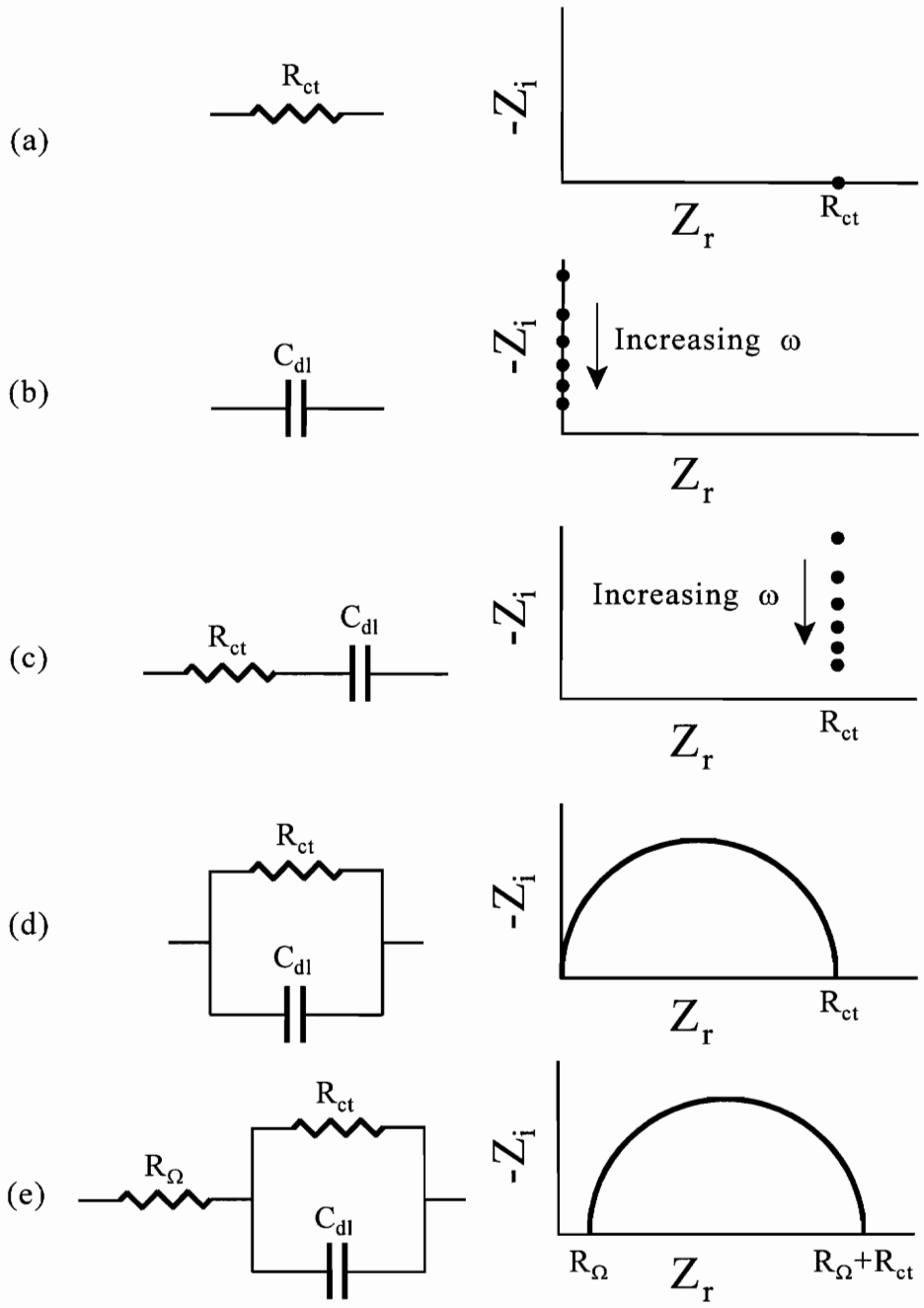

Figure 1.9. Various equivalent circuits and the impedance complex plane plots.

b. Warburg impedance

In a diffusion controlled system, it was found (Southampton Electrochemistry Group, 1985) that,

$$Z = R_{ct} + \frac{\sigma}{\omega^{1/2}} - j\frac{\sigma}{\omega^{1/2}} \qquad \textbf{(1.21)}$$

where

$$\sigma = \frac{RT}{2^{1/2}n^2F^2AD^{1/2}}\left(\frac{1}{c_{O,b}} + \frac{1}{c_{R,b}}\right) \qquad \textbf{(1.22)}$$

where A is the electrode area, D is the diffusion coefficient for species in solution, and $c_{O,b}$ and $c_{R,b}$ are bulk concentrations.

Let

$$Z_W = \frac{\sigma}{\omega^{1/2}} - j\frac{\sigma}{\omega^{1/2}} \qquad \textbf{(1.23)}$$

then

$$Z = R_{ct} + Z_W \qquad \textbf{(1.24)}$$

This is the sum of two terms, a simple resistance component which is small when i_0 (exchange current) is large, and a reactance which is a frequency-dependent resistance. This special resistance, Z_W, is called Warburg impedance, and σ is called Warburg coefficient. In the complex plane, the Warburg impedance is a straight line with a slope of 1.

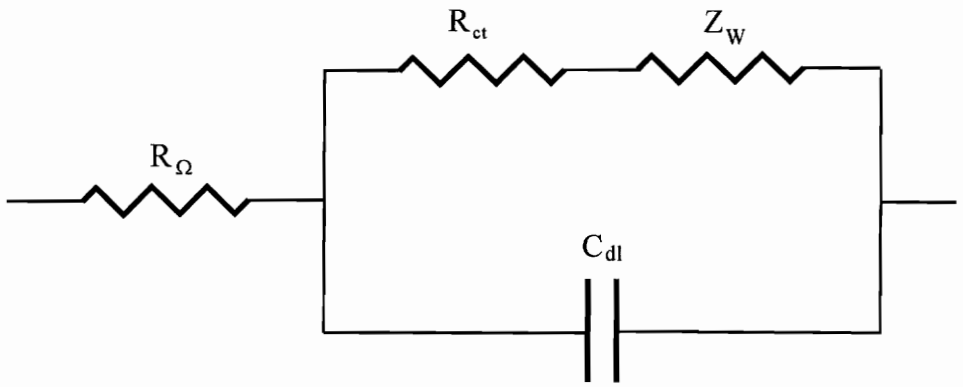

Figure 1.10. Equivalent electronic circuit for an electrochemical cell with Warburg impedance (after Southampton Electrochemistry Group, 1985).

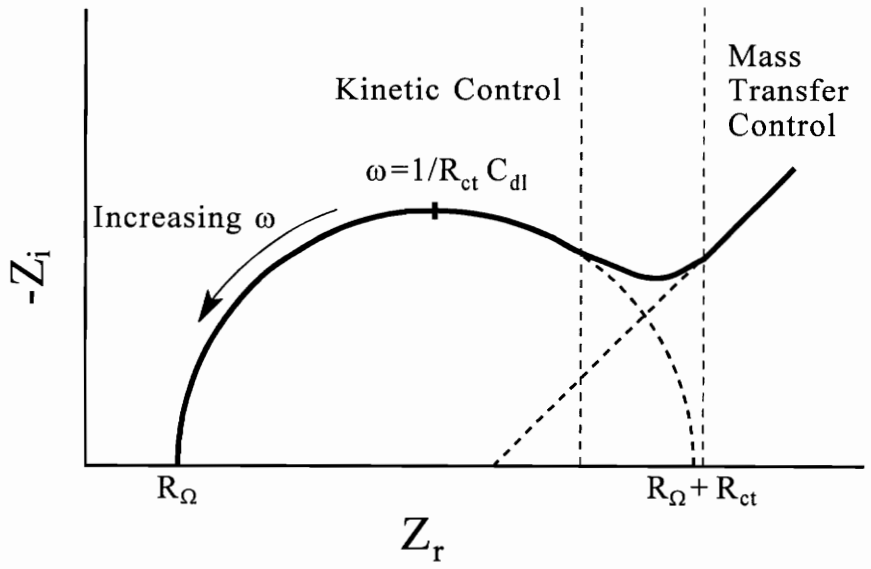

Figure 1.11. Impedance complex plane plot for the equivalent circuit of Figure 1.10 (after Southampton Electrochemistry Group, 1985).

The relative size of R_{ct} and Z_W at any given frequency is a measure of the balance between kinetic and diffusion control. The equivalent circuit of such a system is shown in Figure 1.10. The complex plane impedance plot for this circuit is shown in Figure 1.11. In this plot, both the kinetically controlled (semicircular, high frequency) and mass transfer controlled (linear, unity slope, low frequency) regions are displayed.

c. Impedance at semiconductor-solution interface

As discussed in Section 1.2.2 (b), the total capacitance at the semiconductor-solution interface can be considered as the space charge layer, Helmholtz layer, and diffuse layer capacitances in series. The equivalent electronic circuit for a semiconductor-solution interface is illustrated in Figure 1.12, which can be compared to the equivalent electronic circuit for a metal-solution interface shown in Figure 1.7. In Figure 1.12, C_{SC} is the space charge layer capacitance and C_{dl} is the double layer capacitance. The impedance complex plane plot for the equivalent circuit in Figure 1.12 will be the same as that in Figure 1.8, but the capacitance is the total capacitance, as given by equation 1.10.

1.2.4. Electrochemical Studies of Pyrite and Galena

a. Crystal structure of pyrite and galena

Pyrite (FeS_2) has the halite (NaCl) type structure (Figure 1.13 (a)) (Vaughan and Craig, 1978). The ionic model of pyrite is $Fe^{2+}(S_2)^{2-}$, with the disulfide anion pairs (S_2^{2-}) lying at the center of the cube and the mid-points of the cube edges. Each S atom is coordinated to three Fe atoms and one S atom (Figure 1.13 (b)) and each Fe atom is

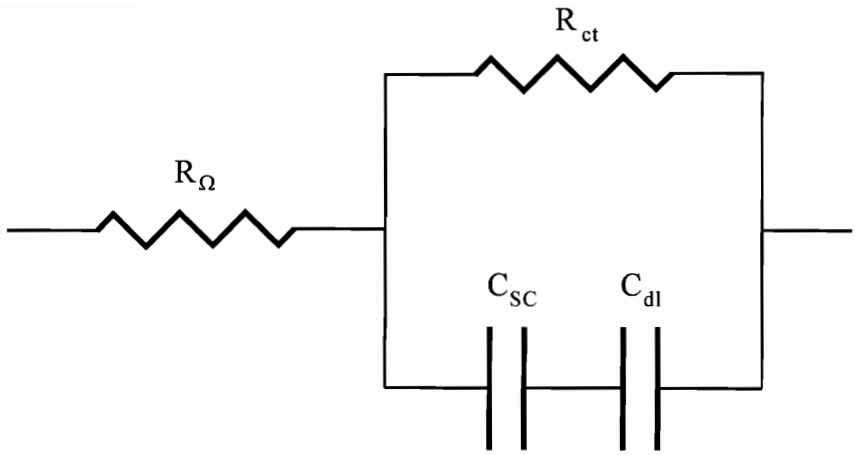

Figure 1.12. Equivalent electronic circuit for a semiconductor-solution interface of a simple electrochemical cell.

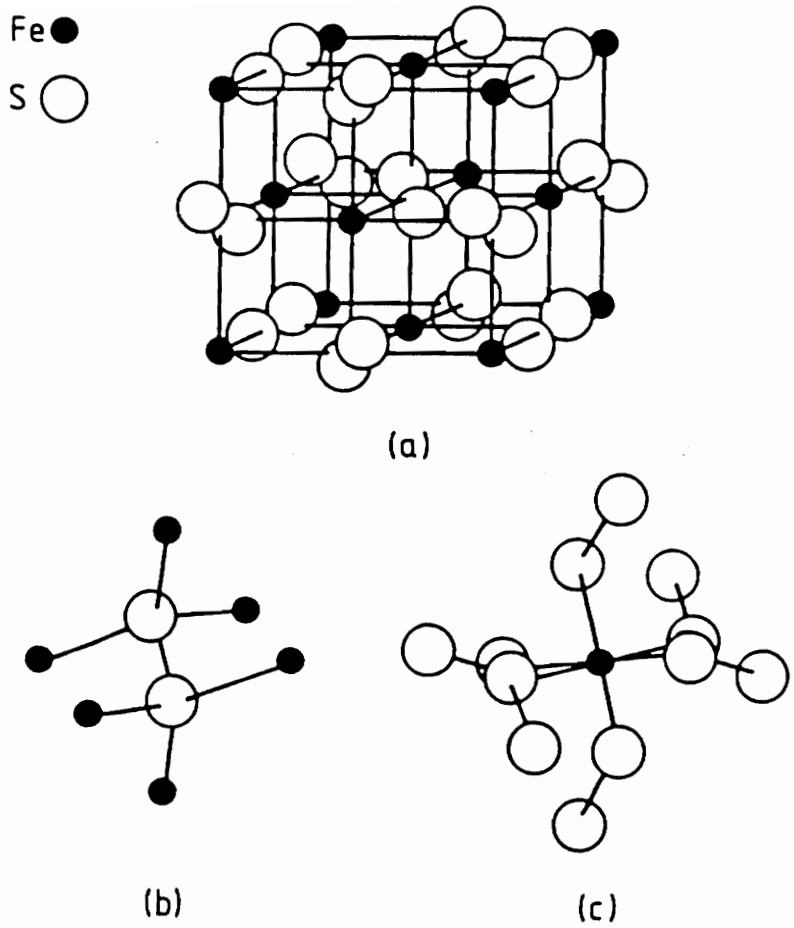

Figure 1.13. Pyrite structure (a); the nearest-neighbor coordination of sulfur atom (b); and the nearest-neighbor coordination of iron atom (c) (after Ennaoui, Fiechter, Jaegermann and Tributsch, 1986).

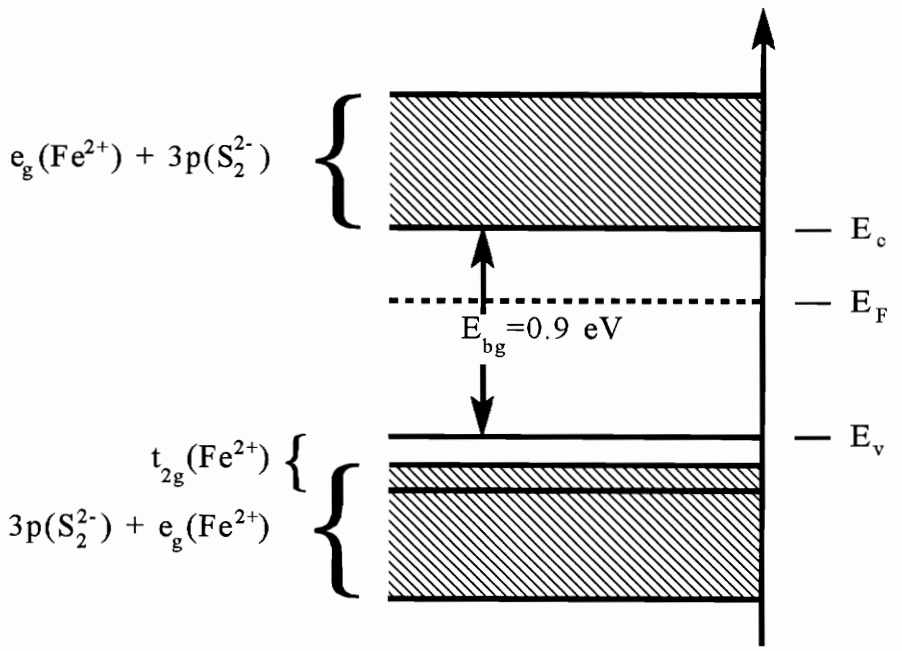

Figure 1.14. Schematic energy band diagram of pyrite (after Jaegermann and Tributsch, 1983).

coordinated to four S atoms (Figure 1.13 (c)). Pyrite is found with both n- and p-type semiconduction. The energy gap of 0.9 eV is essentially the crystal-field splitting of the occupied t_{2g} levels and unoccupied e_g levels (Figure 1.14) (Jaegermann and Tributsch, 1983). Conduction electrons are nearly two orders of magnitude more mobile than holes, and n-type pyrite has a lower resistivity than p-type pyrite (Shuey, 1975). The resistivity is about $1x10^{-3}$ ohm-m for n-type, $3x10^{-2}$ ohm-m for p-type.

Galena (PbS) also has a halite (NaCl) type structure. The unit cell is a face-centered cube, with cubic close-packing of the anions in planes parallel to (111), and both cations and anions are in regular octahedral six-fold coordination (Vaughan and Craig, 1978). Galena is also highly brittle and is easily cleaved along the (100) plane. Galena is found with both n-type and p-type semiconduction. P-type is more resistive than n-type by one order of magnitude (Shuey, 1975). The internuclear distance is smaller than the sum of the ionic radii, suggesting some covalency. Band structure calculation (Vaughan and Craig, 1978) shows that the bottom of the conduction band has Pb(6p) character, and the top of the valence band S(3p) and Pb(6s) characters. The energy gap of galena is about 0.37 eV at room temperature (Shuey, 1975).

The physical properties of pyrite and galena are listed in Table 1.1.

b. Electrochemical studies of pyrite and galena

Most sulfides are thermodynamically unstable in the presence of oxygen (Vaughan and Craig, 1978). When fresh sulfide surfaces are exposed by mining, crushing, or grinding, some degree of oxidation of the surface is expected. The reactions responsible

Table 1.1. Physical properties of pyrite and galena (adapted from Vaughan and Craig, 1978)

Physical properties	Pyrite	Galena
1. Composition	FeS_2	PbS
2. Crystal system	cubic	cubic
3. Space group	P_{a3}	F_{m3m}
4. Crystal structure, a(Å)	5.42	5.94
5. Magnetic property	diamagnetic	diamagnetic
6. Conduction type	semiconductor, n or p	semiconductor, n or p
7. Energy gap	≈ 0.9	0.37

for producing oxide or hydroxide layers on sulfides are electrochemical in nature, with the oxidation reactions of sulfide minerals being coupled with the reduction of dissolved oxygen (Biegler, Rand and Woods, 1975). For a number of sulfides, superficial oxidation is believed to produce excess sulfur in the surface region, which leads to collectorless or "self-induced" flotation (Trahar, 1984).

Sulfide minerals are neither strongly hydrophilic nor strongly hydrophobic (Finkelstein, Allison, Lovell and Stewart, 1975). They are predominantly covalently bonded and the inability of sulfide minerals to form hydrogen bonds with water is the principal reason for sulfides not being strongly hydrophilic. Sulfide minerals are also not strongly hydrophobic due to the presence of broken or unsaturated bonds at the cleavage plane or the fractured surface (excluding layer type sulfide minerals). Kocabag, Kelsall and Shergold (1990a and b) showed that when pyrite is free of oxidation products it is oleophilic, but it is hydrophilic with respect to gas bubble. Formation of sulfur by oxidation at $pH < 4$ will increase oleophilicity. In neutral and alkaline solutions, oleophilicity decreases with oxidation due to the formation of $Fe(OH)_2$ and $Fe(OH)_3$ on the surface. Unoxidized galena is oleophilic in a mineral/oil/water system but hydrophilic in a mineral/gas/water system. Oxidation decreases oleophilicity in neutral and alkaline solutions due to the formation of $Pb(OH)_2$ or metal sulfoxy compounds. In acid solutions, oleophilicity increases with oxidation due to the formation of sulfur on the surface.

The sulfur-rich layer produced by superficial oxidation of sulfide minerals can

exist either as polysulfide (Luttrell and Yoon, 1984a and b; Yoon, Lagno, Luttrell and Mielczarski, 1991), metal-deficient sulfide (Buckley and Woods, 1984 and 1987), or elemental sulfur (Richardson and Maust, 1976; Gardner and Woods, 1979). XPS results by Buckley, Hamilton and Woods (1985) have shown that the oxidation of sulfide minerals involves progressive removal of metal atoms leaving metal-deficient sulfides with sulfur lattices little altered from the original structure. They suggested that metal-deficient layers are probably stabilized by the underlying mineral lattice. Elemental sulfur and sulfur-oxygen species can be formed at strongly oxidizing conditions. Elemental sulfur can be detected at low temperature (150 K) in high vacuum, but it disappears at room temperature because it is volatile.

In long term air oxidation, the oxidation products on pyrite surfaces were detected by XPS as Fe_3O_4 and SO_4^{2-} and, in electrochemical oxidation, as Fe_2O_3 and SO_4^{2-} (Ennaoui, Fiechter, Jaegermann and Tributsch, 1986). Ar ion etching of pyrite surface leads to the formation of FeS (Liu, Pettenkofer and Tributsch, 1988) because sulfur is preferentially sputtered. XPS on *in vacuo* cleaved pyrite (100) surface (Pettenkofer, Jaegermann, Tributsch, Kuhlenbeck, Braun and Bernstorff, 1988) indicated three sulfur states present at the surface: the S(2p) peak for bulk FeS_2 at 162.7 eV, surface FeS_2 at 162 eV and an FeS-like state at 161.2 eV.

In situ Raman spectroscopy studies of the electrochemically oxidized pyrite indicated the presence of sulfur and polysulfides on the electrode surface (Mycroft, Bancroft, McIntyre, Lorimer and Hill, 1990; Zhu, Li, Bobily and Wadsworth, 1992; Li

and Wadsworth, 1993; Turcotte, Benner, Riley, Li, Wadsworth and Bodily, 1993). Elemental sulfur was detected by electrochemically oxidizing pyrite in acid, neutral and weak alkaline solutions, but not in strong alkaline solutions. Polysulfides were identified as the oxidation intermediates. At different pHs, the optimum potential range for sulfur formation is different. The lower potential limits for sulfur formation are 1.05 V at pH 2.7 and pH 9.2, and 0.65 V at pH 6.5 (Li and Wadsworth, 1993). Turcotte, Benner, Riley, Li, Wadsworth and Bodily (1993) also showed that, at pH 6.5, elemental sulfur was present on pyrite surface at potentials above 0.42 V. Polysulfide was also detected. Elemental sulfur was observed on galena at potentials higher than 0.38 V at pH 6.5. These optimum potential ranges for sulfur formation have significant meaning if sulfur acts as a passive film for inhibiting pyrite oxidation.

The anodic behavior of pyrite in acid solution was studied by Biegler and Swift (1979). They concluded that the overall anodic reaction is a combination of two pathways leading to elemental sulfur and sulfate. Sulfate yield increases with increasing potential. Elemental sulfur is not an intermediate in the sulfate route. Sulfate is formed by the initial adsorption of hydroxyl radicals and oxygen atoms from water. The elemental sulfur can be reduced at lower potentials (Hamilton and Woods, 1981). It is generally accepted that the oxidation of pyrite can be described by the following overall reactions (Peters and Majima, 1968; Bailey and Peters, 1976; Peters, 1977; Hamilton and Woods, 1981).

In acidic solution,

$$FeS_2 = Fe^{2+} + 2S^0 + 2e^- \quad (1.25)$$

In neutral and alkaline solution,

$$FeS_2 + 2H_2O = Fe(OH)_2 + 2S^0 + 2H^+ + 2e^- \quad (1.26)$$

$$FeS_2 + 3H_2O = Fe(OH)_3 + 2S^0 + 3H^+ + 3e^- \quad (1.27)$$

and at high anodic potential,

$$FeS_2 + 11H_2O = Fe(OH)_3 + 2SO_4^{2-} + 19H^+ + 15e^- \quad (1.28)$$

If metal-deficient sulfide or polysulfide formed (Luttrell and Yoon, 1984a and b; Buckley and Woods, 1984 and 1987; Yoon, Lagno, Luttrell and Mielczarski, 1991) rather than elemental sulfur, reactions 1.25, 1.26 and 1.27 can be reformulated as:

$$FeS_2 = xFe^{2+} + Fe_{1-x}S_2 + 2xe^- \quad (1.29)$$

$$FeS_2 + 2xH_2O = xFe(OH)_2 + Fe_{1-x}S_2 + 2xH^+ + 2xe^- \quad (1.30)$$

$$FeS_2 + 3xH_2O = xFe(OH)_3 + Fe_{1-x}S_2 + 3xH^+ + 3xe^- \quad (1.31)$$

The electrochemistry of galena in electrolyte solutions has been studied through the use of linear sweep voltammetry (Richardson and Maust, 1976; Paul, Nicol, Diggle and Saunders, 1978a and b; Gardner and Woods, 1979; Pritzker and Yoon, 1988). In acid media, galena oxidation produces lead ion and sulfur according to the following reaction:

$$PbS = Pb^{2+} + S^0 + 2e^- \quad (1.32)$$

In neutral and alkaline solution, a monolayer of PbO and S^0 is formed on the surface of galena:

$$PbS + H_2O = PbO + S^0 + 2H^+ + 2e^- \quad (1.33)$$

Oxy-sulfur species can only formed at high potentials (higher than 0.75 V) (Buckley, Hamilton, and Woods, 1985):

$$PbS + 4H_2O = PbSO_4 + 8H^+ + 8e^- \quad (1.34)$$

If metal-deficient sulfide or polysulfide is proposed as the oxidation product (Luttrell and Yoon, 1984a and b; Buckley and Woods, 1984 and 1987; Yoon, Lagno, Luttrell and Mielczarski, 1991), the reactions can be expressed by:

$$PbS = xPb^{2+} + Pb_{1-x}S + 2xe^- \quad (1.35)$$

$$PbS + xH_2O = xPbO + Pb_{1-x}S + 2xH^+ + 2xe^- \quad (1.36)$$

c. Effect of semiconducting properties of pyrite and galena on electrochemical behavior and flotation

Most sulfide minerals are semiconductors (Shuey, 1975; Vaughan and Craig, 1978). As discussed in Section 1.2.2, semiconducting electrodes have several unique characteristics which arise from the two energetically different pathways for charge transfer, *i.e.*, via the conduction and valence bands, and from the relatively low

(compared to a metal) and variable concentrations of conduction band electrons and valence band holes (Dewald, 1960). Because of these features which distinguish redox processes at semiconductors from those at metals, the oxidation and reduction of sulfides and their flotation response can be expected to be dependent on their semiconducting properties. However, nearly all research directed at determining details of the reactions between semiconducting sulfides and thiol collectors assume, *a priori*, that the electrodes behave as metals. The few studies that have attempted to correlate semiconducting properties with oxidation behavior and flotation have been conflicting or controversial. There are two reasons why controversial results have been obtained. First, naturally occurring sulfide minerals may have widely varying compositions and impurity contents, and, therefore, varying semiconducting properties, making it difficult to correlate charge transfer processes occurring at the surface with semiconducting properties. Second, most electrochemical studies relating to flotation have been conducted on ground electrodes. Grinding is known to create defect levels in the surface region that could mask the semiconducting characteristics of the electrodes (Many, Goldstein and Grover, 1971). Recombination generally occurs through defect levels and a large density of defects induced by grinding would be expected to reduce carrier lifetimes (Scanlon, 1957) and hence the magnitude of photoeffects. Similarly, carrier trapping in defect levels induced by grinding may pin the Fermi level in the surface region so the space charge region is not readily polarized with applied potentials.

Several studies have been directed at the relationship between the semiconducting

properties of pyrite and its oxidation behavior. Shuey (1975) reported that both n- and p-type ore pyrites are present in nature. Esposito, Chander and Aplan (1987) and Briceno and Chander (1988) concluded that ore-pyrite was n-type and coal-pyrite was p-type, while studies on the possible use of pyrite and other d-band semiconductors as photoanodes for solar energy conversion indicate that most pyrite is n-type (Salvador, Tafalla, Tributsch and Wetzel, 1991; Mishra and Osseo-Asare, 1988a and b, 1992). Pyrite specimens from different sources and with different semiconducting properties (n-type, n-type metallic and p-type) were studied for their electrochemical oxygen reduction behavior in acid solution (Biegler, 1976). The oxygen reduction behavior varied on different samples, but the variations could not be correlated with the semiconducting type. Biegler and Swift (1979) also showed that the semiconducting properties of pyrite do not significantly influence the kinetics of its anodic oxidation.

The photoelectrochemistry of n-type pyrite has been characterized (Jaegermann and Tributsch, 1983; Ennaoui and Tributsch, 1984; Ennaoui, Fiechter, Goslowsky and Tributsch, 1985; Ennaoui, Fiechter, Jaegermann and Tributsch, 1986). They showed that illuminated pyrite cannot photo-evolve oxygen but photo-corrodes to iron sulfate. They concluded that interfacial iron cannot form a complex which leads to oxygen evolution, while interfacially bound oxygen is transferred to the sulfur ligand which is oxidized to SO_4^{2-}.

There have been several studies of the effect of semiconducting properties on the electrochemistry and flotation of galena (Guarnaschelli, 1970; Richardson and Maust,

1976; Richardson and Edelstein, 1978; Grandke and Cardona, 1980; Richardson and O'Dell, 1985; Fletcher and Horne, 1991). Plaksin and Shafeev (1960) first suggested that the semiconducting properties of some sulfides might be significant in flotation. For galena, they suggested that oxygen chemisorption could localize conduction band electrons at the surface, giving rise to an underlying positive space charge layer (depletion layer on n-type galena) that facilitates oxidation reactions involving xanthate collectors. The formation of a depletion layer due to the oxidation of freshly cleaved galena electrodes has been confirmed (Richardson and O'Dell, 1985). Eadington and Prosser (1969) studied the oxidation rate of galena of controlled non-stoichiometry. They concluded that lead-rich samples oxidizes much slower than sulfur-rich samples. Springer (1970) showed that sulfur-rich sulfides show p-type conductivity and metal-excess ones n-type, and concluded that the electronic conduction properties do not normally play a significant role in hydrometallurgical oxidation and dissolution reactions. While Eadington (1973) observed two distinct reaction stages in galena oxidation. In the initial period, the reactivity of n-type galena is faster than p-type and it can be enhanced by illumination. After reaction proceeds for less than a monolayer, the reaction rate decreased considerably and independent of the original electronic nature of the solid. Since most of the reaction will occur at the slower rate after the first monolayer dissolved, they concluded that the overall leaching rate will be similar.

1.3. Objective

The major objective of this work was to better understand the initial oxidation behavior of pyrite. This topic is of considerable technological importance because the oxidation of pyrite leads to acid mine drainage (AMD), which is one of the most severe environmental problems caused by mining. AMD arises from the oxidation of pyrite and other iron containing sulfide minerals.

To study the initial oxidation of pyrite, fresh surfaces were created by fracturing electrodes *in situ*. The current at the surface during fracture and the voltammetric behavior of pyrite after fracture were used to study its oxidation behavior.

Another objective of this study was to determine how the sources of pyrite, hence, its solid state properties influence its initial oxidation. For this purpose, photocurrent measurement was conducted on fractured pyrite electrodes. For comparison, photocurrent studies were also conducted on galena electrodes. Galena was chosen because of its well-characterized semiconducting properties, and its behavior could be compared with that of pyrite. Electrochemical impedance measurements were initiated to further characterize the interfacial properties of fractured and abraded pyrite electrodes.

Chapter 2. Experimental

2.1. Materials

2.1.1. Mineral Samples

Hand selected pyrite samples from Lorgono, Spain or Huanzala, Peru, in the shape of cubes, were used for this study. Pyrite samples from Zacatecas, Mexico; Taipai, Taiwan; Black sea region, Turkey; Melissa, Illinois; and Lake balkhash, Russia were also studied. Galena samples were from Galena, Kansas, and obtained from a single large crystals of cluster. No visible impurities or inclusions were present in the pyrite and galena samples.

2.1.2. Chemicals and Solution

The pH 4.6 buffer solution was made of 0.05 M sodium acetate ($CH_3COONa.3H_2O$, crystalline) and 0.05 M acetic acid (CH_3COOH, glacial, sequencing grade, aldehyde free). The pH 9.2 buffer solution was made with 0.05 M sodium tetraborate (borax, $Na_2B_4O_7.10H_2O$, crystalline). All chemicals used were certified A.C.S. grade made by Fisher Scientific. All of the solutions were made using double distilled and deionized water (resistivity 18 megohm-cm).

2.1.3. Equipment

The potentiostat used in this study was a Model 273 potentiostat/galvanostat (EG&G Princeton Applied Research). The potentiostat was controlled by an IBM

personal computer. The light source for the photocurrent measurement was an 100 watt tungsten-halogen lamp housed by an Oriel 60008 light housing (Oriel Corporation). An oscilloscope (Tektronix, Inc., Model 7613) was used to observe the transient photocurrent. For some experiments, the transient photocurrent was photographed using a polaroid scope camera. For photocurrent-potential and impedance measurements, a lock-in amplifier (EG&G Princeton Applied Research, Model 5208) was used. The dependence of photocurrent on potential was recorded using an X-Y recorder (Hewlett Packard, Model 7015).

2.2. Electrode Design

Pyrite samples were cut with a low speed diamond saw to dimensions of approximately 2x2x10 mm. Galena samples were cleaved using a razor blade. The cleaved samples were rectangular in shape, and all of its surfaces were freshly cleaved.

A copper electrical lead was attached to one of the 2×2 mm faces with either conducting epoxy or indium solder. These specimens were mounted on the end of an 8 mm O.D. Pyrex tube using nonconducting epoxy. The epoxy was also used to encapsulate the electrical contact and approximately one half of the electrode; the half of the electrode not encapsulated protruded out of the epoxy, and was in contact with the electrolyte when the sample was mounted in an electrochemical cell. The electrode is illustrated in Figure 2.1. A sharp tap on the protruding portion with a glass rod nearly always resulted in fracture with the new surface flush with the epoxy.

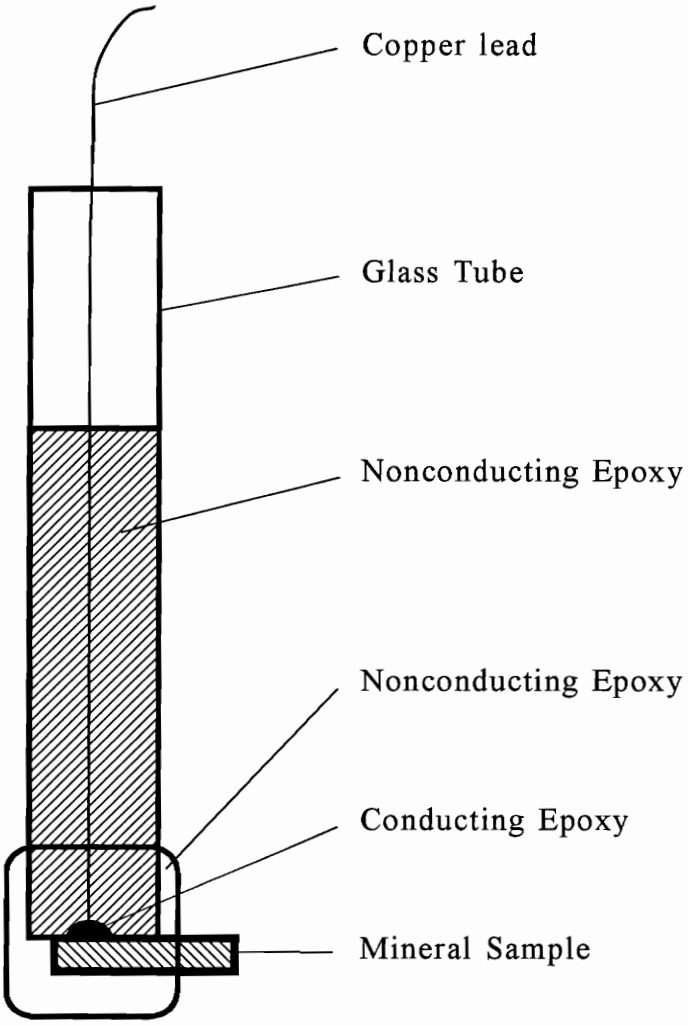

Figure 2.1. Electrode.

2.3. Electrochemical Cell Design

The electrochemical cell was a standard three-electrode cell, with a quartz optical window, as illustrated in Figure 2.2. The total volume of the cell was about 200 ml. The top of the cell was made of nylon and contained ports for the working electrode, reference electrode, gas inlet, gas outlet, and for inserting a glass rod used to fracture the electrode. The counter electrode compartment was connected to the cell through a glass frit. Mineral electrodes were used as the working electrode. The counter electrode consisted of a piece of platinum screen spot-welded to a platinum wire. A saturated calomel electrode (SCE) was used as the reference electrode, and the potentials were converted to the standard hydrogen electrode (SHE) scale by adding 0.2415 V.

2.4. Experimental Setup

A diagram of the electrochemical setup and equipment for current-time, voltammetry, photocurrent, and impedance measurements are shown in Figure 2.3. Model 270 Electrochemical Analysis System (EG&G Princeton Applied Research, version 3.00) was used for the current-time, voltammetry and photocurrent-potential measurements. The Model 378 Electrochemical Impedance System (EG&G Princeton Applied Research, version 2.70) was used for the impedance measurement.

2.5. Procedures

Before experiments, the solutions were sparged with nitrogen for about two hours

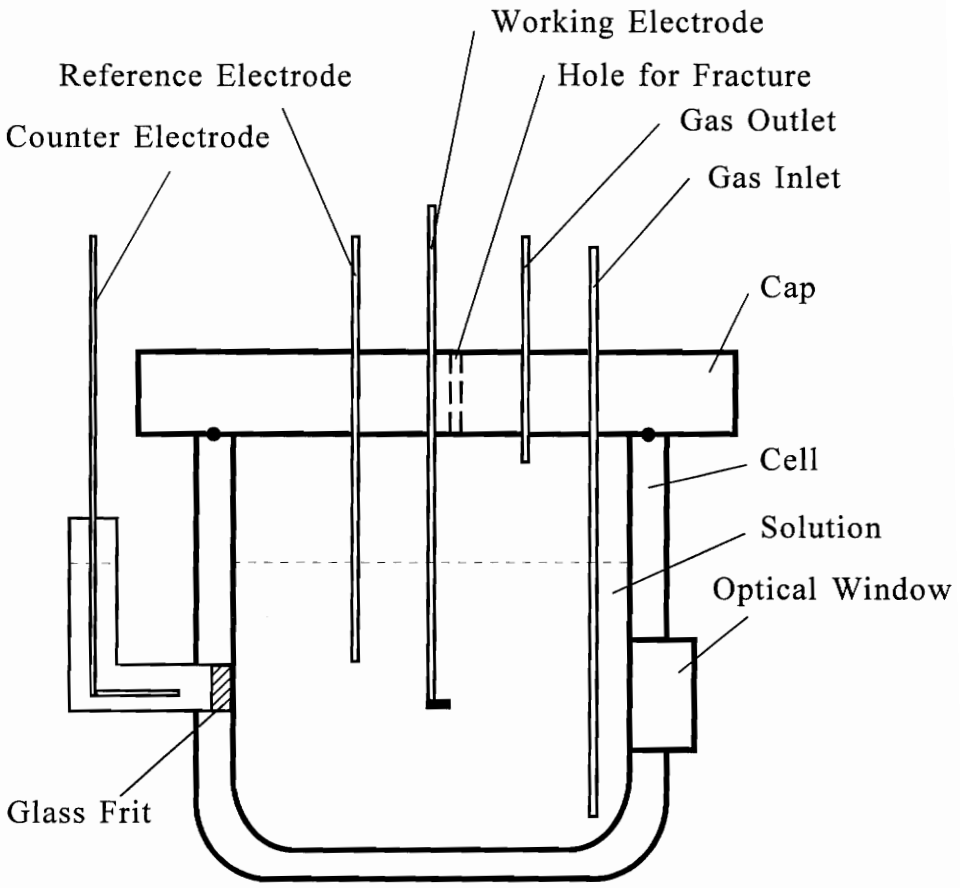

Figure 2.2. Electrochemical cell.

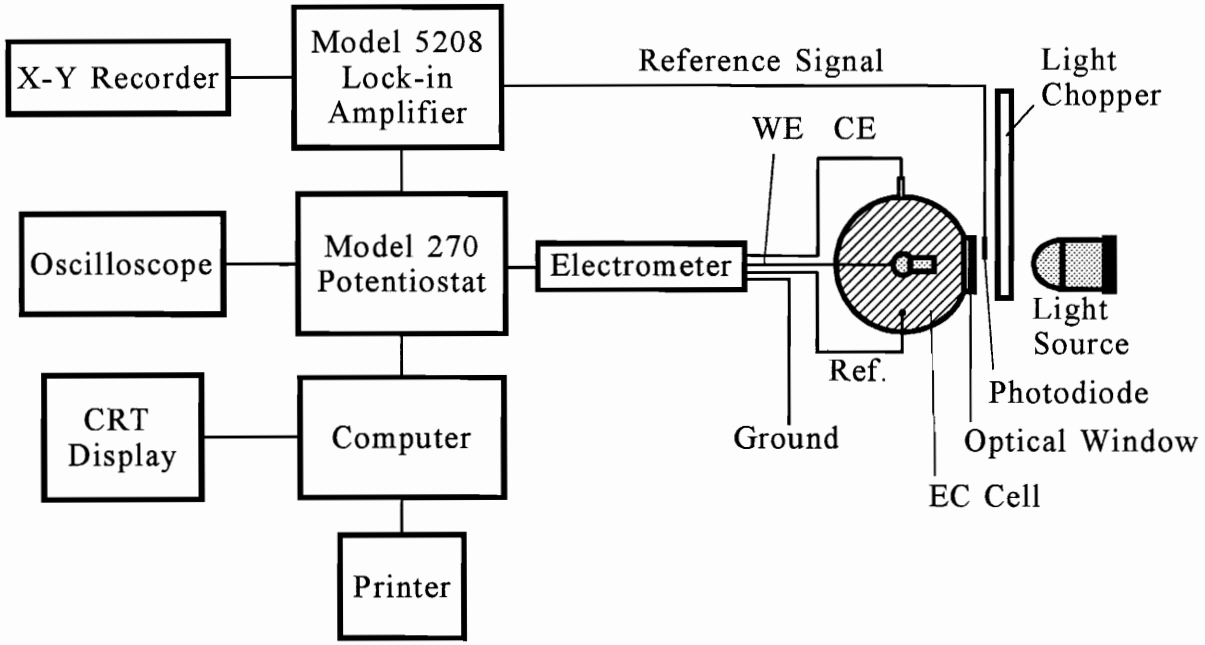

Figure 2.3. Experimental setup for the (photo)electrochemical measurement, WE=working electrode, Ref=reference electrode, CE=counter electrode.

to eliminate dissolved oxygen. For current-time measurements during fracture, chronoamperometry software (Model 270 Electrochemical Analysis System) was used. The electrodes were potentiostated at selected potentials before and after fracture.

For the photocurrent-potential measurement, chopped illumination was produced by a homemade light chopper. The chopper speed was about 1600 rpm with light-on and light-off durations of approximately 1.3 msec and 17.4 msec, respectively. The transient photocurrent was studied by photographing the signal with the scope camera. The in-phase component of the photocurrent was measured with a PAR 5208 lock-in amplifier. The photocurrent-potential curves represent the root-mean-square of the peak of the transient photocurrent averaged for 300 ms.

Electrochemical impedance experiments were conducted using the Model 378 software. The sinusoidal voltage signal for impedance measurements were 10 mV peak-to-peak and the frequency range studied was 100 KHz to 0.05 Hz.

Chapter 3. Electrochemical Studies of Pyrite

3.1. Experimental Results

3.1.1. Current-Time Measurement on *In Situ* Fractured Pyrite Electrodes

Through out the experiment, pyrite samples from Lorgono, Spain and Huanzala, Peru were used, except that in Section 3.1.3.(d), where pyrite from other sources were also used. Figures 3.1 and 3.2 illustrate the typical curves of current as a function of time after fracturing mineral pyrite electrodes in, respectively, pH 4.6 and pH 9.2 buffer solutions. Before discussing these curves, it is worthwhile pointing out the similarity between chronoamperometry on a fractured surface to the better-known technique of controlled potential step chronoamperometry for studying electroactive species in solution. In the latter, the potential is stepped from an electrochemically inactive region to a value where an electroactive species is rapidly reduced or oxidized. This requires, initially, a large current to reduce or oxidize those species within the reaction layer at the surface. Charging of the double layer and redox processes involving any adsorbed species are also fast processes (Bard and Faulkner, 1980) that contribute to the initial current. The current then decays as a concentration gradient that controls the diffusion of the electroactive species to the surface develops. The present experiments differ from the usual controlled potential step method in several aspects. First, the electroactive species is the pyrite electrode itself. Second, the potential step experienced at fracture

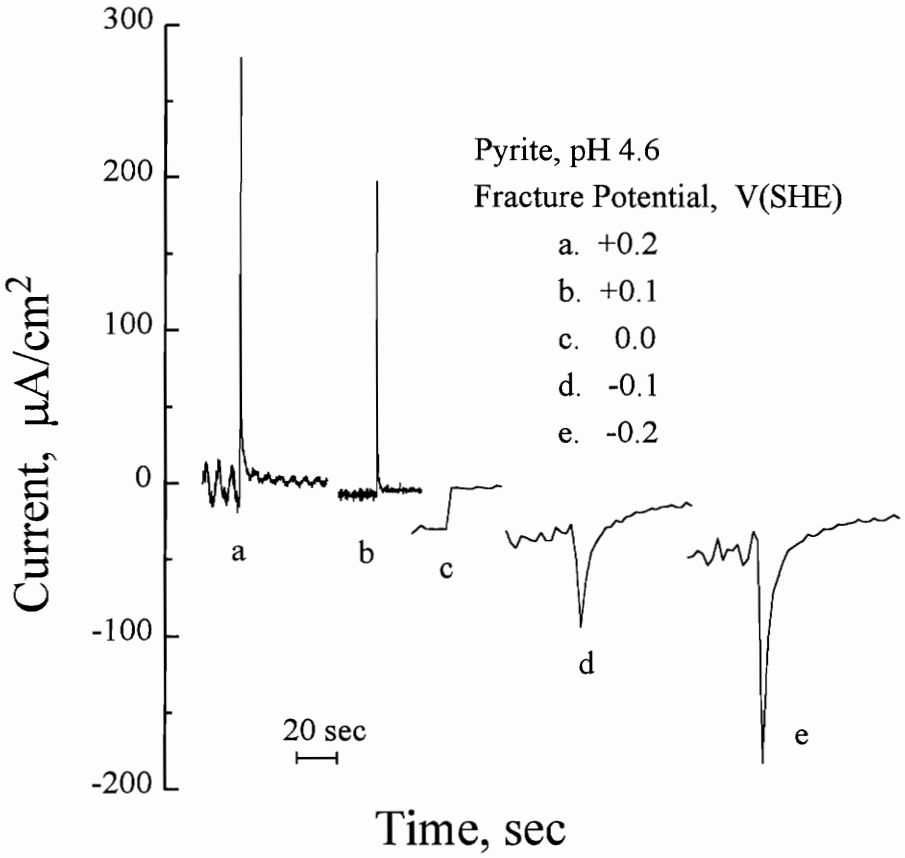

Figure 3.1. Current-time curves for *in situ* fractured pyrite electrodes held at various potentials. pH 4.6 buffer solution.

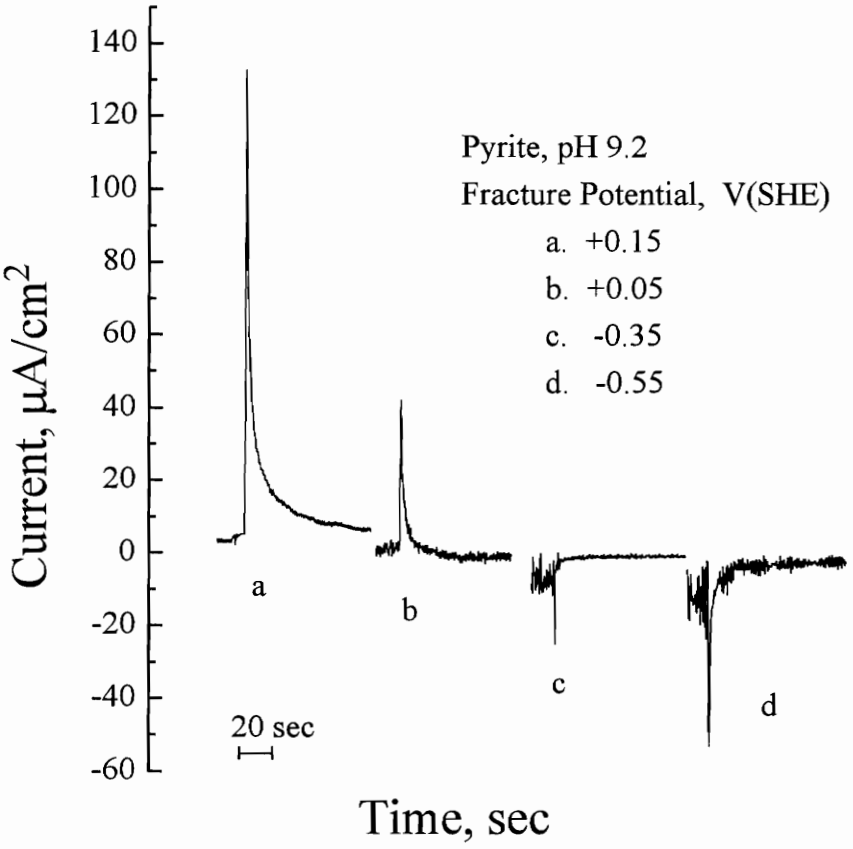

Figure 3.2. Current-time curves for *in situ* fractured pyrite electrodes held at various potentials. pH 9.2 buffer solution.

represents the difference between the applied potential and the potential a newly created surface assumes at the instant of fracture. Third, fracture momentarily destroys the preexisting double layer, and a double layer must be formed on the new surface. Based on these comparisons, it is believed that the initial spike observed on the current-time curves at the moment of fracture represents a combination of double layer charging and faradaic oxidation (or reduction) of the fresh pyrite surfaces. Double layer charging is fast compared to the time scales of Figures 3.1 and 3.2, and thus the decay in the current after the initial spike is believed to represent primarily faradaic reactions involving pyrite.

Each of the electrodes were potentiostated at the potentials indicated on the curves for a few minutes before fracture to allow residual currents to decay to constant, steady state values. The current density is expressed using the measured geometric area of the electrode after fracture. Before fracture, the apparent surface area of the electrode exposed to solution was in the range of 5 to 15 times of the geometric area of the fractured surface. Since the area before fracture is much larger than the area after fracture, only the current densities after fracture is meaningful. Although the assumed fracture surface was carefully delineated, the fractured surface of pyrite was irregular, and the true area was believed to be two to four times the geometric area. There was a residual, steady state current on the electrodes prior to fracture that was very close to zero at anodic potentials and became more cathodic with increasing negative potentials. This current represented the reduction of the residual oxygen on the electrode surface,

and hence increased with increasing negative potential. From Figure 3.1, at pH 4.6, an anodic current was observed when the pyrite electrode was fractured at 0.2 V and 0.1 V, establishing that pyrite undergoes spontaneous oxidation at these potentials. Cathodic currents were observed when pyrite was fractured at -0.1 V and -0.2 V, establishing that pyrite undergoes spontaneous reduction at these potentials. The current observed at fracture changed from anodic to cathodic between 0.1 V and -0.1 V, and thus the potential at which pyrite is stable is between these values. It is believed to be close to 0.0 V (curve (c)) at this pH. The slight step change in current during fracture observed for curve (c) was believed to represent primarily a decrease in the amount of oxygen reduced due to the sudden decrease in surface area of the electrode after fracture.

Similar result was obtained at pH 9.2, which is shown in Figure 3.2. An anodic current was observed when the pyrite electrode was fractured at potentials 0.15 V and 0.05 V and a cathodic current was observed when pyrite was fractured at potentials of -0.35 V and -0.55 V. The stable potential is believed to be close to -0.3 V at this pH.

The most significant features of the current-time curves in Figures 3.1 and 3.2 are the dependence of both the sign and magnitude of the current on potential and the apparent existence of a unique potential where new surfaces of pyrite do not react, i.e., the potential where there is no current flow at fracture. This occurs at 0 V at pH 4.6 (Figure 3.1) and -0.3 V at pH 9.2 (Figure 3.2). Previous studies (Richardson, Li and Yoon, 1992) have shown that fresh pyrite produced by fracture on open-circuit, i.e., without potentiostating the electrodes, assumed an instantaneous potential several hundred

millivolts more negative than the rest potential. The potential then increased more slowly back to the usual rest potential. It can be reasoned that a freshly created pyrite surface should instantaneously assume a potential that is within the thermodynamic stability domain of pyrite, with the actual value being dependent on soluble ion concentrations at the surface. If this instantaneous fracture potential is known for a given solution, and the electrodes held at this potential during fracture, a freshly created surface should have no tendency to react. This is consistent with the results of Figures 3.1 and 3.2; surfaces created at $\approx$ 0 V at pH 4.6 and at $\approx$ -0.3 V at pH 9.2 appear to be stable, i.e., faradaic reactions on these surfaces appear to be negligible as long as the potentials are maintained at these unique fracture potentials. Therefore, the fracture potentials where no significant current flows may be referred to as "stable" potentials. It should be noted that the instantaneous potential at fracture is several hundred millivolts more negative than the steady state rest potentials.

The charges passed immediately after fracture, obtained by integrating the current-time curves (Figures 3.1 and 3.2), are shown in Figures 3.3 and 3.4. The crystal structure of pyrite is face-centered cubic, with a unit cell length of 5.42 Å (Vaughan and Craig, 1978). The molecular density on (100) surface is 6.8×10^{14} molecules/cm^2. If the oxidation and reduction reactions on pyrite occur by one-electron processes, the charge expected for the reaction of one monolayer of pyrite is 109 μC/cm^2. For a two-electron process (as in reactions 3.3 and 3.8 below), the charge anticipated for one monolayer would correspond to 218 μC/cm^2. Figure 3.3 indicates that, when pyrite was fractured

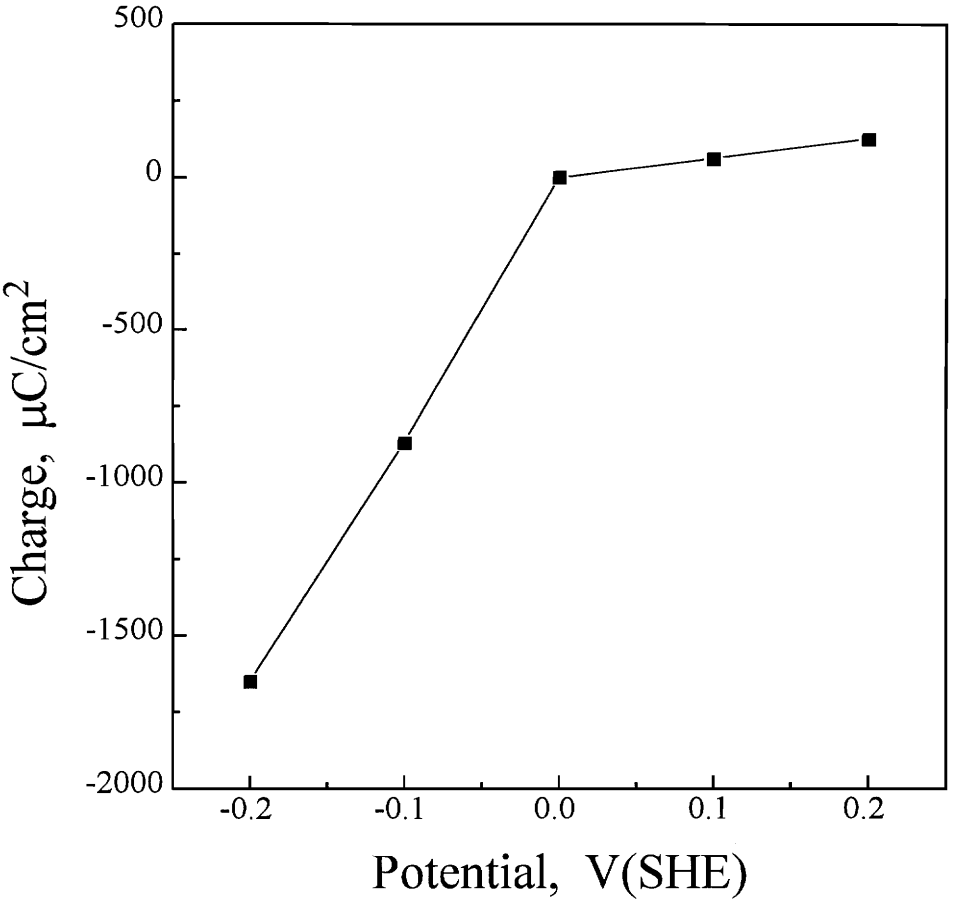

Figure 3.3. Charge-potential curve obtained by integrating the current-time curves shown in Figure 3.1.

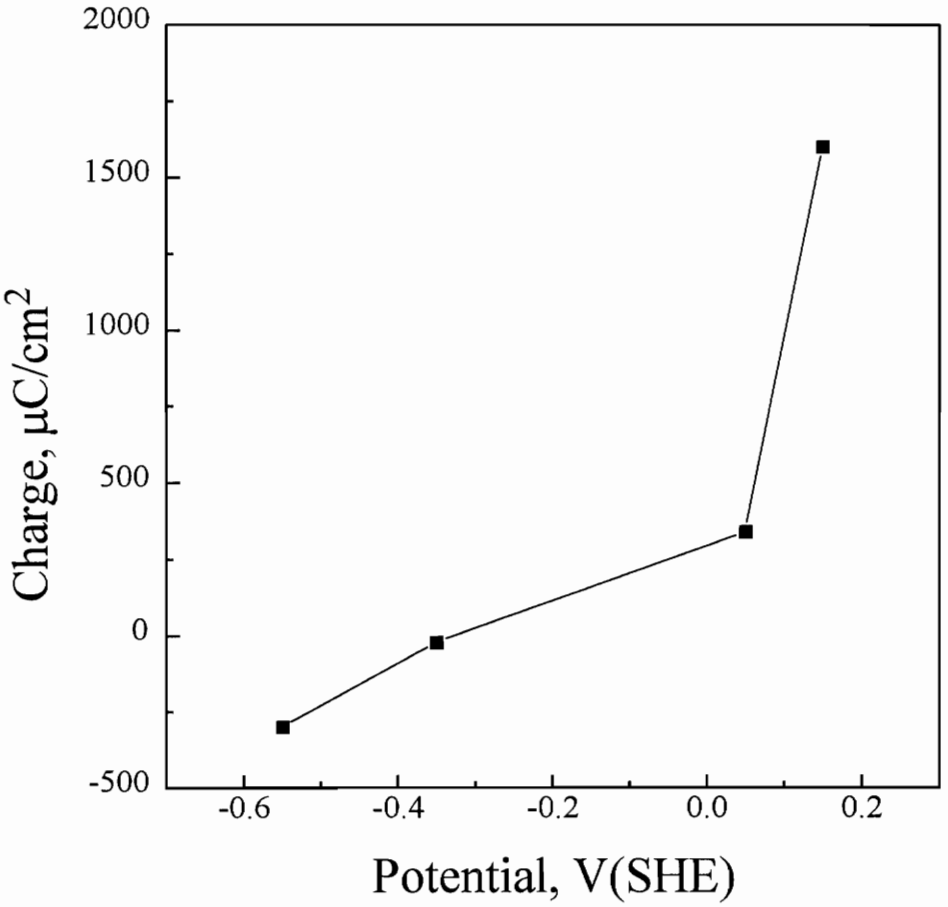

Figure 3.4. Charge-potential curve obtained by integrating the current-time curves shown in Figure 3.2.

while holding the potential in the range of -0.1 to 0.2 V, less than a monolayer of pyrite was oxidized or reduced assuming a two-electron process. The potential at which pyrite is stable is around 0 V at pH 4.6. Figure 3.3 also suggests that pyrite is more easily reduced at potentials below the stable potential than it is oxidized at potentials above the stable potential.

Figure 3.4 indicates that when pyrite was fractured while holding the potential in the range of -0.5 to -0.1 V at pH 9.2, less than a monolayer of pyrite was oxidized or reduced assuming a two-electron process. In contrast to the behavior at pH 4.6, at pH 9.2, pyrite is more easily oxidized at potentials above the stable potential than it is reduced at potentials below the stable potential. Therefore, the tendencies of pyrite to be reduced or oxidized outside of the stable potential are different at pH 4.6 and pH 9.2. The reason for this difference is not clear.

Between pH 4.6 and 9.2, the stable potential changes 0.065 V per pH unit. This is close to 0.059, which would be the value expected for a reaction involving H^+ or OH^- where one electron is passed for each H^+ or OH^- ion. This is in agreement with the oxidation mechanism proposed by Biegler and Swift (1979). They proposed that the slow step in sulfate formation on pyrite occurs somewhere during the addition of the first or second oxygen atom to a sulfur atom. From electrochemical kinetic theory, they suggested that the process involves direct transfer of oxygen from water to sulfur atoms in the pyrite lattice, with oxygen addition occurring through adsorption and deprotonation of water molecules according to a series of equations such as:

$$FeS_2 + H_2O \rightleftharpoons FeS_2(OH)_{ads} + H^+ + e^- \quad (3.1)$$

$$FeS_2(OH)_{ads} \rightleftharpoons FeS_2(O)_{ads} + H^+ + e^- \quad (3.2)$$

with the second charge transfer step (reaction 3.2) being rate-determining. They were unable to determine at which stage desorption of a sulfur-oxygen species takes place. In reaction 3.2, one electron is passed for each H^+ ion.

3.1.2. Cyclic Voltammetry on *In Situ* Fractured Electrodes

Most electrochemical studies on pyrite have been conducted on surfaces that have been either dry- or wet-abraded (Peters and Majima, 1968; Janetski, Woodburn and Woods, 1977; Hamilton and Woods, 1981; Mishra and Osseo-Asare, 1988a and b; Ramprakash, Koch and Woods, 1991; Chander, Briceno and Pang, 1992; Ahmed and Giziewicz, 1992). Abrasion may cause extensive pre-oxidation and the introduction of lattice defects in the surface region, both of which may affect electron transfer processes. Surfaces abraded under water (Buckley and Woods, 1987) were shown to undergo stoichiometric alteration, with iron-rich and sulfur-rich regions formed. After exposure to air for a few minutes, iron oxide and iron-deficient sulfide were formed. Therefore, on abraded surface of pyrite, the composition is not stoichiometric pyrite. Some mechanical damages at the surface and in the bulk immediately beneath the surface is expected. This is also true for other sulfide minerals.

Some voltammograms on pyrite electrodes were obtained by beginning the sweeps from the open circuit potential of ground or abraded electrodes (Hamilton and Woods,

1981, Ramprakash, Koch and Woods, 1991). At open circuit, the outermost surfaces are oxidized pyrite. In the subsequent potential scan, the anodic or cathodic processes appear to be dominated by the oxidation or reduction of these pre-existing oxidation products. Cathodic or anodic treatment of the electrode before sweeping (Peters and Majima, 1968; Chmielewski and Wheelock, 1990) changed the electrode surfaces, but the treated surfaces probably contain oxidation or reduction products. The products of oxidation or reduction may be soluble, the reactions during a sweep may be irreversible (Hamilton and Woods, 1981). In the present study, in order to study the oxidation/reduction behavior of pure pyrite (neither oxidized nor reduced), electrodes were fractured when holding at the stable potential where no current was passed during fracture. The electrode was then swept positively or negatively from the fracture potential in order to study the oxidation or reduction behavior of pure pyrite.

Figures 3.5 shows the voltammetry curve for the first positive-going sweep beginning from the stable potential at pH 4.6. A small anodic peak is observed at 0.15 V and an anodic wave begins at 0.25 V. The small peak must be due to the oxidation of pure pyrite by a reaction of the form (Peters and Majima, 1968; Bailey and Peters, 1976; Peters, 1977; Hamilton and Woods, 1981):

$$FeS_2 = Fe^{2+} + 2S^0 + 2e^- \qquad (3.3)$$

and the large anodic wave may be due to the reaction,

$$FeS_2 + 8H_2O = Fe^{2+} + 2SO_4^{2-} + 16H^+ + 14e^- \qquad (3.4)$$

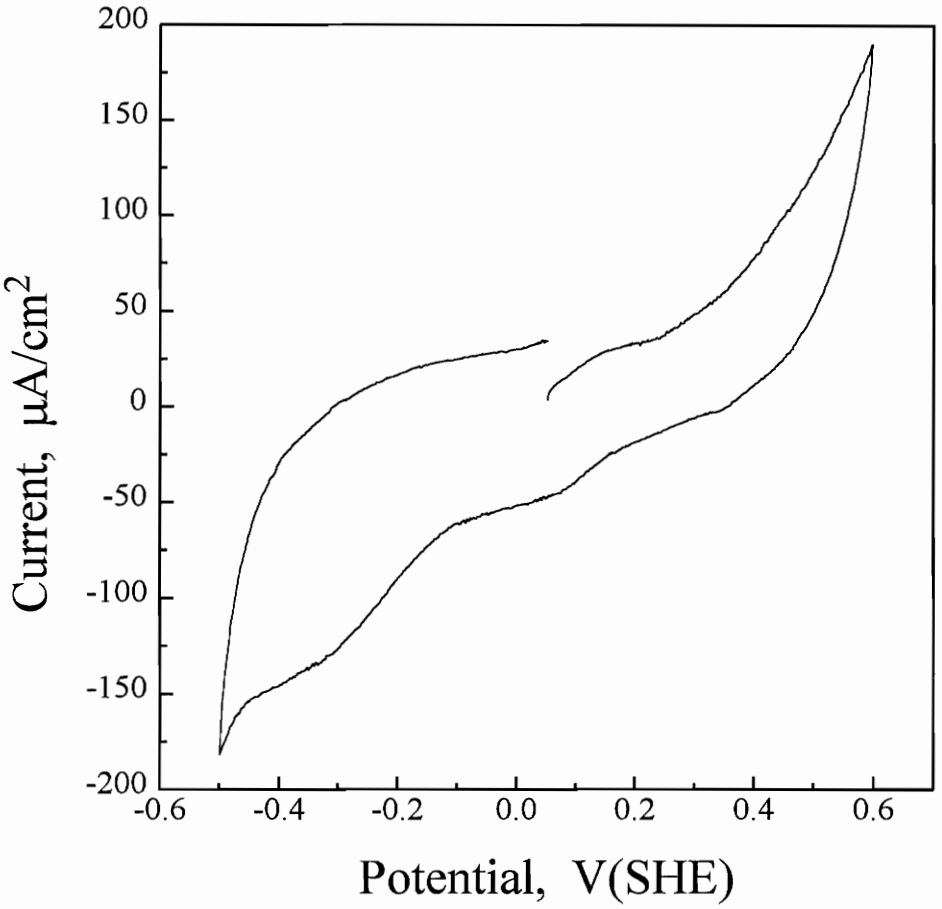

Figure 3.5. The first sweep voltammogram for a freshly fractured pyrite electrode in pH 4.6 buffer solution. The electrode was held at 0 V during and after fracture until sweep begins. No current passed during fracture. The sweep begins in the positive-going direction from the fracture potential. Sweep rate 50 mV/sec.

or, at potentials higher than -0.4 V,

$$FeS_2 + 11H_2O = Fe(OH)_3 + 2SO_4^{2-} + 19H^+ + 15e^- \quad (3.5)$$

On the subsequent cathodic sweeps, a small cathodic wave is observed at 0.05 V and a large wave begins at -0.1 V. The small cathodic wave at 0.05 V can be assigned to the reduction of ferric hydroxide formed by reaction 3.5 (Hamilton and Woods, 1981):

$$Fe(OH)_3 + 3H^+ + e^- = Fe^{2+} + 3H_2O \quad (3.6)$$

and the large wave may be due to the reduction of sulfur,

$$S^0 + 2H^+ + 2e^- = H_2S \quad (3.7)$$

or, at lower potentials, the reduction of pyrite:

$$FeS_2 + 2H^+ + 2e^- = FeS + H_2S \quad (3.8)$$

If metal-deficient sulfide or polysulfide (Luttrell and Yoon, 1984a and b; Buckley and Woods, 1984 and 1987; Yoon, Lagno, Luttrell and Mielczarski, 1991), rather than elemental sulfur is formed, reaction 3.3 can be rewritten as:

$$FeS_2 = xFe^{2+} + Fe_{1-x}S_2 + 2xe^- \quad (3.9)$$

Figures 3.6 shows the voltammetry curve for the first negative-going sweep beginning from the stable potential. Two cathodic waves were observed which begin at 0 V and -0.15 V respectively. The first wave must be due to the reduction of pure pyrite, which can be expressed by reactions 3.8. The second wave may be due to the

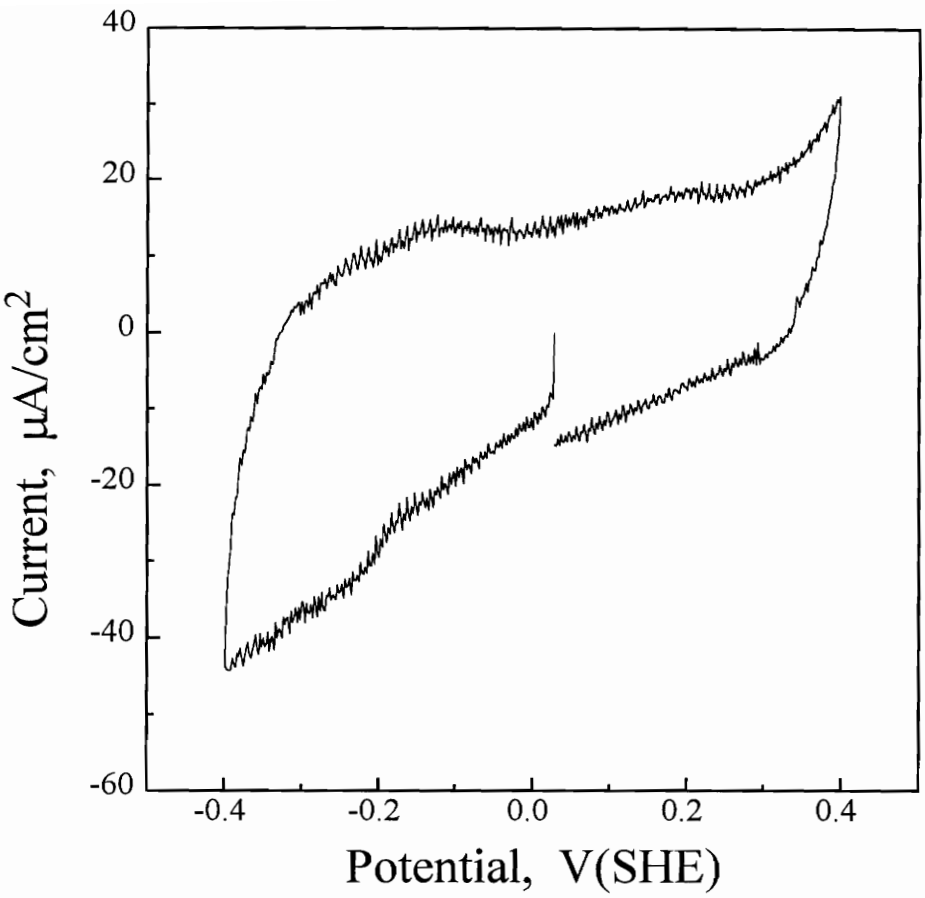

Figure 3.6. The first sweep voltammogram for a freshly fractured pyrite electrode in pH 4.6 buffer solution. The electrode was held at 0 V during and after fracture until sweep begins. No current passed during fracture. The sweep begins in the negative-going direction from the fracture potential. Sweep rate 50 mV/sec.

further reduction of FeS, or the reduction of pyrite. Two small anodic processes are observed at around -0.12 V and 0.2 V, and another, larger anodic process begins at 0.3 V. The first anodic process at -0.12 V may be due to the reverse of reaction 3.8. The other two anodic processes are believed to represent the oxidation of pyrite, as expressed by reactions 3.3 and 3.4.

Figure 3.7 shows the charge obtained by integrating the voltammetry curve of Figure 3.5. For a two electron process, the charge passed should be 218 $\mu C/cm^2$ for one monolayer of pyrite. The charge measured from 0 V to 0.25 V on the positive sweep is 104 $\mu C/cm^2$. This suggests that less than one half of a monolayer of pyrite is oxidized by reaction 3.3. The charge passed for the anodic process at potentials positive of 0.25 V is about 900 $\mu C/cm^2$. For a 14- and a 15-electron processes, which correspond to reactions 3.4 and 3.5, the charge passed should be 1526 $\mu C/cm^2$ and 1635 $\mu C/cm^2$, respectively, for one monolayer pyrite. This suggests that less than one monolayer of pyrite is oxidized by reactions 3.4 and 3.5 at potentials between 0.25 V and 0.6 V.

The charge passed in the potential range between 0.35 V and -0.1 V on the negative going sweep is about 290 $\mu C/cm^2$, suggesting that less than one monolayer of $Fe(OH)_3$ was formed on the pyrite surface by reaction 3.5. The total charge passed for the cathodic process at potentials from -0.1 V to -0.5 V is about 1130 $\mu C/cm^2$, this charge is due to the reduction of S^0 and FeS_2. It is believed that less than a monolayer of S^0 is formed by reaction 3.3.

Figure 3.8 shows the charge passed that was obtained by integrating the

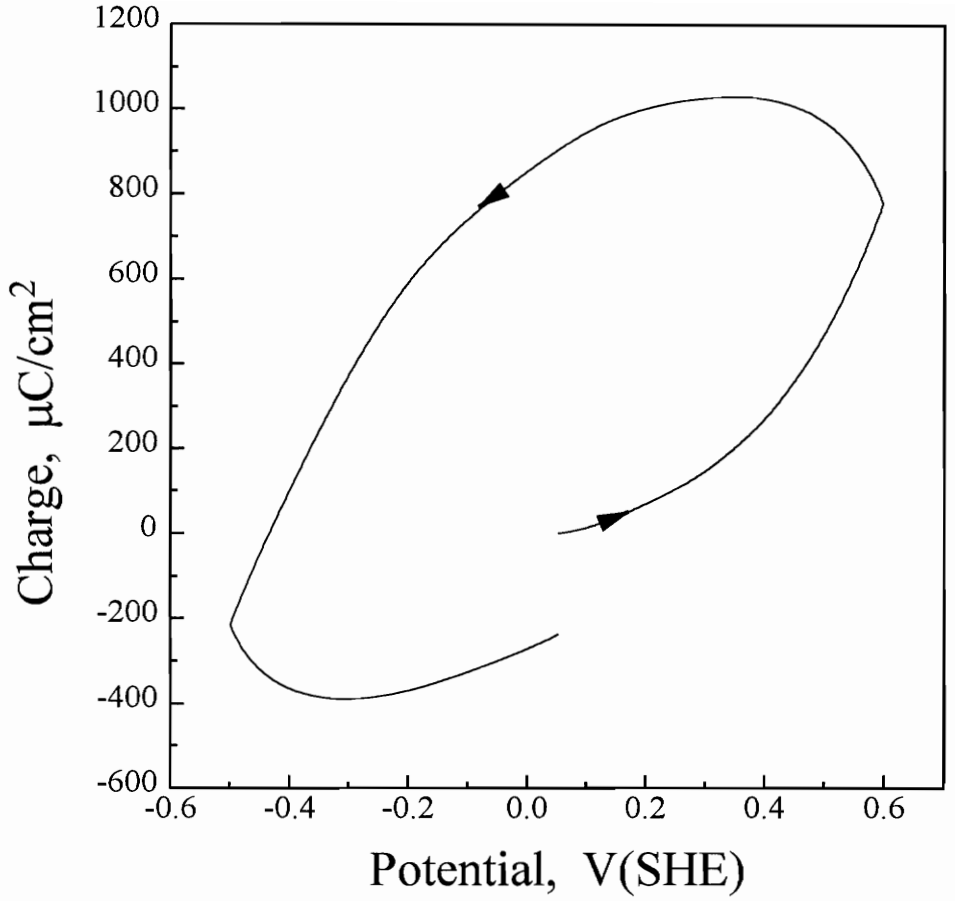

Figure 3.7. Charge-potential curve obtained by integrating the voltammetry curve shown in Figure 3.5.

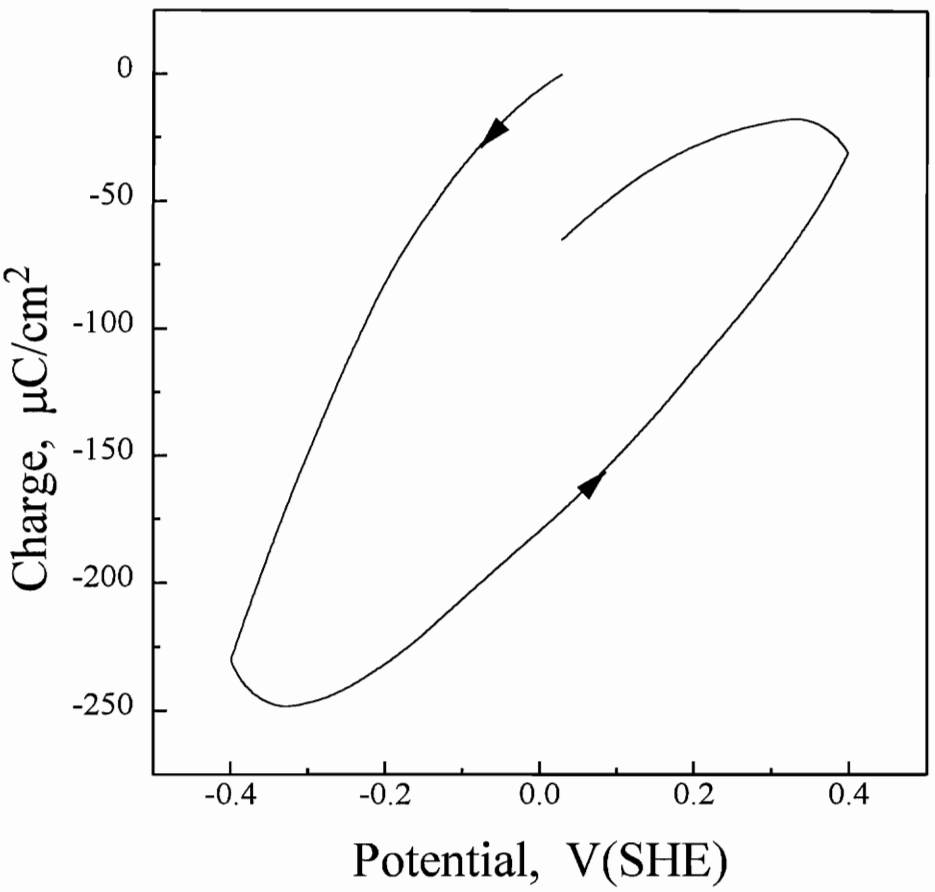

Figure 3.8. Charge-potential curve obtained by integrating the voltammetry curve shown in Figure 3.6.

voltammetry curve of Figure 3.6. Reaction 3.8 is a two electron process, and the charge passed during the cathodic sweep indicates that less than one monolayer of pyrite was reduced in the cathodic process, from 0 V to -0.4 V then to -0.3 V.

3.1.3. Photoelectrochemical Measurement

a. Photocurrent measurement on fractured electrodes

Figure 3.9 illustrates the typical transient photocurrent induced on a pyrite electrode by chopped illumination. The photocurrent transient rises and falls with the incident light intensity. The instantaneous, or fast, response of the photocurrent is of interest in this work, because this component provides information on the sign and magnitude of the band bending (Many, Goldstein and Grover, 1971). The instantaneous photocurrent on pyrite is anodic, indicating the bands are bent upwards at the surface. During the full-on period of illumination, the photocurrent decays towards zero rather rapidly. This is consistent with the observation that usually no significant photocurrents are observed with steady illumination. The decay of the photocurrent during the on-cycle of illumination and the absence of a photocurrent with steady illumination has been reported for other semiconducting electrodes and attributed to a back reaction of highly reactive photo-oxidized products such that there is no net current, the net process at the surface being electron-hole recombination (Hardee and Bard, 1966).

During the off-cycle, a photocurrent of opposite sign and smaller in magnitude is produced. This component arises from the charge and potential rearrangement that occurs at the interface when the sample is illuminated. Under illumination at a fixed

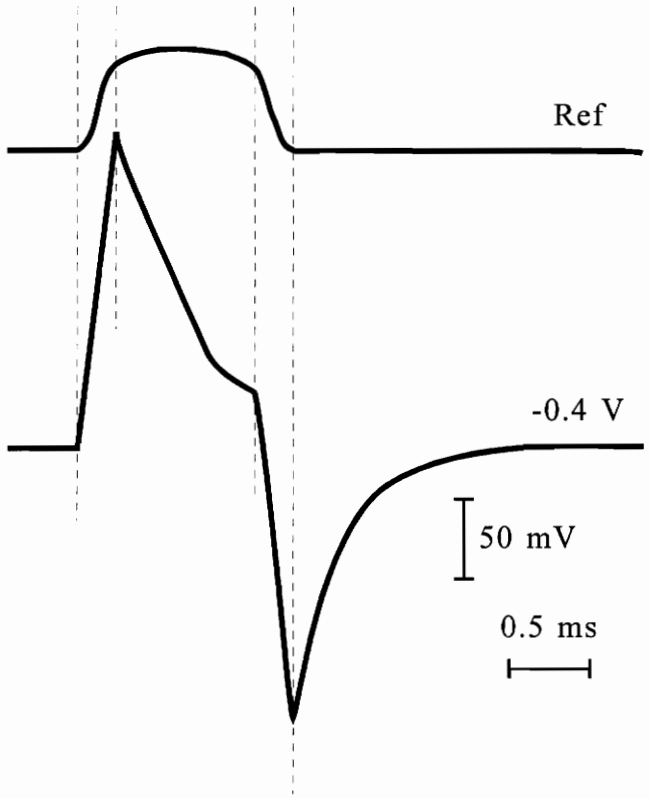

Figure 3.9. Transient photocurrent for a fractured pyrite electrode at -0.4 V during the negative-going sweep in pH 4.6 buffer solution. Top trace shows the reference signal from the CdS photoresistor placed close to the quartz window.

potential, an adjustment occurs in the potential drop across the Helmholtz layer and the space charge layer. When illumination terminates, the interface readjusts to the dark equilibrium condition which requires an opposite charge flow.

Figure 3.10 shows the voltammogram and photocurrent-potential curves of a fractured pyrite electrode for different lower potential limits at pH 4.6. The photocurrent represents the root-mean-square (rms) of the instantaneous photocurrent induced by sudden illumination, i.e., the rms of the maximum transient photocurrent, as illustrated in Figure 3.9. The signal was averaged over 300 ms. The change in the rms of the photocurrent during a potential sweep is shown in Figure 3.10. The most interesting characteristics of the curves in Figure 3.10 are:

1. over the potential range studied, only an anodic photocurrent is observed. This indicates that the bands of pyrite are bent upwards. This must be the result of a negative charge giving rise to an underlying space charge layer that is depleted in electrons and enriched in holes;

2. significant cathodic decomposition of pyrite begins at -0.6 V (Figure 3.10 (a)) and there is a close correlation between the decomposition of pyrite and the decrease in the photocurrent to zero.

The rapid increase in cathodic current at potentials negative of -0.6 V indicates the aggressive decomposition of pyrite by the reaction:

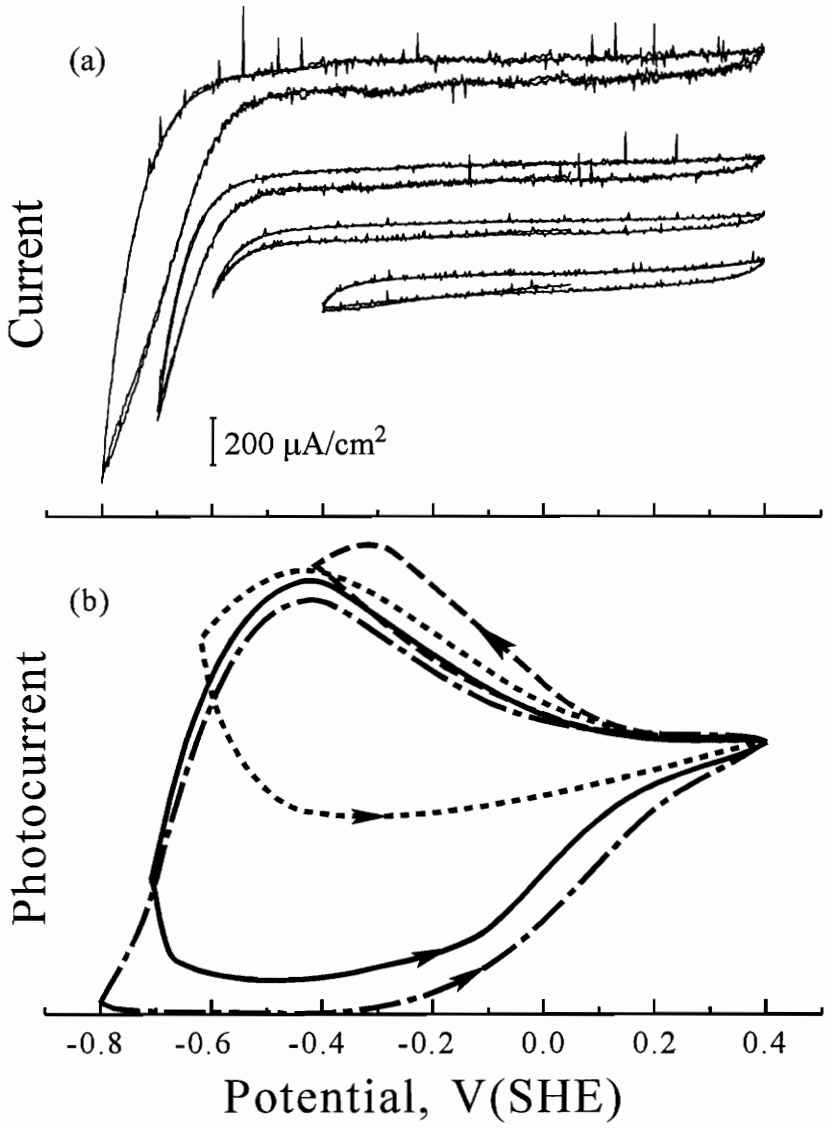

Figure 3.10. The effect of lower potential limit on the voltammetry (a) and photocurrent-potential (b) curves of a fractured pyrite electrode in pH 4.6 buffer solution, sweep rate 20 mV/sec.

$$FeS_2 + 4H^+ + 4e^- = Fe^0 + 2H_2S \qquad (3.10)$$

On the negative-going sweep, the photocurrent approaches zero when the lower potential limit is $<$-0.6 V. The necessity to cathodically decompose pyrite at potentials $<$-0.6 V to reduce the photocurrent to zero establishes that the surface of pyrite must be cathodically decomposed in order to attain the flat band potential.

No reversal in the sign of the photocurrent on pyrite has been observed, even under strong negative polarization. This indicates that this pyrite electrode is highly n-type, possibly degenerate. With strong negative potentials, the Fermi level at the surface approaches the conduction band edge at the flat band potential, and the large electron density in the conduction band prevents downward band bending and the associated cathodic photocurrent.

Figure 3.11 illustrates a typical photocurrent-potential curve obtained on a fractured pyrite surface at pH 9.2. The anodic and cathodic limits were restricted to the range of 0.15 to -0.55 V to prevent extensive oxidation or reduction in the surface region. The photocurrent is anodic in the potential range shown, again indicating that a depletion layer (upward band bending) is present on the n-type pyrite.

The most significant point concerning Figure 3.11 is that the photocurrent is nearly insensitive to changes in electrode potential, as long as the negative potential limit is more positive than the decomposition potential of pyrite. This strongly suggests that the band edges are strongly pinned over the potential range of 0.15 to -0.55 V. It will

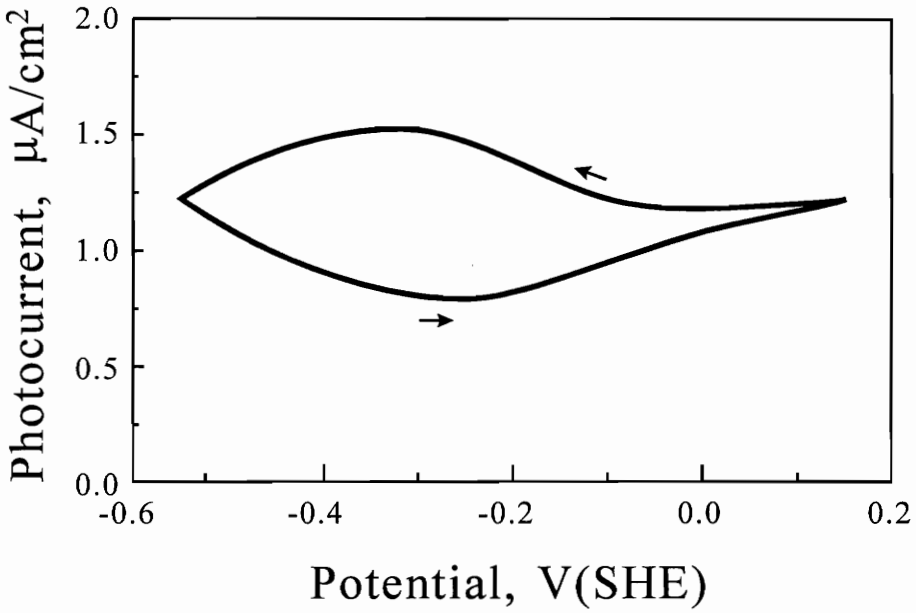

Figure 3.11. Photocurrent-potential curve for a fractured pyrite electrode in pH 9.2 buffer solution, sweep rate 20 mV/sec.

be shown in the next paragraph that the slight hysteresis in the photocurrent between the negative and positive going scans is associated with the photo-oxidation of reaction products at the surface and not with changes in band bending.

Figure 3.12 shows a voltammetry curve on a fractured pyrite electrode that had been cycled several times after fracture in order to obtain a well-defined oxidation peak at 0.12 V which represents the formation of ferric hydroxide and a well-defined cathodic peak at -0.31 V which represents the reduction of ferric- to ferrous-hydroxide (Hamilton and Woods, 1981). Similar to the behavior shown in Figures 3.10 and 3.11, there is considerable hysteresis between the positive- and negative-going sweeps. It is clear from Figure 3.12 that there is a peak in the anodic photocurrent on the negative going scan that occurs at -0.22 V and that this peak is associated with the reduction of ferric- to ferrous-hydroxide in the voltammetry curve (Figure 3.12(a)). Similar hysteresis in the photoresponse has been reported by Jaegermann and Tributsch (1983) and reflects the fact that photogenerated holes have an oxidizing power that is greater than conduction band electrons by the bandgap energy (Gerischer, 1977). During the negative going scan, $Fe(OH)_2$ is produced by the reaction,

$$Fe(OH)_3 + e^- = Fe(OH)_2 + OH^- \qquad \textbf{(3.11)}$$

which occurs *via* the conduction band and is insensitive to illumination on the n-type pyrite. The chopped light generates holes, h_{vb}^+, in the valence band that re-oxidize a portion of the $Fe(OH)_2$ by the reaction,

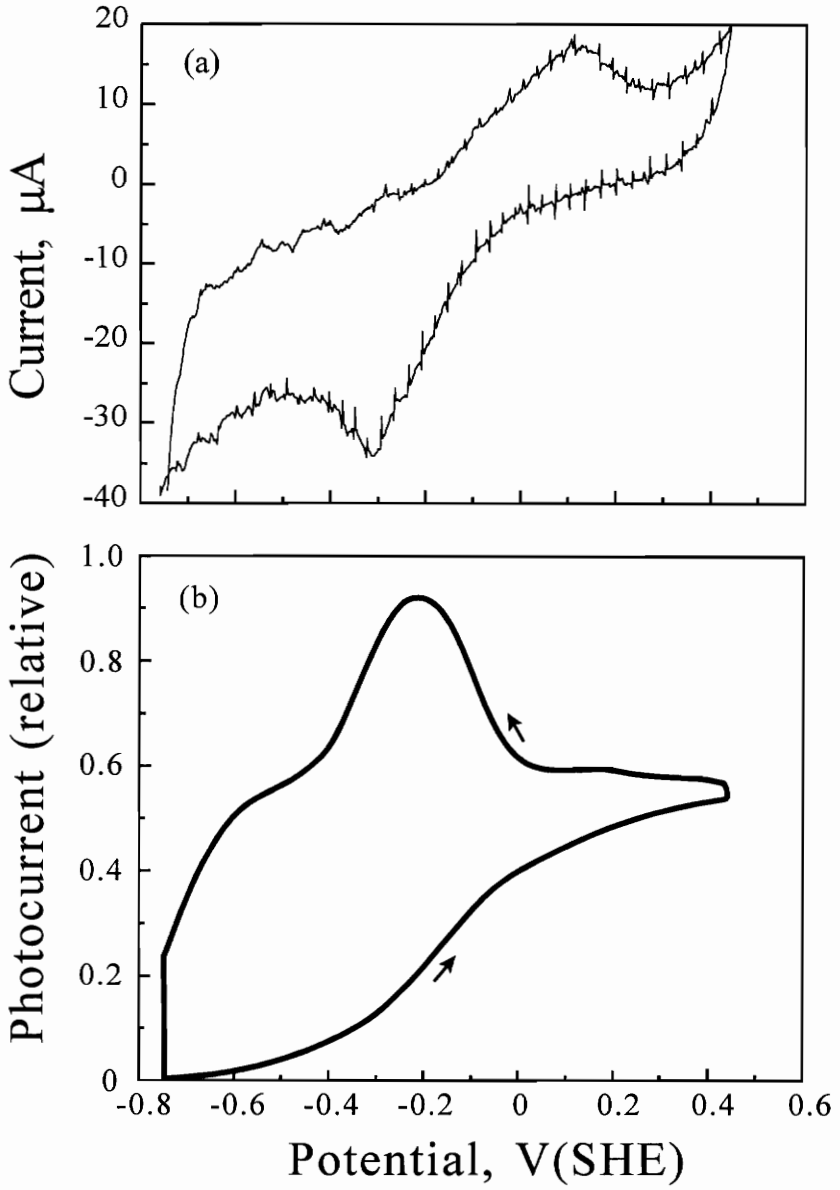

Figure 3.12. Cyclic voltammetry (a) and photocurrent-potential (b) curves for a fractured pyrite electrode after sweep several times in pH 9.2 buffer solution, sweep rate 20 mV/sec.

$$Fe(OH)_2 + h_{vb}^{+} + OH^{-} = Fe(OH)_3 \qquad \textbf{(3.12)}$$

In addition, $FeOH^{+}$ or HS^{-} may be reduction products during the negative going sweep that are produced by reactions involving conduction band electrons. The associated anodic photocurrent would then represent the re-oxidation of these species by capture of photogenerated holes from the valence band.

Figure 3.13 illustrates the photocurrent-potential curves for a fractured pyrite electrode at different pHs. In the pH range from 3.8 to 12.1, the shape of the curves do not change much. The flat band potential of pyrite shifts to lower potentials with increasing pH, but the shift is extremely small, about 0.01 V per pH unit. The fact that the apparent flat band potential (zero photocurrent) is nearly independent of pH may provide evidence that the surface species responsible for the anodic photocurrent (upward band bending) is not related to oxidation reactions of pyrite. On the negative going potential sweep in acid solution, there is one broad anodic photocurrent peak due to the photo-oxidation of the reduction products produced during the sweep. This photo-oxidation peak is independent of pH in acid solutions. In alkaline solutions, there are two distinct photo-oxidation processes that occur during the negative going potential sweep. These give rise to two peaks on the photocurrent-potential curves, as clearly illustrated at pH 7.9. The first peak is believed to be associated with the photo-oxidation of $Fe(OH)_2$ produced during the negative going sweep, the second to the photo-oxidation of HS^{-} to sulfur.

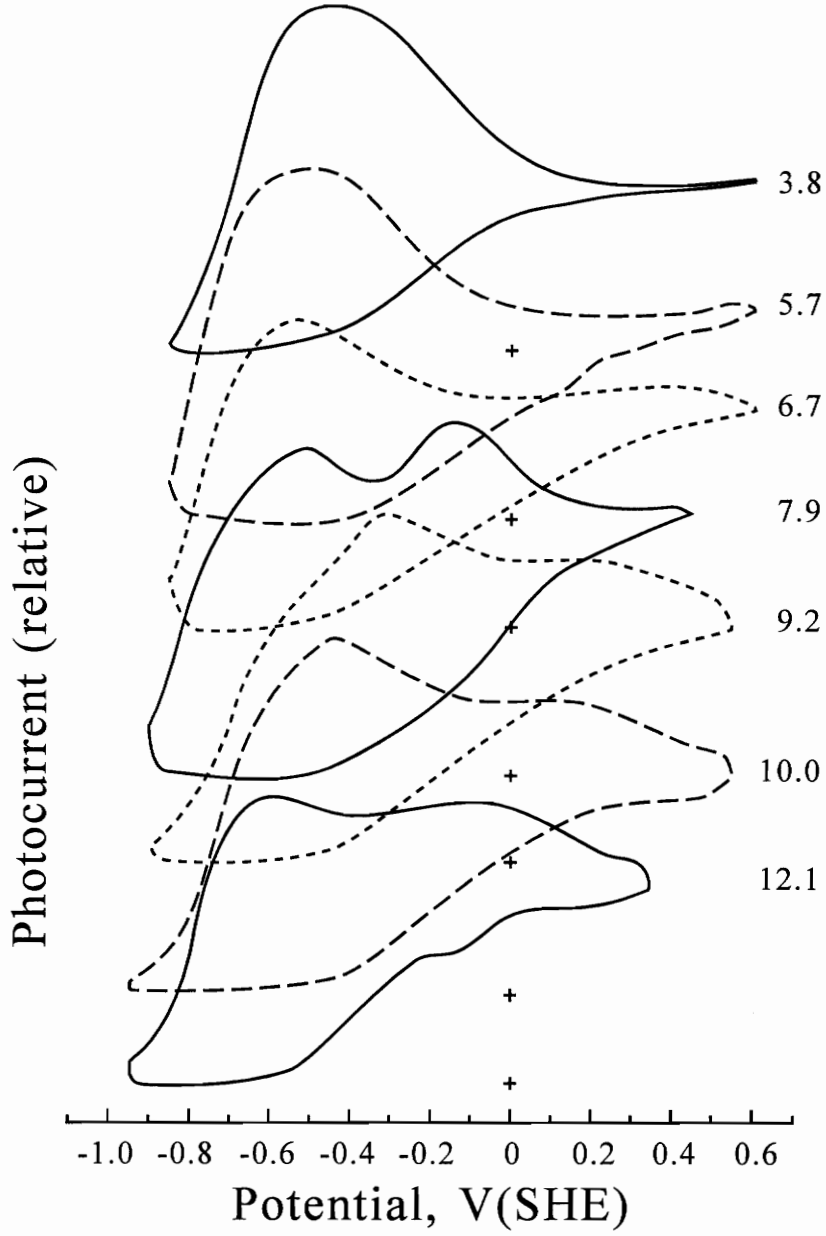

Figure 3.13. Photocurrent-potential curves for a fractured pyrite electrode at different pHs (pH values shown on the right), sweep rate 20 mV/sec.

b. Effect of Na_2S addition on photocurrent-potential measurement

In order to further investigate the relationship between the reactions that occur on pyrite surface and the photoresponse, sulfur was deposited on an electrode by oxidizing HS^- (Walker, Walters and Richardson, 1986). Figure 3.14 shows a cyclic voltammetry curve and the simultaneous photocurrent-potential curve in the presence of $3.3x10^{-3}$ M Na_2S. After adding Na_2S, the magnitude of current and photocurrent increased several times (Figure 3.14) compared to that without Na_2S. The anodic peak near 0.06 V (Figure 3.14 (a)) represents the oxidation of HS^- to S^0, and the cathodic peak at -0.65 V the reverse process (Walker, Walters and Richardson, 1986). At potentials between -0.75 and -0.2 V on the positive potential sweep, the photocurrent is similar to the behavior observed in the absence of hydrosulfide, i.e., zero photocurrent induced by cathodic dissolution of pyrite at -0.75 V and a gradual increase in photocurrent with increasing potential. However, sulfur deposition causes a sudden decrease in the photocurrent at potentials greater than -0.1 V. The decrease may be associated with either a decrease in band bending at the surface, i.e., an apparent shift in the flat band potential to more positive potentials, similar to the model proposed by Jaegermann and Tributsch (1983), and Salvador, Tafalla, Tributsch and Wetzel (1991), or to the formation of a passivating sulfur layer at the surface, which inhibits charge transfer. The decrease in current on the voltammetry curve with sulfur deposition indicates a passivated surface.

However, during the reduction cycle, there is a reduction process on the

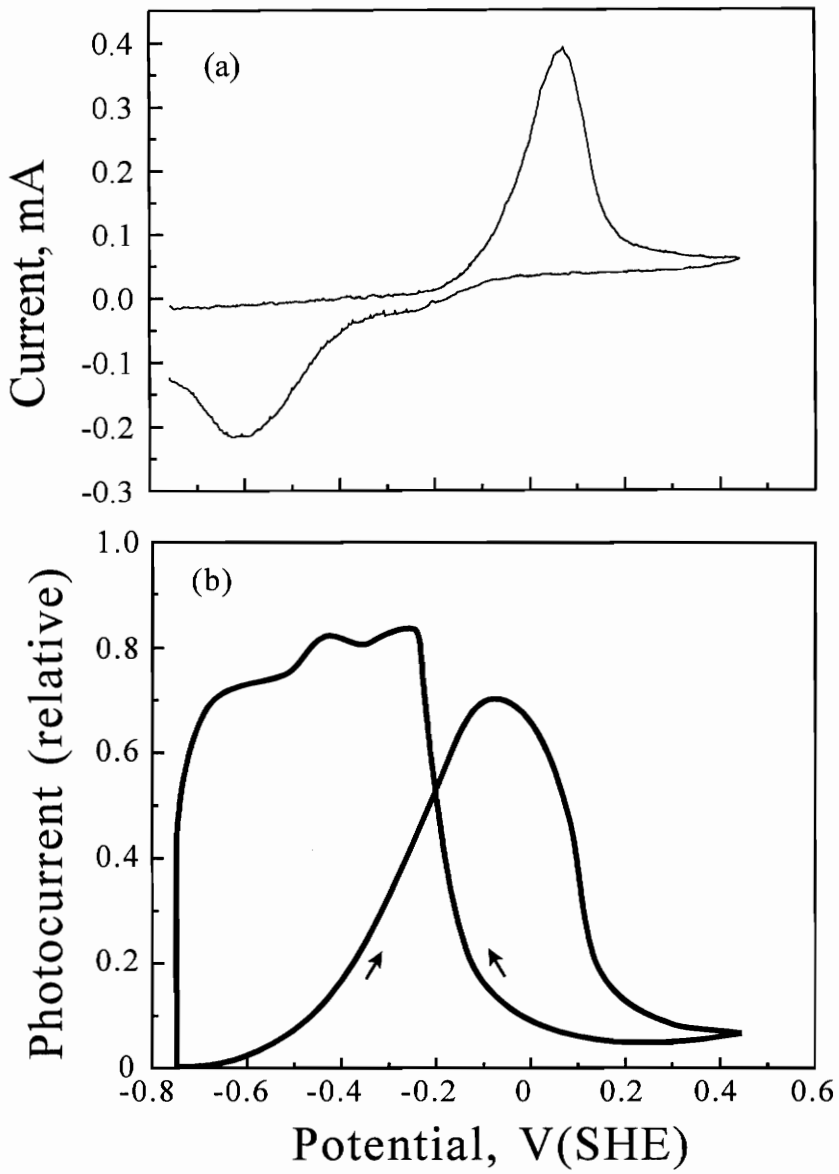

Figure 3.14. Voltammetry (a) and photocurrent-potential (b) curves of a fractured pyrite electrode in 3.3×10^{-3} M Na_2S, sweep rate 5 mV/sec.

voltammetry curve commencing at -0.1 V which precedes the reduction of the sulfur deposited on the positive scan. This may represent the reduction of an adsorbed sulfur species as a precursor to the reduction of elemental sulfur. In the absence of HS^-, $Fe(OH)_3$ is also reduced in this potential range, but its formation is not likely in the presence of HS^-. Interestingly, the photocurrent during the negative going scan rapidly increases before the dominant sulfur reduction process occurs. The overall behavior suggests that sulfur deposition neutralizes the charge on the surface of pyrite that causes upward band bending. With sufficient neutralization of the surface charge, an apparent positive shift of about 1 V occurs in the flat band potential. This is the same behavior observed by others for several different redox couples (Jaegermann and Tributsch, 1983; Mishra and Osseo-Asare, 1988a and b, 1992; Salvador, Tafalla, Tributsch and Wetzel, 1991). It should be noted that the photocurrent does not go entirely to zero with sulfur deposition. Thus the actual flat band potential is not determined. A shift to more positive values is inferred from the decrease in photocurrent.

Metal polysulfide (Yoon, Lagno, Luttrell and Mielczarski, 1991), metal deficient sulfide (Buckley and Woods, 1987), and elemental sulfur (Hamilton and Woods, 1981) have all been postulated as oxidation products that produce excess sulfur on pyrite. The neutralization of the charge on the surface by the oxidation of pyrite to produce excess sulfur at the surface may offer an explanation for the apparent shifts in the band edges of pyrite with the potential of various redox couples.

Table 3.1. Results of the photocurrent measurement on pyrite samples from different sources

Sources of pyrite samples	Photocurrent measurement
Lorgono, Spain	Anodic photocurrent
Huanzala, Peru	Anodic photocurrent, the magnitude is similar to that from Spain
Zacatecas, Mexico	Anodic photocurrent, the magnitude is 2/3 of that from Spain and Peru
Black sea area, Turkey	No photocurrent
Melissa, Illinois, USA	No photocurrent
Lake balkhash, Russia	No photocurrent
Taipai, Taiwan	No photocurrent

c. Photocurrent measurement on pyrite electrodes from different sources

Photocurrent measurements were carried out on pyrite electrodes from several sources. For the mineral pyrite samples from Lorgono, Spain and Huanzala, Peru, no difference was observed in their photocurrent-potential curves. For the pyrite samples from Zacatecas, Mexico, the photocurrent-potential curve is similar to that for the above two samples, but the magnitude is 1/3 smaller. No photocurrent was observed for pyrite samples from other sources, which include samples from Taipai, Taiwan; Black sea region, Turkey; Melissa, Illinois; and Lake balkhash, Russia. The results are listed in Table 3.1. It is believed that samples without a photoresponse may have large defect densities. This defect increases the recombination rate of electrons and holes, thereby reducing the photosensitivity.

d. Photocurrent measurement on abraded electrodes

Several *in situ* fractured electrodes were removed from the cell and wet abraded in pH 4.6 and 9.2 buffer solutions on 600 grit silicon carbide paper. Figure 3.15 shows the photocurrent of an electrode that was fractured and then abraded in pH 9.2 buffer solution (the same electrode as that in Figure 3.11). Usually, abrading a fractured surface with 600 grit SiC paper reduced the photocurrent on pyrite by a factor of 10 to 50, at equivalent light intensities. Because the photocurrents after polishing were reduced to approximately the noise level of our measuring system, no attempt was made to further quantify how Abrasion affects the reactivity of the electrodes for charge transfer processes.

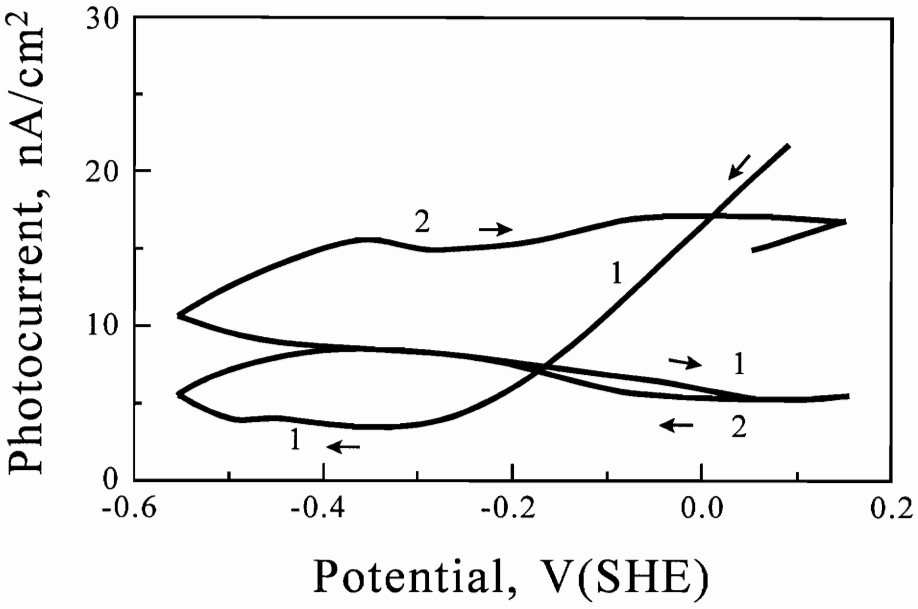

Figure 3.15. Photocurrent-potential curve in pH 9.2 buffer solution for a fractured pyrite electrode that then was wet-abraded with grit 600 silicon carbide paper (the same electrode as that in Figure 3.11), sweep rate 20 mV/sec.

The decrease in the photocurrent of the electrode is believed to be caused by the introduction of defects that greatly increase the recombination rate of electrons and holes generated by illumination. Electron/hole pairs generally recombine through defects, where a charge carrier is localized at a defect and then an oppositely charged carrier recombines through the occupied defect. The increase in recombination rate essentially lowers the steady state concentration of electrons and holes produced by illumination. Defects introduced by abrasion that are located in the space charge region may also trap charge and tend to pin the Fermi level at the surface so that the space charge layer is not readily polarized. However, the Fermi level at the surface of pyrite is already pinned by an intrinsic surface state so that no additional pinning by abrasion induced defects is evident.

Fractured surfaces are probably more similar to the surfaces produced by comminution. Most research in sulfide electrochemistry related to flotation utilizes abraded electrodes. Therefore, the effect of abrasion on adsorption and charge transfer processes at sulfide surfaces is an area that should receive some attention. Controlling the flotation of sulfide minerals often involves the adsorption of relatively small quantities of surfactants. It is the submonolayer quantities that would likely be sensitive to surface defects.

3.1.4. Impedance Measurement

Photocurrent measurements indicate that the space charge layer on pyrite is not polarizable over a wide potential range. Over this potential range, the space charge layer

is not expected to have any charge storage capacity and hence should not contribute a component to the capacitance. Thus, pyrite should behave more like a metal electrode than a semiconducting electrode because the Fermi level at the surface is pinned. It will be shown later that the pinning of the Fermi level is probably an intrinsic surface state.

Figure 3.16 shows the impedance complex plane plot for an abraded pyrite electrode after held at an oxidizing potential of 0.7 V for five minutes. The frequency increases from right to left. Two incomplete semicircles at high frequencies followed by a linear region which appears at lower frequencies are observed. The small, high frequency semicircle does not change with polarization of the electrode and is ascribed to bulk electrolyte behavior.

The larger semicircle is believed to reflect the polarization of the electrode surface and the reactions taking place. In the frequency range where this semicircle is observed, the kinetics for charge transfer processes are slower than that for the diffusion of species in the electrolyte. The charge transfer resistance can be calculated by extrapolating the semicircle so that it intercepts the Z_r axis, and taking the distance between the two Z_r axis intercepts.

At very low frequencies, the impedance plot becomes linear and have a slope of about 45°. In this frequency range, the system is under diffusion control as the kinetics of charge transfer at the electrode-electrolyte interface is much faster than the diffusion of reactants to the surface or products away from the surface. The transition frequency from charge transfer control to diffusion control decreases as the electrode potential is

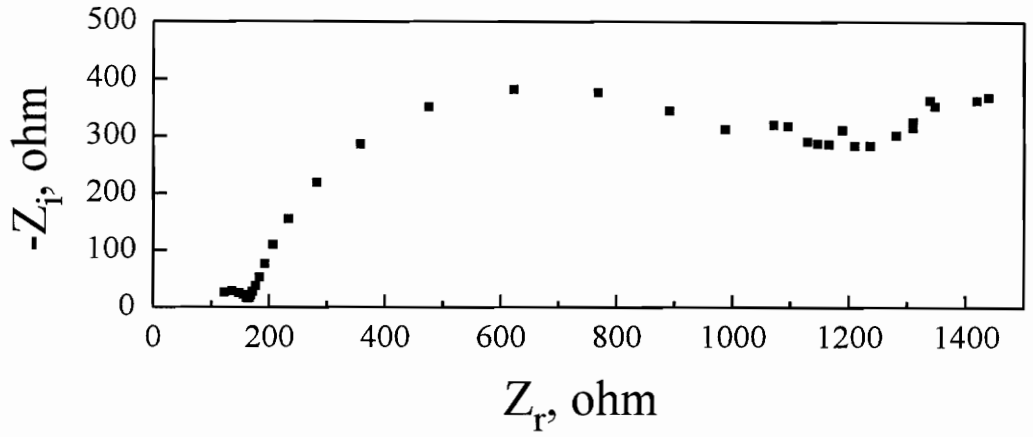

Figure 3.16. Impedance complex plane plot for an abraded pyrite electrode after holding potential at 0.7 V for 5 minutes, pH 9.2 buffer solution. The geometric area of the electrode is 0.16 cm^2.

increased.

Impedance measurements were carried out on abraded pyrite electrodes in the potential range from -1.4 V to 1.5 V(SHE). Well-defined semicircular plots (as shown in Figure 3.16) were only observed at potentials higher than 0.5 V; at lower potentials, only a linear region was observed.

Figure 3.17 shows the charge transfer resistance obtained from the impedance plots. The charge transfer resistance is about 11,300 ohm-cm^2 at 0.5 V and drops rapidly to 396 ohm-cm^2 at 0.6 V. The charge transfer resistance can be accounted for by assuming an insulating sulfur or sulfur-rich layer formed on the surface at oxidizing potentials. It is believed that at 0.5 V a relatively thick, sulfur-rich film is produced on the surface. At potentials more positive than 0.5 V, pyrite and sulfur can be oxidized to sulfate (Hamilton and Woods, 1981; Ahlberg, Forssberg and Wang 1990), causing the charge transfer resistance to decrease.

Figure 3.18 shows the plot of capacitance vs. potential. The capacitance was calculated from the impedance plots using the frequency value at the apexes of the semicircle region (Southampton Electrochemistry Group, 1985):

$$C = \frac{1}{\omega_{max} \cdot R_{ct}} = \frac{1}{2\pi f_{max} \cdot R_{ct}} \qquad (3.13)$$

where f_{max} and ω_{max} are the frequency and angular frequency values, respectively, at the maximum value of $-Z_i$ (see Figure 1.8). The average capacitance is about 35 μF/cm^2 which is larger than the magnitude expected for a space charge layer and is believed to

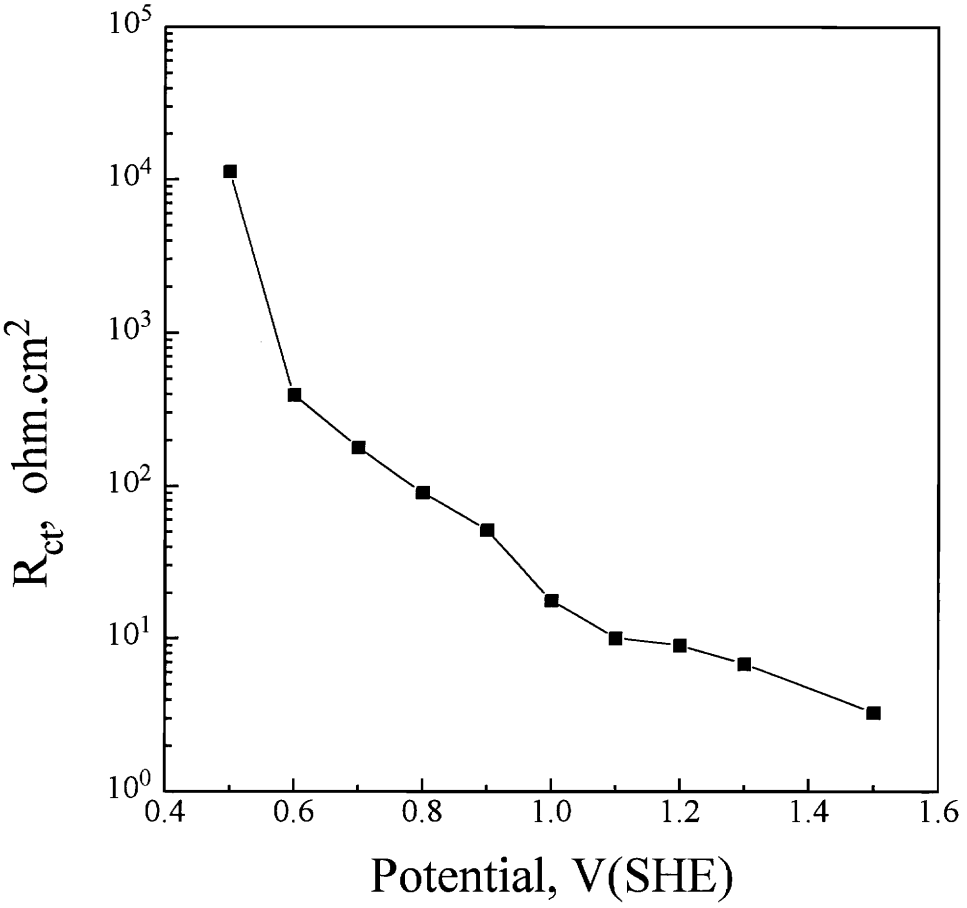

Figure 3.17. Dependence of the calculated charge transfer resistance of abraded pyrite electrode on potential. At each potential, the electrode was abraded using grit 600 carbide paper, then the electrode was held at the potential for 5 minutes before collecting impedance spectra. pH 9.2 buffer solution.

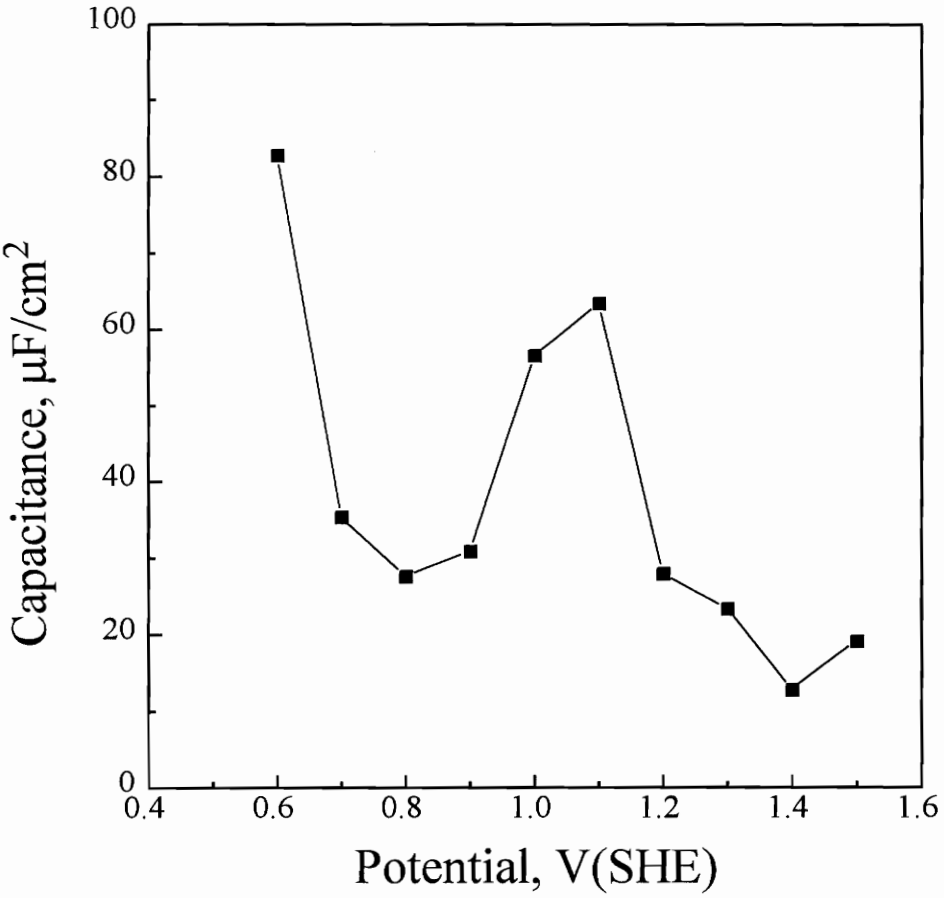

Figure 3.18. Capacitance-potential curve obtained using the data of Figure 3.17.

represent mainly the capacitance of the Helmholtz layer. This is consistent with the pining of the Fermi level indicated by photocurrent measurements. The peak at 1.1 V may be due to an adsorbed species or a surface state on pyrite.

For the complex plane impedance plot in Figure 3.16, the complete electronic equivalent circuit can be drawn as in Figure 3.19, where R_Ω is the uncompensated resistance between the working electrode (pyrite) and the reference electrode. In the present experiment, R_Ω is about 110 ohms. The small semicircle in Figure 3.16 represents solution parameters, as represented by R_s and C_s in Figure 3.19; the large semicircle the electrode parameters. R_s is about 30 ohms and C_s is about 0.13 μF. As shown previously, Figures 3.17 and 3.18 illustrate the charge transfer resistance and capacitance calculated from the large semicircle. At still lower frequencies, R_W dominates, and the reactions at the pyrite electrode are under diffusion control.

Oxygen reduction on pyrite electrodes was studied by Doo and Sohn (1989) in 0.1 M H_2SO_4 and oxygen bubbled solution using impedance spectroscopy. They found that the Warburg impedance is negligible, and that the charge transfer resistance decreased as the potential decreased in the potential range from 0.35 V to 0.15 V. This behavior indicated that the reaction mechanism shifted from a charge transfer process to a diffusion process as the potential decreased.

Overall, the impedance studies suggests that the space charge region of pyrite does not contribute to the interfacial capacitance. This result is consistent with the photocurrent measurements.

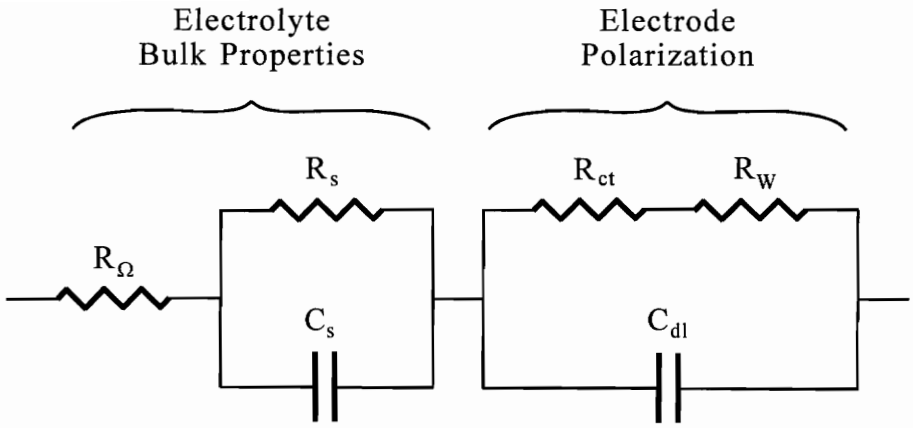

Figure 3.19. The equivalent electronic circuit for the impedance complex plane plot in Figure 3.15.

3.2. Discussion

3.2.1. Incipient Oxidation of Pyrite

Figure 3.20 shows an E_h-pH diagram for pyrite where the stable potentials obtained from Figures 3.1 and 3.2 are plotted. These points clearly lie within the thermodynamic stability domain of pyrite. The chronoamperometry technique developed in the present work is significant because it specifies not only a method of *obtaining* an unreacted pyrite surface, but also a way of *maintaining* an unreacted surface, i.e., fracture pyrite while holding its potential in the region where pyrite is thermodynamically stable. This procedure overcomes one of the usual difficulties of interpreting electrochemical measurements on sulfide electrodes due to the presence of oxidized products arising from the preparation of the electrodes, e.g., products introduced by abrasion. For pyrite, pre-oxidation leads to voltammograms that appear to be dominated by Fe^{o}/Fe^{2+} and Fe^{2+}/Fe^{3+} redox couples. The presence of these species makes it difficult to determine when pyrite itself begins to oxidize to form incipient oxidation products. The identification of the sulfur oxidation products, e.g., polysulfide, metal-deficient sulfide, or elemental sulfur, is of particular interest in flotation and the reactions leading to these products may be masked by iron containing species.

The rest potential of pyrite after exposed to air at pH 0 is 0.62 V as reported by Peters and Majima (1968). Cathodic excursions of pyrite generate a "clean" pyrite surface when the solution is bubbled with helium and the rest potential is between 0.2 and 0.3 V at pH 0, which is much more consistent with the thermodynamically estimated

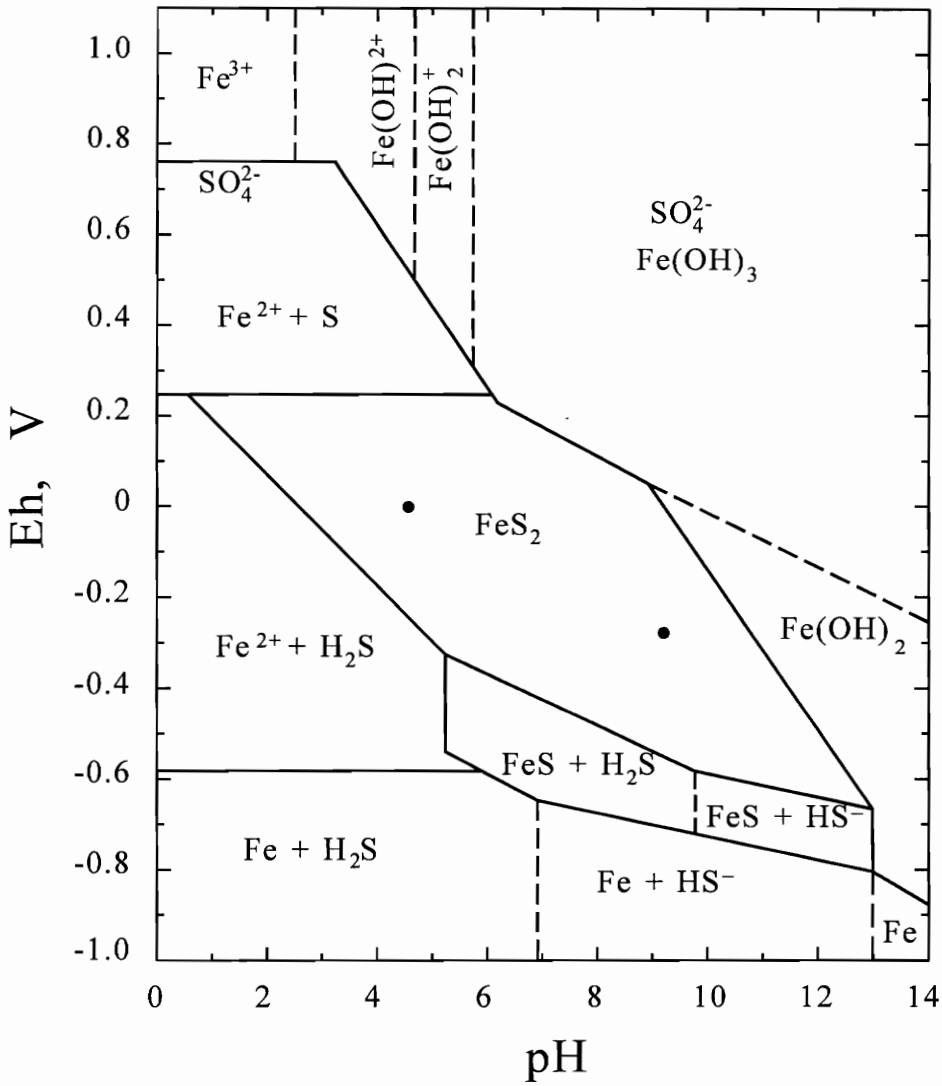

Figure 3.20. E_h-pH diagram for the pyrite-H_2O system at 25°C and for 10^{-5} M dissolved species. Solid circles at pH 4.6 and 9.2 represent the potentials where negligible oxidation and reduction currents occur on fresh surfaces produced by fracture. E_h-pH curve adapted from Kocabag, Shergold and Kelsall (1990b).

reversible potential of pyrite. The two surface states of pyrite are called, respectively, active and passive by Peters and Majima. If a linear relationship of the stable potential of freshly fractured pyrite relative to pH is assumed, the value at pH 0 should be between 0.2 and 0.3 V (Figure 3.20). It is in the same range as the rest potential of the active form. The rest potential of pyrite changes along with the composition of the pyrite surface, and the rest potential determines the oxidation/reduction behavior when pyrite is exposed to air or galvanically contacted with other conducting sulfide minerals. In the passive form, the rest potential of pyrite is higher than that of other sulfide minerals (Majima, 1969). When they are galvanically contacted, in oxygen starvation conditions, pyrite will be reduced and other sulfide minerals will be oxidized; while in the presence of oxygen, the oxidation of the other sulfide mineral will be enhanced. The stable potential of a freshly fractured pyrite or the rest potential of active pyrite is lower than the rest potential of passive pyrite. For a sulfide mineral with a rest potential between those of active and passive pyrite, it will be stabilized when contacted with active pyrite and preferentially corroded when contacted with passive pyrite.

XPS studies showed that the properties of a fractured surface of pyrite differ significantly from those of a surface prepared by grinding (Buckley and Woods, 1987). Their S(2p) spectrum for a freshly fractured surface indicated that only pyritic sulfur was present. The Fe(2p) spectrum showed no evidence of the presence of oxidized iron species in any significant quantity. The S(2p) spectrum for a ground surface was broadened and displayed additional intensity on the high binding energy side. This was

interpreted (Buckley and Woods, 1987) in terms of a shifted component arising from the presence of elemental sulfur formed in the grinding procedure. Some iron oxide was evident in the Fe(2p) spectrum from this surface and it was concluded that grinding had resulted in iron oxide and elemental sulfur. Further evidence proved that, a metal-deficient sulfide rather than elemental sulfur was present at the ground surface of pyrite (Buckley and Woods, 1987). Meyer (1979) found no apparent difference in the polarization behavior of fractured and polished surface of pyrite in 1.5 M H_2SO_4 solution.

3.2.2. Photoelectrochemical Measurement

Measurements of the transient photocurrent on pyrite electrodes show that a depletion layer forms spontaneously on freshly fractured surfaces. The characteristics of the photocurrent-potential curves indicate that the depletion layer arises from an excess of negative charge on the surface that pins the band edges at the surface.

Several characteristics of the photocurrent behavior of pyrite suggest that an intrinsic surface state dominates the interfacial behavior of pyrite. These characteristics are:

1. spontaneous anodic photocurrents on electrodes that are potentiostated, at fracture, under conditions where slight oxidation or slight reduction occurs;

2. weak dependence of the photocurrent on electrode potentials from 0.15 to -0.55 V;

3. the necessity to cathodically decompose pyrite to reach the flat band potential; and

4. the near independence of the photocurrent on pH.

This behavior is consistent with an intrinsic surface state that produces a net negative charge on the surface and an underlying depletion layer (positive space charge layer on the n-type electrodes). The charge in the surface state is not readily neutralized. To the contrary, neutralization requires cathodic decomposition of the surface region of pyrite. Thus, the Fermi energy at the surface is pinned over a wide potential range ($\approx$ -0.55 to 0.15 V), causing a quasi-metallic behavior where changes in electrode potential occur primarily across the Helmholtz layer.

The existence of an intrinsic surface state was suggested by Pettenkofer, Jaegermann, Tributsch, Kuhlenbeck, Braun and Bernstorff (1988), from photoemission studies on synthetic and natural pyrite. They observed three different sulfur states on the vacuum-cleaved (100) surface of pyrite: two attributed to FeS_2 at the surface and in the bulk; the third to an FeS-like surface state. They suggested that the FeS-like state represents a Tamm state arising from the reduced symmetry at the surface. From XPS measurements they reported that both the iron and sulfur 2p levels show chemical shifts from the S_2^{2-} in FeS_2 to S^{2-} in FeS, with Fe remaining nominally as Fe(II).

An intrinsic surface state is also consistent with studies of the photoelectrochemical behavior of pyrite with the redox couples V^{2+}/V^{3+}, Fe^{2+}/Fe^{3+}, Br^-/Br_2, and Cl^-/Cl_2 (Jaegermann and Tributsch, 1983; Salvador, Tafalla, Tributsch and Wetzel, 1991). They studied the anodic photocurrents for these redox couples and found the results were consistent with the band edges shifting with the reversible potential of

the redox couples. These shifts in the band edges with the potential of the redox couple implies that the flat band potential also shifts with the redox couple. They attributed the shifts to a high density of band gap states associated with Fe_2S_3 lattice impurities. Mishra and Osseo-Asare (1988a and b, 1992) observed similar shifts in the band edges of pyrite in acetonitrile with ferrocene and N,N,N',N'-tetramethyl-p-phenylenediamine redox couples. They also attributed the quasi-metallic behavior of pyrite, *i.e.*, pinned surface Fermi energy and large dark currents to surface states. Since Fermi level pinning was observed in the non-aqueous solution, they suggested that the surface states could not be attributed to hydrogen or hydroxyl ion adsorption.

The existence of an intrinsic surface state on pyrite surfaces can logically be assumed to be important in the flotation of pyrite and during the initial stages of the oxidation reactions that lead to acid mine drainage. This is because surface states on pyrite control how a change in interfacial potential is distributed between the Helmholtz layer and the space charge layer of pyrite. The distribution of this potential can be expected to regulate the energetics and kinetics of pyrite oxidation as well as the adsorption of reagents used in flotation.

Chapter 4. Electrochemical Studies of Galena

4.1. Experimental Results

4.1.1. Photocurrent Transients

Figure 4.1 shows typical transient photocurrents induced on a galena electrode by chopped light at several electrode potentials. The photocurrent transients rise and fall with the incident light intensity and with light-on, the transients are anodic at potentials $\geq$ 0.05 V and cathodic at potentials $\leq$ -0.05 V. The sign change in the photocurrent establishes that the apparent flat band potential, V_{fb}, is between these potentials. As shown later, the photocurrent saturates under moderately strong anodic and cathodic bias, with the saturation current at negative potentials slightly larger than that at more positive potentials. Such behavior indicates that this electrode is close to intrinsic or slightly p-type and will be referred to as slightly p-type in the text.

Galena is known (Richardson and Maust, 1976; Eadington and Prosser, 1969; Peters, 1977; Gardner and Woods, 1979) to undergo anodic and cathodic decomposition in acid electrolytes by the respective reactions:

$$PbS + 2h^{+} = Pb^{2+} + S^{0} \qquad (4.1)$$

$E_h = 0.354 + 0.0295\log[Pb^{2+}]$, and

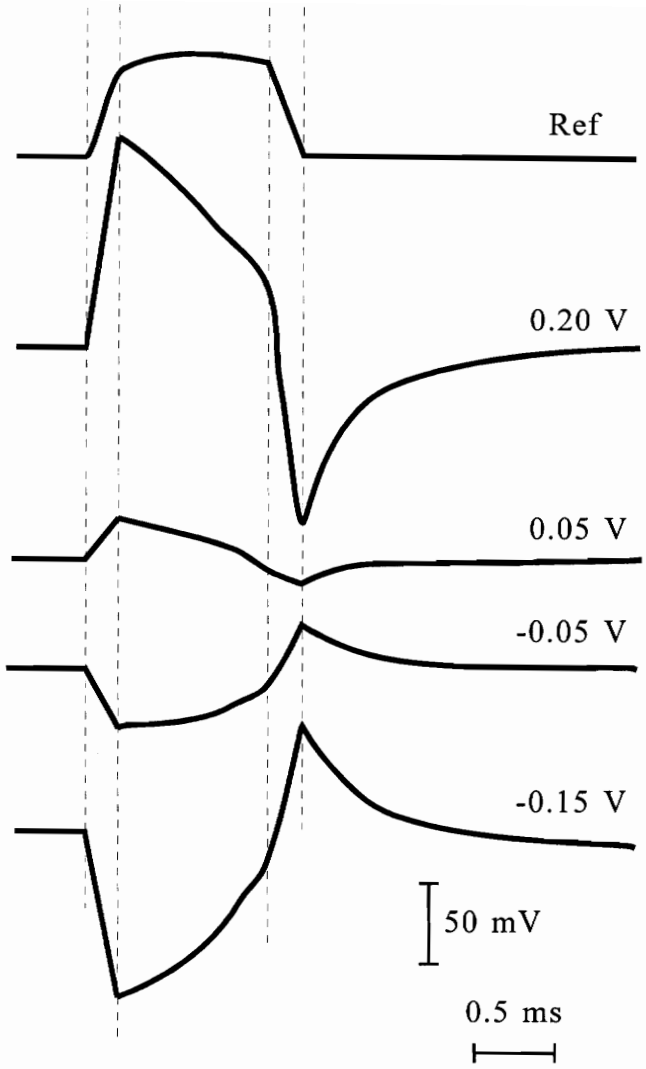

Figure 4.1. Transient photocurrents for a fractured galena electrode at several potentials in pH 4.6 buffer solution. Top trace shows the reference signal from the CdS photoresistor.

$$PbS + 2H^+ + 2e^- = Pb^0 + H_2S \quad (4.2)$$

$E_h = -0.339 - 0.0295\log[H_2S] - 0.0591pH.$

However, there is evidence that lead or sulfur atoms can be removed from a galena surface without forming separate elemental sulfur and elemental lead phases as denoted by reactions 4.1 and 4.2, respectively. Peters (1977) and Sato (1960) have shown that galena, and similar binary sulfide electrodes, can have a continuous range of potentials that is determined by the stoichiometry. Also, XPS and electrochemical studies suggest that the initial oxidation of galena at moderate overpotentials involves removal of lead ions from the mineral lattice with sulfur remaining in normal lattice sites, i.e., incongruent reaction (Buckley, Hamilton and Woods, 1985).

The shape of the voltammetry curves observed for galena electrodes within the stability potential range of the mineral as defined by reactions 4.1 and 4.2 indicates that, in addition to components due to charging of the space charge layer and electrical double layer, there is a contribution from a Faradaic process such as reaction 4.3.

$$PbS + 2xh^+ = Pb_{1-x}S + xPb^{2+} \quad (4.3)$$

The formation of H_2S can arise from removal of lead vacancies generated by reaction 4.3:

$$Pb_{1-x}S + 2xH^+ + 2xe^- = (1-x)PbS + xH_2S \quad (4.4)$$

In addition, sulfur can be removed to form sulfur vacancies:

$$PbS + 2yH^+ + 2ye^- = PbS_{1-y} + yH_2S. \quad (4.5)$$

They suggested that the relative importance of reactions 4.4 and 4.5 depend on the limits of the potential excursion and the potential at which the Pb:S ratio is exactly 1:1.

The photocurrents essentially represent a light-induced acceleration of reaction 4.3 at potentials positive of V_{fb} and reaction 4.5 at potentials negative of V_{fb}. During the full-on period of illumination, the photocurrent decays towards zero rather rapidly. This behavior is similar to that for pyrite, and is consistent with the observation that usually no significant photocurrents are observed with steady illumination. One exception where a large steady cathodic photocurrent was observed will be discussed later. The decay of the photocurrent during the on-cycle of illumination and the absence of a photocurrent with continuous light has been reported for other semiconducting electrodes and attributed to a back reaction of highly reactive photo-oxidized products such that there is no net current, the net process at the surface being electron-hole recombination (Hardee and Bard, 1966). For galena at potentials positive of V_{fb}, the decay of the photocurrent during the full-on cycle may correspond to a progressive increase in the net recombination rate during the light on-cycle. Initial illumination increases the rate of reaction 4.3, which requires two holes for each lead ion dissolved. As the concentration of lead ions at the surface decreases, the concentration of holes trapped at the surface increases, increasing the rate of recombination.

During the off-cycle, a photocurrent of opposite sign and smaller in magnitude

is produced. This component arises from the charge and potential rearrangement that occurs at the interface when the samples are illuminated. The acceleration of reactions 4.3-4.5 by light causes the electrodes to approach a new steady state condition corresponding to the illuminated condition, i.e., it is believed that the surface stoichiometry relative to the bulk of the electrode is uniquely dependent on the electrode potential and illumination conditions. Thus under illumination at a fixed potential, the surface composition of the electrode changes and this causes an adjustment in the potential drop across the Helmholtz layer and the space charge layer. When illumination terminates, the interface readjusts to the dark equilibrium condition which requires an opposite charge flow.

4.1.2. Photocurrent-Potential Scans

Figures 4.2 and 4.3 (bottom curves) show the respective photocurrent-potential curves during potentiodynamic scans for a slightly p-type electrode and a highly n-type electrode. These curves represent the root-mean-square of the peak of the photocurrent transient averaged for 300 ms.

The photocurrent-potential curve of Figure 4.2 has the classic behavior expected for a nearly intrinsic semiconducting electrode, exhibiting both anodic and cathodic photocurrents, consistent with the transient response discussed above. At negative potentials, the photocurrent is cathodic and eventually saturates with decreasing potential; at more positive potentials the photocurrent is anodic and also saturates with increasing potential. The saturation in the photocurrents with increasing negative and positive

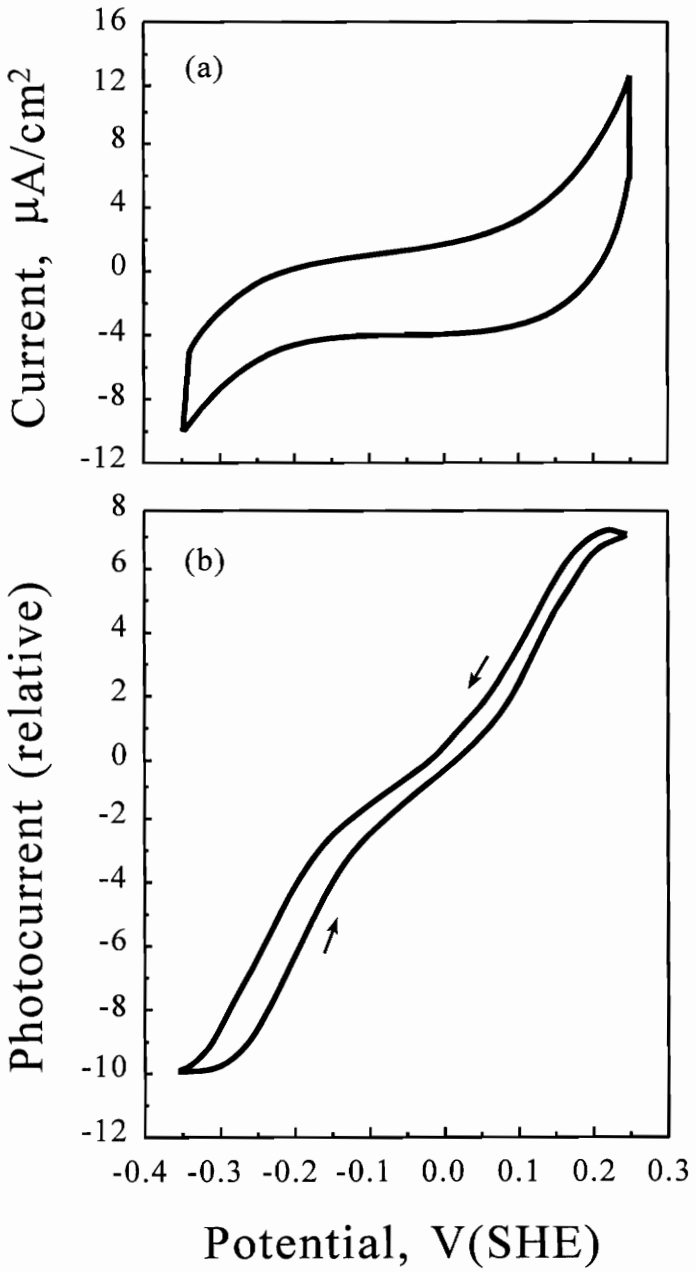

Figure 4.2. Cyclic voltammetry curve (a) and photocurrent-potential curve (b) for a fractured galena electrode of slightly p-type in pH 4.6 buffer solution (the same electrode as that in Figure 4.1). Sweep rate 10 mV/sec.

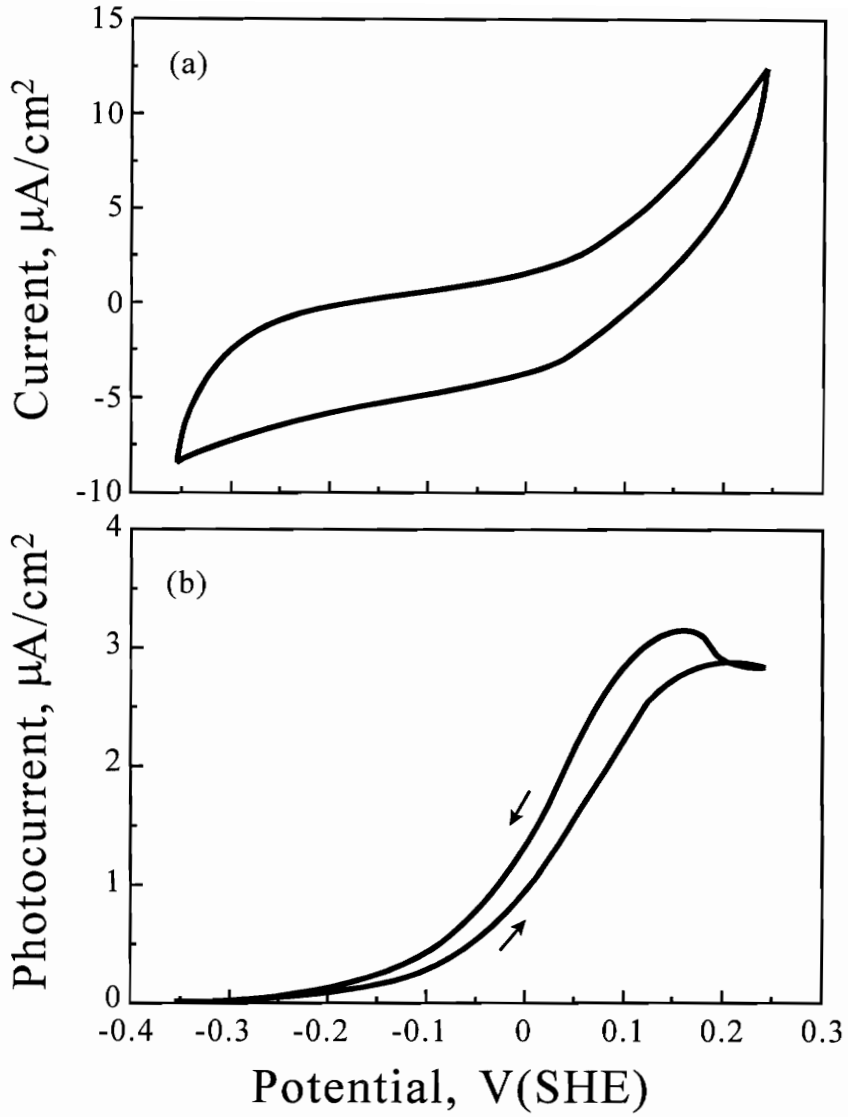

Figure 4.3. Cyclic voltammetry curve (a) and photocurrent-potential curve (b) for a fractured galena electrode of degenerate n-type in pH 4.6 buffer solution. Sweep rate 5 mV/sec.

potentials represents the Fermi level at the surface approaching and eventually becoming pinned at the band edges. With increasingly negative potentials, the Fermi level approaches and eventually merges with the conduction band edge and the surface becomes degenerate in electrons; with increasingly positive potentials, the Fermi level merges with the valence band and the surface becomes degenerate in holes. This electrode is believed to be slightly p-type because the ratio of the saturation currents under strong cathodic and anodic polarization is less than unity, i.e., $I_p(0.25\ V)/I_p(-0.35\ V) = 0.75$ (Dewald, 1960; Frankl and Ulmer, 1960; Gerischer, 1966, 1978; Hardee and Bard, 1977). The flat band potential depends slightly on the direction of polarization and is at approximately 0 V at pH 4.6. The hysteresis in the curves with scan direction decreases with decreasing sweep rate.

For the electrode of Figure 4.3, only anodic photocurrents are observed, with the photocurrent approaching zero at potentials negative of -0.2 V. The absence of a cathodic photocurrent for this electrode at potentials as low as -0.6 V (not shown), establishes that the electrode is highly n-type, probably degenerate. Thus at large negative potentials that tend to bend the bands downward (accumulation layer on the n-type electrode), the surface becomes degenerate at or very near the flat band potential, and no downward band bending occurs. The flat band potential is probably close to but negative of -0.20 V. It cannot be determined precisely because the photocurrent eventually becomes buried in noise during cathodic polarization. At potentials positive of the flat band potential, the anodic photocurrent increases with increasing positive

potential, establishing the progressive formation of a depletion layer at the surface. The photocurrent saturates at 0.2 V, i.e., as the Fermi level at the surface nears the valence band edge. The electrode under anodic polarization represents a degenerate p-type space charge layer on a highly n-type electrode. A highly n-type electrode has been polarized to 0.7 V. The photocurrent remained essentially at the saturation value during the positive scan and during the subsequent negative going scan to about 0.2 V. It then decreased as in Figure 4.3.

We have studied approximately 30 galena electrodes from the same source. Most of the samples have been highly n-type, exhibiting no cathodic photocurrent at large negative potentials. These samples are believed to be degenerate n-type. A few exhibited small cathodic photocurrents that were an order of magnitude less than the anodic saturation photocurrents. These are believed to be highly n-type, but not degenerate. Several electrodes have appeared to be nearly intrinsic or slightly p-type, with the saturation photocurrents under strong cathodic and anodic polarization about equal. Microprobe analysis of a natural crystal from this source showed no major impurities. A polished surface was analyzed in several places, with Pb:S ratios of 1.005, 1.008, 0.992 and 0.995 being obtained.

Usually, over the narrow potential range used in this work, no significant photocurrents were observed with steady illumination. However, one electrode behaved quite differently from the others, having a pronounced cathodic photocurrent under constant illumination with the 100 watt tungsten lamp (Figure 4.4). This curve was

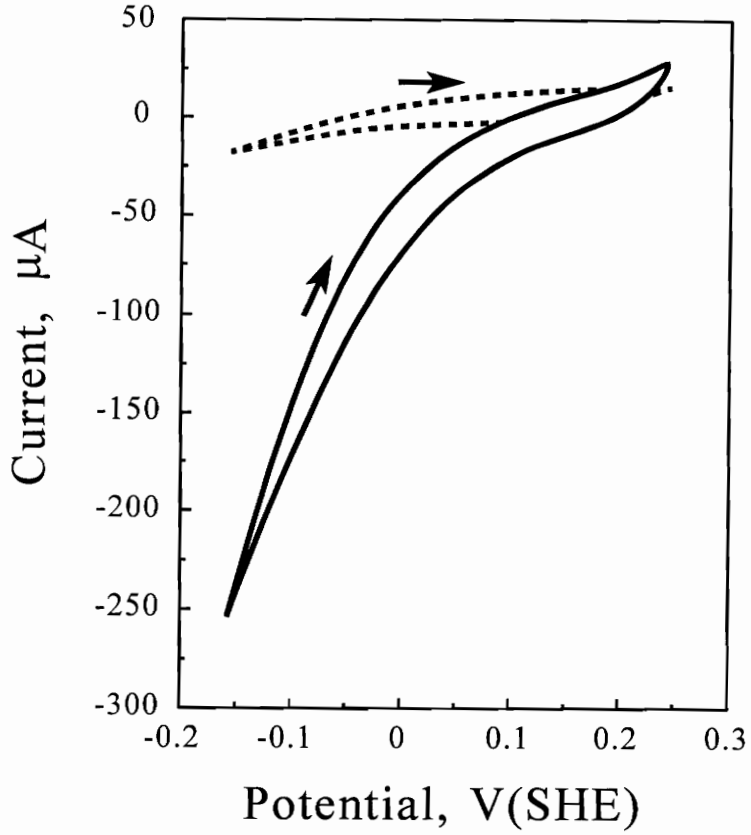

Figure 4.4. Cyclic voltammetry curves in the dark (dashed line) and with steady illumination (solid line) for an "as mounted" galena electrode before fracture in pH 4.6 buffer solution, sweep rate 10 mV/sec.

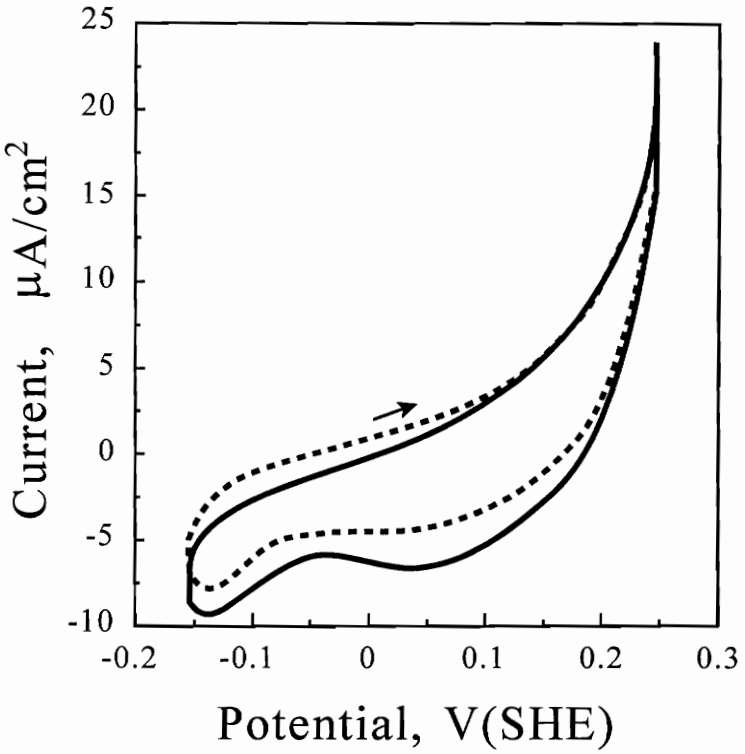

Figure 4.5. Cyclic voltammetry curves in the dark (dashed line) and with steady illumination (solid line) for the electrode of Figure 4.4 after fracture in pH 4.6 buffer solution, sweep rate 10 mV/sec.

obtained on an "as mounted" electrode, i.e., prior to cleavage so that air oxidized surfaces were exposed to the electrolyte. Figure 4.4 suggests this electrode is highly p-type, with the cathodic dissolution processes, reaction 4.2, 4.4 or 4.5 limited by the diffusion of electrons to the surface. Illumination increases the concentration of minority carriers (electrons) causing a large increase in the cathodic current. However, after cleavage, the electrode was only slightly sensitive to steady light (Figure 4.5) and the photocurrent-potential behavior with chopped illumination indicated the bulk was slightly p-type. It is believed that the outer layer of this electrode was highly p-type prior to cleavage, probably due to atmospheric oxidation. The photocurrent represents a light-induced increase in the rate of diffusion of minority carriers (conduction band electrons) to the surface which increases the rate of reaction 4.2 (Gerischer, 1966; Frankl and Ulmer, 1966; Dewald, 1960).

Figures 4.2 and 4.3 (top curves) show the voltammetry curves for the slightly p- and highly n-type electrodes. These curves were obtained simultaneously with the photocurrent-potential curves of Figures 4.2 and 4.3 respectively. Anodic decomposition, reaction 4.1, is evident for both electrodes by the increasing current at potentials above 0.10 V during the positive scan. There is corresponding evidence for cathodic decomposition on the scans at about -0.3 V for the n-type and -0.25 V for the slightly p-type electrodes. A comparison of the voltammetry curves and the photocurrent curves shows that the increases in current on the voltammograms correspond reasonably well with the onset of saturation in the photocurrent, as expected. Over the regions

where the photocurrent is changing most rapidly with electrode potential, the electrodes are nearly inactive. This indicates that major changes in electrode potential over the range of about -0.25 to 0.20 V occur primarily across the space charge layer, with a smaller change occurring in the Helmholtz layer that drives the decomposition of galena. As discussed by Gerischer (1978), when the potentials of reactions 4.1 and 4.2 are, respectively, below the valence band edge, or above the conduction band edge, decomposition by majority carriers, i.e., in the dark, is only possible by polarizing the electrodes to degeneracy. The decomposition potentials of slightly p-type and highly n-type galena are shown in Figure 4.6, where the band edges relative to the reference electrode have been located by using the flat band potential for the slightly p-type electrode of Figure 4.2, i.e., 0 V; and for the highly n-type electrode of Figure 4.3, i.e., -0.25 V. The decomposition potentials essentially represent the limits of stability of galena at pH 4.6 on a Pourbaix diagram. The reversible potential for cathodic decomposition is relatively far above the conduction band edge, consistent with observations that relatively large negative potentials must be applied to actively decompose galena by reaction 4.2, and with Figure 4.4 that shows steady illumination enhances the cathodic decomposition of p-type galena. The anodic decomposition potential is close to the valence band edge for the slightly p-type electrode. This is consistent with the fact that galena appears to readily oxidize in the dark by mixed potential corrosion reactions. It should be noted that galena has a very narrow band gap, 0.37 eV, (Scanlon, 1959), so that thermal generation of minority carriers can be

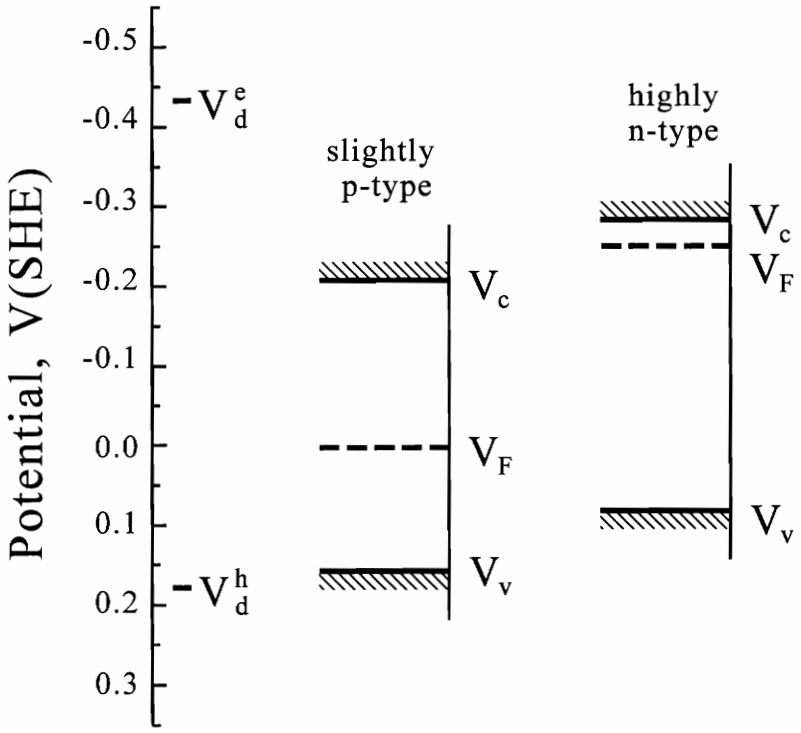

Figure 4.6. Band diagram of galena near the flat band potential on an electrode potential scale. Anodic and cathodic decomposition potentials, V_d^h and V_d^e, are indicated on the diagram, which are calculated from reactions 4.1 and 4.2, respectively.

significant and promote decomposition without degeneracy. Nevertheless, the voltammetry and photocurrent behavior of galena establishes that both the cathodic and anodic decomposition reactions are accelerated when the surface becomes degenerate in electrons and holes, respectively.

The photoelectrochemical behavior of galena is dramatically different than that of pyrite. The reason for the difference is that the space charge layer on galena is readily polarized by applied potentials, whereas the space charge layer on pyrite appears to be pinned so that it does not respond to changes in electrode potential.

4.1.3. Photoresponse of Pure Galena Surfaces

Investigations on pure galena were carried out to evaluate a mechanism recently suggested by Fletcher and Horne (1991) to explain the photoelectrochemical behavior of galena that contained minor elements. These authors recently reported photocurrent measurements on natural galena from Broken Hill, Australia at pH 9.2 and obtained results that differed from previous photovoltage measurements at pH 9.2 (Richardson and O'Dell, 1985). For their specimens of natural galena, the photocurrent was predominantly cathodic with smaller anodic photocurrents observed at the negative and positive limits of the potential excursions. This gave two zero crossings of the photocurrent. They postulated the existence of a p-type layer on the electrode as a result of the preferential migration of monovalent impurities over trivalent impurities to the surface. They suggested that n-type galena containing monovalent impurities such as Ag^+ and Cu^+ should not be considered a pure electronic conductor but a mixed ionic

and electronic conductor. The essential point of their argument was that monovalent impurities in galena migrated to the surface under the influence of the electric field in the space charge layer, causing an inversion of the electric field and converting a layer at the surface to a p-type semiconductor. They stated that "the migration of impurities is missing from the semiconductor model of Plaksin and coworkers and radically changes the interpretation of experimental data". They also stated that they could find no evidence for a lead-deficient phase in conflict with previous XPS and electrochemical studies (Buckley and Woods, 1984, 1990).

To determine whether the presence of minor elements plays a significant role in photoelectrochemical behavior, as suggested by Fletcher and Horne (1991), studies have been carried out on a synthetic lead sulfide electrode. This sample was reported to be p-type through control of the stoichiometry and 99.99% pure. Microprobe analysis of a polished surface of a fragment from this crystal revealed no impurities. The Pb:S ratios obtained from microprobe analysis indicated a 1:1 stoichiometry to within the accuracy of the probe, i.e., $\pm 0.05\%$. The synthetic galena electrode had a photocurrent-potential curve nearly identical to the slightly p-type electrode of Figure 4.2, i.e., one flat-band potential between 0.05 and -0.05 V depending on the direction of polarization, well-defined saturation photocurrents, with that under cathodic bias larger than that under anodic bias indicating a p-type electrode, and no minima and maxima in the photocurrent-potential curve. Thus, the presence of impurity elements is not important in determining the photoelectrochemical behavior of galena.

Buckley and Woods (1984) studied the oxidation of natural galena by electron spectroscopy and found the initial oxidation of galena to be incongruent in that lead oxide species were formed without any significant change in the sulfur environment being apparent. It could be argued that this behavior arises from diffusion of minor elements in the mineral to the surface to replace the lead atoms removed. Indeed, extended leaching of lead from the mineral did result in a concentration of impurities at the surface although such a process was not apparent in the initial stages of oxidation. In order to determine whether incongruent initial oxidation is a manifestation of the presence of impurity elements in the mineral lattice, the initial oxidation behavior of the pure synthetic galena was determined by XPS. The Pb(4f) and O(1s) photoelectron spectra from a fracture surface exposed to air for no more than 1 minute indicated that more oxidation had occurred than at similarly treated surfaces of natural galena examined in previous studies. Nevertheless, the corresponding S(2p) spectrum was indistinguishable from that for natural galena fractured under nitrogen, consisting of only one doublet at a $(2p)_{3/2}$ binding energy of 160.4 eV. Thus, as with natural galena containing minor elements (Buckley and Woods, 1984) despite clear evidence for oxidation of some of the lead to hydrated lead oxide, all sulfur remained as sulfide in an essentially unaltered electronic environment. After further exposure to air for periods of up to 24 h, the Pb(4f) spectra revealed the presence of a higher concentration of lead-oxygen species at the surface. The O(ls) binding energy remained predominantly at 531 eV, consistent with the oxidized species being hydrated lead oxide. As in the case of brief exposure to

air, however, the S(2p) spectra were indistinguishable from the spectrum for unoxidized galena; there was no evidence for the presence of a S(2p) doublet at a $(2p)_{3/2}$ binding energy within the range 161.5-163 eV corresponding to oligosulfide species, or near 163.5 eV which would have indicated the formation of some elemental sulfur, or for peaks at binding energies between 164 and 170 eV from sulfur-oxygen species. No impurity elements were evident from the survey spectra for any of the surfaces characterized.

4.1.4. Photoresponse of Abraded Galena Surfaces

Conventional electrochemical studies related to the flotation of galena have generally been conducted on abraded or polished surfaces. Where comparisons have been made between the behavior of abraded and cleaved surfaces, similar results have been obtained. Thus, the characteristics of voltammograms for the oxidation reactions of galena in buffer solutions (Richardson and Maust, 1976) and for the interaction of this mineral with ethyl xanthate (Richardson and O'Dell, 1985) were found to be the same for both methods of generating fresh surfaces. Furthermore, we have found no difference in the surface composition of abraded and cleaved galena using XPS. However, photoelectrochemical behavior is expected to be more sensitive to changes brought about by surface treatment than can be detected by XPS, or than is important in voltammetric investigations. For example, it is well-documented that abrasive treatments can strongly alter the electronic structure of semiconductor surfaces (Many, Goldstein and Grover, 1971).

In order to determine how abrasion influences the photoelectrochemical response of galena, several electrodes that were studied as cleaved surfaces were removed from the cell, immediately wet-abraded (pH 4.6 buffer solution) with 600 grit silicon carbide paper, and immediately re-inserted in the cell. Abrasion had a dramatic effect, not only reducing the magnitude of the photocurrents, but causing considerable structure and sign changes to appear in the photocurrent-potential curves. Figure 4.7 shows a photocurrent-potential curve obtained after abrading the surface of the highly n-type electrode used to obtain the data in Figure 4.3. After abrasion, the photocurrent is predominantly cathodic and similar to the shape obtained by Fletcher and Horne (1991), although displaying greater hysteresis. However, during the scans large shifts in the phase angle between the maximum in the photocurrent and the chopper reference signal occurred that indicated the transient response of the electrodes to light changed with abrasion. Figure 4.8 shows oscilloscope traces of the photocurrent at several electrode potentials for the abraded electrode. Comparison of these curves with those of Figure 4.1 shows that the transient photocurrent on abraded electrodes is composed of at least two separate components. The first is an anodic photocurrent, in phase with the incident light intensity, that is only observed at high positive potentials. This anodic component of the photocurrent "appears" to decay rapidly once the incident light reaches full intensity. The second process gives rise to a cathodic photocurrent. The cathodic component is slower than the anodic component and gives rise to a maximum that is delayed with respect to the incident light intensity, except at the more negative potentials, explaining the phase shifts

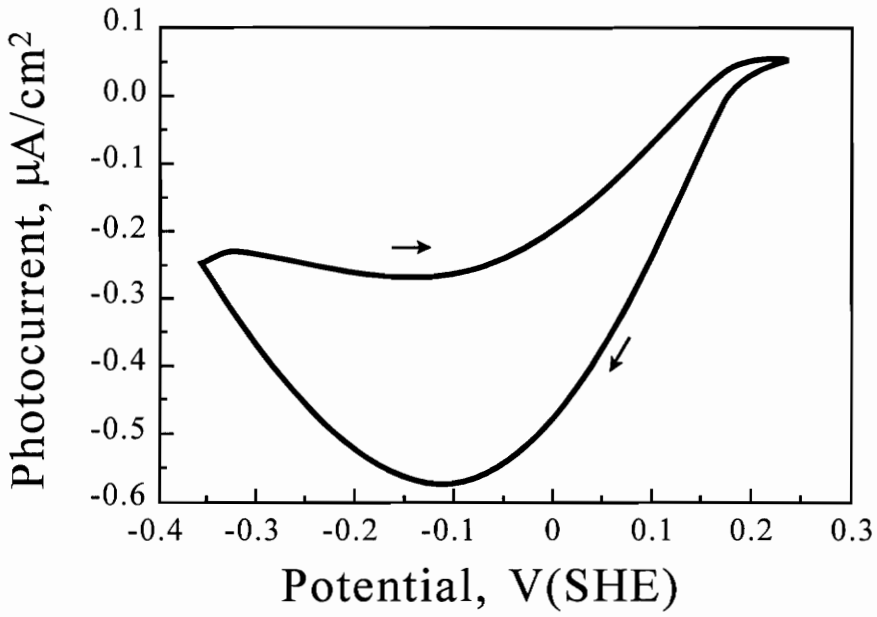

Figure 4.7. Photocurrent-potential curve for an abraded galena electrode of degenerate n-type (the same electrode as that in Figure 4.3) in pH 4.6 buffer solution. Sweep rate 5 mV/sec.

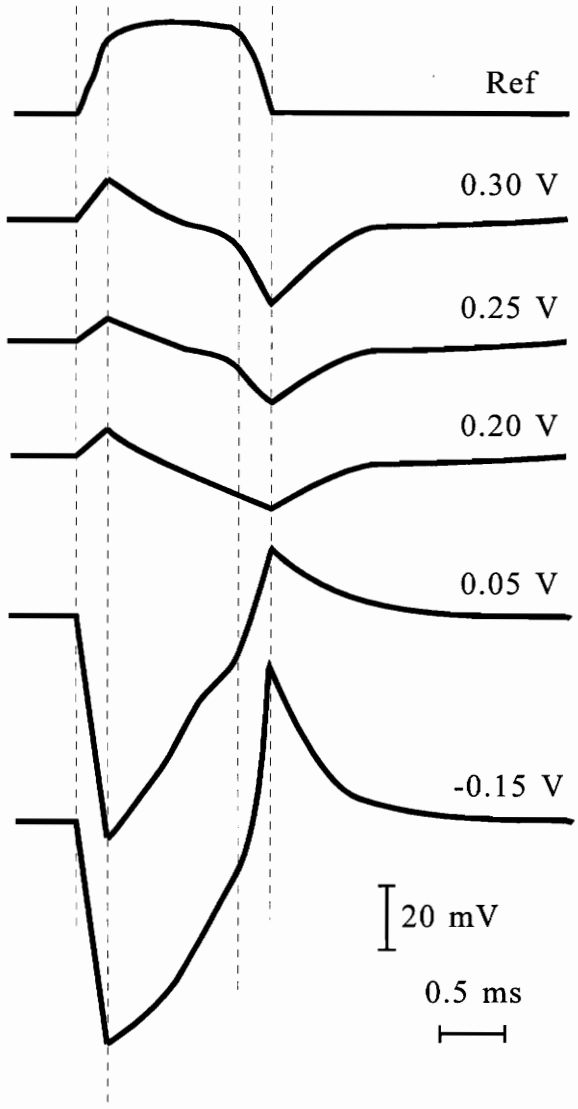

Figure 4.8. Transient photocurrents of an abraded galena electrode (the same electrode as that in Figure 4.7) in pH 4.6 buffer solution. Top trace shows the reference signal from CdS photoresistor.

observed during the potential scans. It was also observed that the exact shape and zero crossings of the photocurrent-potential curves depended on the potential at which the phase and amplitudes of the lock-in amplifier were adjusted, as expected from an examination of Figure 4.8.

The transient photocurrents on abraded surfaces are complex and not yet understood. It is suggested that the intense local heating in the presence of oxygen alters the surface to produce a p-type layer. Oxygen is a well-known reagent for increasing the p-type conductivity of lead sulfide to make it more sensitive as an IR detector (Scanlon, 1959). It is believed oxygen is incorporated in the lattice during abrasion, converting the surface to p-type. The p-type layer is believed to be much thicker than the width of the space charge layer and is expected to have a large defect density. Lattice defects in lead sulfide are known to act as recombination centers (Scanlon, 1957), greatly reducing the lifetimes of photogenerated electrons and holes, accounting for the decreased photosensitivity of the abraded electrodes. Lattice defects in the space charge region may also store charge, thus pinning the Fermi level at the surface. The space charge layer of abraded surfaces is thus expected to be more difficult to polarize than that of cleaved surfaces.

The existence of two components to the photocurrent also makes it difficult to determine the flat band potential. The two components may arise from the existence of two diffuse space charge regions on abraded surfaces, the first associated with the usual space charge layer just beneath the surface; the second with the n-p, or p- to more -p

junction that delineates the damaged abraded region (more p-type) from the underlying bulk (more n-type). The electric fields in both of these regions influence the migration of photogenerated carriers to the surface, and different migration times may be responsible for the two temporally separate processes.

The behavior of the p-type synthetic lead sulfide after abrading the surface is essentially the same as the natural crystals, i.e. primarily cathodic photocurrents. Also, studies on abraded, slighty p-type surfaces (not shown) gave results similar to those observed in Figures 4.7 and 4.8, i.e., the photocurrents were primarily cathodic at all potentials whereas before abrasion only anodic photocurrents were observed. It is clear that abrasion drastically changes the electronic structure at the surface of galena electrodes. It can be concluded that it is the alteration of the surface caused by the abrasion process that changes galena from n-type to more p-type in the surface region, and not the migration of monovalent impurities to the surface as proposed by Fletcher and Horne (1991).

4.1.5. Flat-Band Potential vs. pH

It is of interest to determine the effect of pH on the flat band potential of galena. Figure 4.9 shows the results. The flat band potentials were determined by averaging the flat band potentials on the negative going and the positive going sweeps. It can be observed that the flat band potential decreases with the increase of solution pH for this galena electrode. It is believed that two processes are involved from pH 3 to pH 11, one process occurs below pH 4.6 and has a slope of 0.176; the other process above pH 4.6

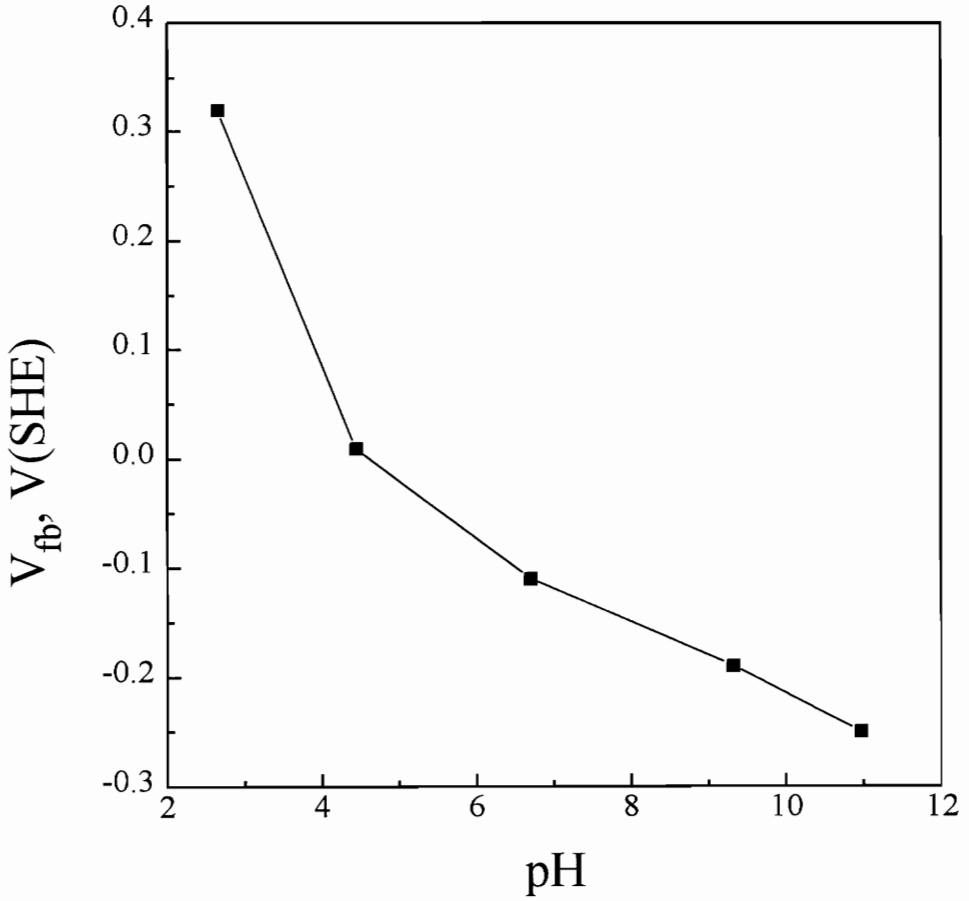

Figure 4.9. Flat band potential change with solution pH for a galena electrode (the same electrode as that in Figure 4.2), pH 4.6 buffer solution, sweep rate 10 mV/sec.

with a slope of 0.038. According to reaction 4.1, at acidic solutions, the decomposition of galena is pH independent. In neutral and alkaline solution, PbO and S^0 are formed on the surface of galena:

$$PbS + H_2O = PbO + S^0 + 2H^+ + 2e^- \quad (4.6)$$

For this reaction, the slope should be 0.0591 V per pH unit.

For most semiconductors, it has been observed that the flat band potential is dependent on pH (Crundwell, 1988), a shift of 0.0591 V per pH unit being recorded, due to the adsorption of H^+ or OH^-. Ginley and Butler (1978) found a similar dependence of the flat band potential of CdS electrode on pH, and concluded that the HS^- and H^+ ions were the potential determining species. It is apparent that, in the case of Figure 4.9, H^+ and OH^- are not the only charge determining ions for galena.

4.2. DISCUSSION

The observation that the initial oxidation reaction at fracture surfaces of the pure synthetic (p-type) galena is similar to that at fresh surfaces of natural (n-type) galena indicates that the incongruent nature of this reaction is not a result of the presence of impurity elements in the mineral lattice or of a particular imbalance in stoichiometry. In each case, the sulfur atoms are not directly involved in the initial oxidation of the surface, and the electronic environment of the sulfur atoms near a slightly oxidized surface remains essentially the same as that for the sulfur atoms at an unoxidized surface.

The fact that such an incongruent reaction might result in a stoichiometry in the near surface region that lies outside the range observed for stable bulk phases should not be a cause for concern, as the near-surface region of the lattice should be regarded as a surface phase rendered metastable by the presence of oxygen, or the lead-oxygen species, at the solid/air interface or by underlying PbS lattice. On the other hand the *rate* of the initial oxidation reaction may well be influenced by the initial carrier type or impurities; the initial oxidation rate appeared to be significantly greater at fracture surfaces of the synthetic galena than at natural galena surfaces, although subsequent oxidation over a 24 h period did not occur more rapidly than for the natural mineral.

The finite slopes of the voltammetry curves (double layer charging currents should give nearly zero slopes), and the behavior of the photocurrent-potential curves can be accounted for by assuming that the oxidation and reduction of galena over the nearly inactive region are continuous functions of electrode potential, as expressed by reactions 4.3-4.5. As mentioned previously, these reactions are consistent with observations that binary electrodes can have a continuous range of electrode potentials that is determined by their stoichiometry (Peters, 1977; Sato, 1960). They also substantiate previous XPS studies on natural galena and the present XPS investigations on pure galena that show the lattice environment of sulfur is not substantially changed by moderate oxidation that leaches lead from the surface or forms a lead oxide overlayer.

It is known that lead and sulfur vacancies in the PbS lattice are produced by deviations in stoichiometry (Scanlon, 1959). In the pure, nonstoichiometric crystal, an

excess of metal atoms produces an n-type semiconductor; an excess of sulfur atoms produces a p-type semiconductor. It is also generally assumed that the ratio of charge carriers to vacancies is unity. Extending this argument to the surface of galena, reactions 4.3 and 4.5 imply that lead vacancies are created by oxidation and sulfur vacancies by reduction. It is assumed that they represent precursor processes that eventually lead to reactions 4.1 and 4.2 in which second solid phases are formed on the electrode. It should be noted that in the case of reaction 4.1, the second phase may be a metal polysulfide PbS_n (Yoon, Lagno, Luttrell and Mielczarski, 1991).

The importance of vacancies produced at the surface as a result of reduction or oxidation lies in their influence on the interfacial charge. It is generally assumed that two holes can become localized at lead vacancies produced by reaction 4.3 to form a neutral acceptor level, V_{Pb}^{++}

$$V_{Pb} + 2h_{vb}^{+} = V_{Pb}^{++} \qquad \textbf{(4.7)}$$

that can become ionized to form a deep negatively charged acceptor level, V_{pb}^{+}

$$V_{Pb}^{++} = V_{Pb}^{+} + h_{vb}^{+} \qquad \textbf{(4.8)}$$

Similarly, sulfur vacancies produced by reaction 4.5 can trap two electrons to form a neutral shallow donor level, V_S^{--}

$$V_S + 2e_{cb}^{-} = V_S^{--} \qquad \textbf{(4.9)}$$

that can become ionized to form a deep positively charged donor level, V_S^{-}

$$V_S^{--} = V_S^{-} + e_{cb}^{-} \qquad \textbf{(4.10)}$$

Previous studies established (Richardson and O'Dell, 1985) that *in situ* cleaved galena assumes the flat band potential at the instant of cleavage, and thus the cleavage potentials increase with decreasing (increasing) electron (hole) concentrations. The assumption of the flat band potential establishes that there is no net surface charge at cleavage that is compensated by the space charge layer of galena. This implies that no rapid adsorption of charged species (hydrogen or hydroxyl ions) occurs and that there are no occupied intrinsic surface states. It also implies that the vacancy (and impurity) concentrations are uniform from the bulk to the surface. The potential assumed at the instant of cleavage represents the difference in the Fermi energy between the galena and the reference electrode. This difference in potential occurs solely across the Helmholtz layer. This explains previous observations and the present results that V_{fb} increases as the bulk carrier density changes from n- to p-type as clearly shown in Figures 4.2 and 4.3. With subsequent oxidation, which occurs spontaneously on fresh cleavage surfaces when dissolved oxygen is present, lead is removed from the surface, creating an excess concentration of lead vacancies at the surface which act as acceptor-like surface states, which may be singly or doubly ionized. The upward band bending represents the underlying positive space charge layer that compensates the excess negative charge localized on lead vacancies.

Reduction of galena reverses this process. If the electrode has been previously

oxidized to form lead vacancies, reduction may remove excess sulfur. Since it is known that lead and sulfur vacancies can exist simultaneously, the reduction process may be viewed as either compensating, or annihilating, lead vacancies that exist in excess in the surface region. If the reduction process involves sulfur that is adjacent to an existing lead vacancy, the process is probably close to annihilation, whereas if sulfur reduction occurs at sites removed from a lead vacancy, a compensating, positively charged, donor is created. Eventually, negative polarization produces an excess of sulfur vacancies at the surface and a net positive surface charge that causes downward band bending. Of course, on the highly n-type electrode, the Fermi level becomes pinned at the conduction band edge and downward band bending does not occur.

Previous studies (Richardson and O'Dell, 1985) and the present work establish that galena electrodes assume the flat band potential at the instant of cleavage, and V_{fb} increases as the bulk carrier density changes from n- to p-type as clearly shown in Figures 4.2 and 4.3. With subsequent oxidation, which occurs spontaneously on fresh cleavage surfaces when dissolved oxygen is present, lead is removed from the surface, creating an excess concentration of lead vacancies at the surface which act as acceptor like surface states, which may be singly or doubly ionized. The upward band bending represents the underlying positive space charge layer that compensates the excess negative charge localized on lead vacancies.

Reduction of galena reverses this process. If the electrode has been previously oxidized to form lead vacancies, reduction may remove excess sulfur. Since it is known

that lead and sulfur vacancies can exist simultaneously, the reduction process may be viewed as either compensating, or annihilating, lead vacancies that exist in excess in the surface region. If the reduction process involves sulfur that is adjacent to an existing lead vacancy, the process is probably close to annihilation, whereas if sulfur reduction occurs at sites removed from a lead vacancy, a compensating, positively charged, donor is created. Eventually, negative polarization produces an excess of sulfur vacancies at the surface and a net positive charge that causes downward band bending. Of course, on the highly n-type electrode, the Fermi level becomes pinned at the conduction band edge and downward band bending does not occur.

Chapter 5. Summary and Conclusions

This research was undertaken to obtain a better understanding of the initial oxidation of pyrite and to determine if the solid state properties of pyrite influence its oxidation behavior. The oxidation of pyrite is industrially important due to the fact that most base metal and precious metal mines and many coal mines contain pyrite. When pyrite is oxidized, it leads to the production of acid waters. Acid mine drainage from past mining practices has caused, and continues to cause, significant environmental damages. It was the aim of this research to better understand pyrite oxidation so that better predictive testing methods can be developed to evaluate waste from new mining operations with regard to their potential to generate acid water. Better models to predict the potential of mine waste to generate acid water would help assure that future mining operations can minimize the acid mine drainage problem.

A new method to prepare fresh, i.e., unoxidized, pyrite surfaces for study was developed as a part of this work. This method employed *in situ* fracture where pyrite electrodes were fractured under an electrolyte. It was found that:

1. a unique potential exists at which freshly fractured pyrite undergoes neither oxidation nor reduction. This is referred to as the "stable" potential of pyrite and is pH dependent;
2. the initial oxidation of freshly fractured pyrite starting from the

"stable" potential occurs about 200 mV more negative than the potentials reported in the literature for pyrite oxidation;

3. the abraded pyrite electrodes usually used for electrochemical studies have an oxidation layer ($Fe(OH)_3$, Fe_2O_3, etc.) on the surface that appears to dominate the electrochemical behavior. In fact, in voltammetry, the oxidation of $Fe(OH)_2$ to $Fe(OH)_3$ on abraded electrodes masks the initial oxidation of pyrite.

Photoelectrochemical and impedance studies were used to determine if the solid state properties of pyrite are important in its electrochemical behavior. The photoelectrochemical studies on pyrite samples from Huanzala, Peru and Lorgono, Spain showed that:

1. spontaneous anodic photocurrents are present on electrodes that are potentiostated, at fracture, under conditions where only slight oxidation or slight reduction occurs. The anodic photocurrents establish that the energy bands of pyrite are bent upward corresponding to a depletion layer on n-type pyrite;

2. no cathodic photocurrents are observed on pyrite even under strong cathodic polarization, indicating the pyrite electrodes were all highly n-type;

3. it is necessary to cathodically decompose pyrite to reach the flat band potential.

The characteristics of the photocurrent-potential curves indicate that the depletion layer arises from an excess of negative charge trapped in an intrinsic, acceptor-like surface state on the fractured pyrite surface. The positive depletion layer forms just beneath the surface to compensate the negative charge in surface state.

Studies of pyrite samples from several different sources established that significant differences occur in their photoresponse. Samples from Peru (Huanzala), Spain (Lorgono), and Mexico (Zacatecas) exhibit relatively large photocurrents. The photocurrents were always anodic, approaching zero at strong negative potentials. No cathodic photocurrents were observed even under strong cathodic polarization, consistent with the conclusion that all of the natural samples were highly n-type.

Pyrite samples from Taiwan (Taipai), Turkey (Black sea region), Illinois (Melissa), and Russia (Lake balkhash) exhibited no photocurrents. The absence of photosensitivity indicates that these samples contain high concentrations of recombination centers. The rapid recombination of photo-generated electrons and holes in these samples essentially reduced the photocurrents to values that could not be detected.

Impedance studies supported the photocurrent measurements in that impedance does not appear to reflect the space charge layer, i.e., the bands are pinned so that pyrite is metallic-like. It appears that at high potentials (>0.5 V), a high resistance layer is formed. The high resistance is believed due to the formation of an elemental sulfur or sulfur-rich layer on the surface.

Studies were also conducted on natural galena electrodes. Galena is a well-known

semiconducting electrode and the major purpose of these studies was to compare its behavior with that of pyrite. It was found that, in contrast to pyrite, galena has a space charge layer that is easily polarizable. It was also found that the semiconducting types were different for galena electrodes from the same source. They vary from highly n-type to slightly p-type.

Prior to this study, most electrochemical studies on sulfide minerals have been conducted on surfaces that had been abraded or polished. It has been shown in this work that abrading or polishing both pyrite and galena has a dramatic effect on their electronic structure. On pyrite, abrasion reduces the photocurrent by over an order of magnitude. On galena, abrasion also reduces the magnitude of the photocurrent, but most importantly, abrasion converts the surface of n-type galena to p-type.

The work reported in this thesis represents, to the author's best knowledge, the first systematic attempt to correlate the oxidation of pyrite with its solid state properties for the purpose of better understanding acid water production in pyritic mine waste. This work required the development of a new technique, *in situ* fracture, to produce fresh pyrite surfaces so that the very initial stages of pyrite oxidation could be studied. It also required the application of a technique, photocurrent measurement, that has not been previously employed to study pyrite oxidation and acid mine drainage.

The major accomplishment of this study has been to show that these techniques of preparing fresh surfaces and characterizing the semiconducting properties can be applied to pyrite and the information obtained can be used to better understand pyrite

oxidation. With respect to pyrite oxidation, it is significant that fresh surfaces oxidize at potentials about 200 mV more negative than reported in the literature for the oxidation of abraded electrodes. It is also significant that this work shows a negative charge layer forms spontaneously on pyrite when a fresh surface is produced.

Pyrite samples from seven different sources were used in this work. Unfortunately, none of these appeared to be p-type. Those from three sources were highly n-type and those from the other four sources had such large densities of recombination centers that the semiconducting type could not be determined by photocurrent measurements. For this reason, a definitive conclusion as to how the semiconducting properties of pyrite affect its initial oxidation will require further studies. In particular, studies are required on p-type electrodes to compare with the present studies on n-type electrodes. The work described in this thesis provides the techniques and base line data for these further studies.

Chapter 6. Recommendations for Future Work

Further work must be done to fully characterize the semiconducting properties of pyrite from a wide variety of sources. Although some of the pyrites used in this study were not very photosensitive, the use of a higher intensity light source and measurement at faster time may increase the photoresponse of these pyrite samples. This requires obtaining pyrite samples of different semiconducting types, and more research is needed to relate the initial oxidation rate to semiconducting type.

Pyrite is photoactive with visible light, and therefore its oxidation may be sensitive to sunlight, as suggested by Jaegermann and Tributsch (1983). The photocorrosion of pyrite in the environment may be another factor in AMD.

References

Adamson, A.W., 1990, *Physical Chemistry of Surfaces*, Fifth Edition, John Wiley & Sons.

Ahlberg, E., Forssberg, K.S.E., and Wang, X., 1990, "The Surface oxidation of pyrite in alkaline solution," *Journal of Applied Electrochemistry*, **20**, 1033-1039.

Ahmed, S.M., and Giziewicz, E., 1992, "Electrochemical studies of iron sulphides in relation to their atmospheric oxidation and prevention of acid drainage; Part-II," In: Woods, R., and Richardson, P.E., eds., *Proceedings of the Third International Symposium on Electrochemistry in Mineral and Metal Processing III*, Proceedings Volume 92-17, The Electrochemical Society, Inc., Pennington, NJ, 372-390.

Bailey, L.K., and Peters, E., 1976, "Decomposition of pyrite in acids by pressure leaching and anodization: The case for an electrochemical mechanism," *Canadian Metallurgical Quarterly*, **15**, 333-344.

Ball, B. and Richard, R.S., 1976, "Chemistry of pyrite flotation and depression," In: Fuerstenau, M.C., ed., *Flotation*, A.M. Gaudin Memorial Volume, AIME, New York, N.Y., 458-483.

Bard, A.J., and Faulkner, L.R., 1980, *Electrochemical Methods--Fundamentals and Applications*, Johnson Wiley & Sons.

Biegler, T., Rand, D.A.J., and Woods, R., 1975, "Oxygen reduction on sulphide minerals. Part I. Kinetics and mechanism at rotated pyrite electrodes," *Journal of Electroanalytical Chemistry*, **60**, 151-162.

Biegler, T., 1976, "Oxygen reduction on sulphide minerals. Part II. Relation between activity and semiconducting properties of pyrite electrodes," *Journal of Electroanalytical Chemistry*, **70**, 265-275.

Biegler, T., and Swift, D.A., 1979, "Anodic behavior of pyrite in acid solutions," *Electrochimica Acta*, **24**, 415-420.

Bockris, J.O'M., and Reddy, A.K.N., 1970, *Modern Electrochemistry*, Volume 2,

Plenum Press, New York.

Briceno, A. and Chander, S., 1988, "An electrochemical characterization of pyrites from coal and ore sources," *International Journal of Mineral Processing*, **24**:73-80.

Buckley, A.N., Hamilton, I.C. and Woods, R., 1985, "Investigation of the surface oxidation of sulfide minerals by linear potential sweep voltammetry and x-ray photoelectron spectroscopy," In: Forssberg, K.S.E., ed., *Flotation of Sulfide Minerals*, Elsevier, 41-60.

Buckley, A.N., and Riley, K.W., 1991, "Self-induced floatability of sulphide minerals: Examination of recent evidence for elemental sulphur as the hydrophobic entity." *Surface and Interface Analysis*, **17**, 655-659.

Buckley A.N., and Woods, R., 1984, "An X-ray photoelectron spectroscopic study of the oxidation of galena," *Applications of Surface Science*, **17**, 401-414.

Buckley, A.N., and Woods, R., 1987, "The surface oxidation of pyrite," *Applied Surface Science*, **27**, 437-452.

Buckley, A.N., and Woods, R., 1990, "X-ray photoelectron spectroscopic and electrochemical studies of the interaction of xanthate with galena in relation to the mechanism proposed by Page and Hazell," *International Journal of Mineral Processing*, **28**, 301-311.

Byerly, D.W., 1990, "Guidelines for handling excavated acid-producing materials," Department of Transportation, Federal Highway Administration, Document: DOT-FHWA-FL-90-007, Sept. 1990.

Chander, S., Briceno, A., and Pang, J., 1992, "On the mechanism of sulfur oxidation in pyrite," *Society for Mining, Metallurgy, and Exploration, Inc., preprint # 92-240*, 1-15.

Chmielewski, T., and Wheelock, T.D., 1990, "Some electrochemical aspects of pyrite hydrophobicity--Investigation on cleaved electrodes," *Journal of Mining & Metallurgy (Glasnik Rudarstva I Metalurgije)*, **26**, 133-144.

Crundwell, F.K., 1988, "The Influence of the electronic structure of solids on the anodic dissolution and leaching of semiconducting sulphide minerals," *Hydrometallurgy*, **21**, 155-190.

Dewald, J.F., 1960, "Semiconductor electrodes," In: Hannay, N.B., ed., *Semiconductors*, Rheinhold, New York, 727-752.

Doo, S.G., and Sohn, H.J., 1989, "Electrochemical reduction of oxygen on a pyrite surface," *Minerals & Metallurgical Processing*, November 1989, 201-205.

Doyle, F.M., 1990, "Acid mine drainage from sulphide ore deposits." In: Gray, P.M.J., Bowyer, Castle, J.F., Vaughan, D.J. and Warner, N.A., eds., *Sulphide Deposits-Their Origin and Processing*, The Institute of Mining and Metallurgy, 301-310.

Doyle, F.M., and Mirza, A.H., 1990, "Understanding the mechanisms and kinetics of acid and heavy metals release from pyritic wastes," In: Doyle, F.M., ed., *Proceedings of the Western Regional Symposium on Mining and Mineral Processing Wastes*, Society of the Mining Engineers, Littleton, Colorado, 43-51.

Eadington, P. and Prosser, A.P., 1969, "Oxidation of lead sulphide in aqueous suspensions," *Transactions of the Institution of Mining and Metallurgy, Section C: Mineral Processing and Extractive Metallurgy*, 78, 74-82.

Eadington, P., 1973, "Leaching of illuminated lead sulphide with nitric acid as a function of the solid-state electronic properties," *Transactions of the Institution of Mining and Metallurgy, Section C: Mineral Processing and Extractive Metallurgy*, 82, 158-161.

Ennaoui, A., Fiechter, S., Goslowsky, H., and Tributsch, H., 1985, "Photoactive synthetic polycrystalline pyrite (FeS_2)," *Journal of the Electrochemical Society*, **132**, 1579-1582.

Ennaoui, A., Fiechter, S., Jaegermann, W., and Tributsch, H., 1986, "Photoelectrochemistry of highly quantum efficient single-crystalline n-FeS_2 (pyrite)," *Journal of the Electrochemical Society*, **133**, 97-106.

Ennaoui, A., and Tributsch, H., 1984, "Iron sulphide solar cells," *Solar Cells*, **13**, 197-200.

Esposito, M.C., Chander, S., and Aplan, F.F., 1987, "Characterization of pyrite from coal sources," In: Vassiliou, A.H., ed., *Process Metallurgy, VII*, TMS/AIME, 475-493.

Everett, P.K., 1982, In: Osseo-Asare, K. and Miller, J.D., eds., *Hydrometallurgy Research, Development and Plant Practice*, AIME, Warrendale, PA, 165.

Ferreira, R.C., 1975, "High-temperature E-pH diagrams for the systems S-H_2O, Cu-S-

H_2O and Fe-S-H_2O" In: Burkin, A.R., ed., *Leaching and Reduction in Hydrometallurgy*, The Institution of Mining and Metallurgy, 67-83.

Finkelstein, N.P., Allison, S.A., Lovell, V.M., and Stewart, B.V., 1975, "Natural and induced hydrophobicity in sulfide mineral systems," In: Somasundaran, P., and Grieves, R.B., eds., *Advances in Interfacial Phenomena of Particulate/Solution/Gas Systems; Application to Flotation Research, AIChE Symposium Series, Volume 71, Number 150*, 165-175.

Finklea, H.O., 1988, "Semiconductor Electrode Concepts and Technology," In: Finklea, H.O., ed., *Semiconductor Electrodes*, Elsevier, 1-42.

Fletcher, S., and Horne, M.D., 1991, "Some photoelectrochemical insights into galena flotation," *International Journal of Mineral Processing*, **33**, 145-163.

Frankl, D.R., and Ulmer, E.A., 1966, "Theory of the small-signal photovoltage at semiconductor surfaces," *Surface Science*, **6**, 115-123.

Gardner, J.R., and Woods, R., 1979, "A study of the surface oxidation of galena using cyclic voltammetry," *Journal of Electroanalytical Chemistry*, **100**, 447-459.

Gerischer, H., 1966, "Electrochemical behavior of semiconductors under illumination," *Journal of the Electrochemical Society*, **113**, 1174-1182.

Gerischer, H., 1978, "Electrolytic decomposition and photodecomposition of compound semiconductors in contact with electrolytes," *Journal of Vacuum Science and Technology* **15**, 1422-1428.

Ginley, D.S., and Butler, M.A., 1978, "Flatband potential of cadmium sulfide (CdS) photoanodes and its dependence on surface ion effects," *Journal of the Electrochemical Society*, **125**, 1968-1974.

Grandke, T., and Cardona, M., 1980, "Electronic properties of clean and oxygen covered (100) cleaved surfaces of PbS," *Surface Science*, **92**, 385-392.

Guarnaschelli, C., 1970, "Adsorption of xanthate on illuminated lead and zinc sulfides," *Transactions of the Society of Mining Engineers, AIME*, **247**, 324-329.

Hamilton, I.C., and Woods, R., 1981, "An investigation of surface oxidation of pyrite and pyrrhotite by linear potential sweep voltammetry," *Journal of Electroanalytical Chemistry*, **118**, 327-343.

Hardee, K.L., and Bard, A.J., 1977, "Semiconductor electrodes X. Photoelectrochemical behavior of several polycrystalline metal oxide electrodes in aqueous solutions," *Journal of the Electrochemical Society*, **124**, 215-223.

Jaegermann, W., and Tributsch, H., 1983, "Photoelectrochemical reactions of FeS_2 (pyrite) with H_2O and reducing agents," *Journal of Applied Electrochemistry*, **13**, 743-750.

Janetski, N.D., Woodburn, S.I., and Woods, R., 1977, "An electrochemical investigation of pyrite flotation and depression," *International Journal of Mineral Processing*, **4**, 227-239.

Kittel, C., 1968, *Introduction to Solid State Physics*, third edition, John Wiley & Sons, Inc., New York.

Kocabag, D., Kelsall, G.H., and Shergold, H.L., 1990a, "Natural oleophilicity /hydrophobicity of sulphide minerals, I. Galena," *International Journal of Mineral Processing*, **29**, 195-210.

Kocabag, D., Kelsall, G.H., and Shergold, H.L., 1990b, "Natural oleophilicity /hydrophobicity of sulphide minerals, II. Pyrite," *International Journal of Mineral Processing*, **29**, 211-219.

Leppinen, J.O., and Basilio, C.I., and Yoon, R.H., 1988, "Spectroelectrochemical study of ethyl xanthate adsorption on sulfide minerals," In: Richardson, P.E., and Woods, R., eds., *Proceedings of the Third International Symposium on Electrochemistry in Mineral and Metal Processing II*, Proceedings Volume 88-21, The Electrochemical Society, Inc., Pennington, NJ, 49-65.

Li, J., and Wadsworth, M.E., 1993, "Raman spectroscopy of electrochemically oxidized pyrite and optimum conditions for sulfur formation," In: Hiskey, J.B., and Warren, G.W., eds., *Hydrometallurgy Fundamentals, Technology and Innovations*, Society for Mining, Metallurgy, and Exploration, Inc., Littleton, Colorado, 127-141.

Liu, C., Pettenkofer, C., and Tributsch, H., 1988, "Enhancement of photoactivity in pyrite (FeS_2) interfaces by photoelectrochemical processes," *Surface Science*, **204**, 537-554.

Luttrell, G.H., and Yoon, R.H., 1984a, "The collectorless flotation of chalcopyrite ores using sodium sulfide," *International Journal of Mineral Processing*, **13**, 271-283.

Luttrell, G.H., and Yoon, R.H., 1984b, "Surface studies of the collectorless flotation of chalcopyrite," *Colloids and Surfaces*, **12**, 239-254.

Luttrell, G.H., and Yoon, R.H., 1992. In: Proceedings of the Coal Preparation '92 Conference, May 3-7, Cincinnati, Ohio.

Majima, H., 1969, "How Oxidation affects selective flotation of complex sulphide ores," *Canadian Metallurgical Quarterly*, **8**, 269-273.

Manocha, A.S., and Park, R.L., 1977, "Flotation related ESCA studies on PbS surfaces," *Applications of Surface Science*, **1**, 129-141.

Many, A. Goldstein, Y., and Grover, N.B., 1971, *Semiconductor surfaces*, chapter 9, Elsevier, New York.

Meyer, R.E., 1979, "Electrochemistry of FeS_2," *Journal of Electroanalytical Chemistry*, **101**, 59-71.

Meyers, R.A., 1977, *Coal Desulfurization*, Marcel Dekker, New York.

Mishra, K.K., and Osseo-Asare, K., 1988a, "Electrodeposition of H^+ on oxide layers at pyrite (FeS_2) surfaces," *Journal of the Electrochemical Society*, **135**, 1898-1901.

Mishra, K.K., and Osseo-Asare, K., 1988b, "Aspects of the interfacial electrochemistry of semiconductor pyrite (FeS_2)," *Journal of the Electrochemical Society*, **135**, 2502-2509.

Mishra, K.K., and Osseo-Asare, K., 1992, "Fermi level pinning at pyrite (FeS_2)/electrolyte junctions," *Journal of the Electrochemical Society*, **139**, 749-752

Mycroft, J.R., Bancroft, G.L., McIntyre, N.S., Lorimer, J.W., and Hill, I.R., 1990, "Detection of sulphur and polysulphides on electrochemically oxidized pyrite surfaces by X-ray photoelectron spectroscopy and Raman spectroscopy," *Journal of Electroanalytical Chemistry*, **292**, 139-152.

Paul, R.L., Nicol, M.J., Diggle, J.W., and Saunders, 1978a, "The Electrochemical behavior of galena (Lead sulphide)--I. Anodic dissolution," *Electrochimica Acta*, **23**, 625-633.

Paul, R.L., Nicol, M.J., Diggle, J.W., and Saunders, 1978b, "The Electrochemical behavior of galena (Lead sulphide)--II. Cathodic reduction," *Electrochimica Acta*, **23**, 635-639.

Peters, E., 1977, "Electrochemistry of sulfide minerals," In: Bockris, J.,O'M, Rand, D.A.J., and Welsch, B.J., eds., *Trends in Electrochemistry*, Plenum Press, New York, NY, 267-290,

Peters, E., and Majima, H., 1968, "Electrochemical reactions of pyrite in acid perchlorate solutions," *Canadian Metallurgical Quarterly*, **7**, 111-117.

Pettenkofer, C., Jaegermann, W., Tributsch, H., Kuhlenbeck, H., Braun, W. and Bernstorff, W., 1988, "Surface core level shifts on cleaved FeS_2 (100) surfaces," 249-251.

Plaksin, I.N., and Shafeev, R. Sh., 1960, "The influence of certain semiconducting properties of the surface on the reaction between xanthate and galenite," *Proceedings, Physical Chemistry Section*, **132**, 421-423.

Pritzker, M.D., and Yoon, R.H., 1988, "A voltammetric study of galena immersed in acetate solution at pH 4.6," *Journal of Applied Electrochemistry*, **18**, 323-332.

Ramprakash, Y., Koch, D.F.A., Woods, R., 1991, "The Interaction of iron species with pyrite surfaces," *Journal of Applied Electrochemistry*, **21**, 531-536.

Redon, A.M., Vigneron, J., Heindl, R., Sella, C., Martin, C., and Dalbera, 1981, "Differences in the optical and photoelectrochemical behaviors of single-crystal and amorphous ferric oxide," *Solar Cells*, **3**, 179-186.

Richardson, P.E., and Edelstein, D.L., 1978, "The Effect of the space charge layer of galena on the kinetics of the oxygen reduction reaction," In: Richardson, P.E., Hyde, G.R., and Ojalvo, M.S., eds., *The Physical Chemistry of Mineral-Reagent Interactions in Sulfide Flotation*, U.S. Department of the Interior, Bureau of Mines, Information Circular 8818, 72-99.

Richardson, P.E., Li, Y.Q., and Yoon, R.H., 1992, "The photoelectrochemistry of *in-situ* fractured pyrite electrodes," In: Woods, R., and Richardson, P.E., eds., *Proceedings of the Third International Symposium on Electrochemistry in Mineral and Metal Processing III*, Proceedings Volume 92-17, The Electrochemical Society, Inc., Pennington, NJ, 342-353.

Richardson, P.E., and Maust, E.E., Jr., 1976, "Surface stoichiometry of galena in aqueous electrolytes and its effect on xanthate interactions," In: Fuerstenau, M.C., ed., *Flotation, A.M. Gaudin Memorial Volume*, 364-392.

Richardson, P.E., and O'Dell, C.S., 1985, "Semiconducting characteristics of galena electrodes--Relation to mineral flotation," *Journal of the Electrochemical Society*, **132**, 1350-1356.

Richardson, P.E., Yoon, R.H., Woods, R., and Buckley, A.N., 1994, "The photoelectrochemistry of galena," **International Journal of Mineral Processing**, (to be published).

Salvador, P., Tafalla, D., Tributsch, H., and Wetzel, H., 1991, "Reaction mechanism at the n-FeS_2/I interface," *Journal of the Electrochemical Society*, **138**, 3361-3369.

Sato, M., 1960, "Oxidation of sulfide ore bodies, II. Oxidation mechanisms of sulfide minerals at 25^{0}C," *Economic Geology*, **55**, 1202-1231.

Scanlon, W.W., 1957, "Lifetime of carriers in lead sulfide," *Physics Review*, **106**, 718-720.

Scanlon, W.W., 1959, "Polar semiconductors," In: Seitz, F., and Turnbull, D., eds., *Solid State Physics, Advances in Research and Applications*, **9**, 83-137.

Shuey, R.T., 1975, *Semiconducting ore minerals*, Elsevier.

Singer, P.C., and Stumm, W., 1970, "Acid Mine Drainage: The rate determining step," *Science*, **167**, 1121-1123.

Southampton Electrochemistry Group (Greef, R., Peat, R., Peter, L.M., Pletcher, D., and Robinson, J.), 1985, *Instrumental Methods in Electrochemistry*, Ellis Horwood Limited.

Springer, G., 1970, "Observations on the electrochemical reactivity of semiconducting minerals," *Transactions of the Institution of Mining and Metallurgy, Section C: Mineral Processing and Extractive Metallurgy*, **79**, 11-14.

Sutherland, K.L., and Wark, I.W., 1955, *Principles of Flotation*, Australian Institute of Mining and Metallurgy, Melbourne.

Trahar, W.J., 1984, "The influence of pulp potential in sulphide flotation," In: Jones, M.H., and Woodcock, J.T., eds., *Principles of Mineral Flotation, The Wark Symposium*, Australasian Institute of Mining and Metallurgy, 117-135.

Turcotte, S.B., Benner, R.E., Riley, A.M., Li, J., Wadsworth, M.E., and Bodily,

D.M., 1993, "Surface analysis of electrochemically oxidized metal sulfides using Raman spectroscopy," *Journal of Electroanalytical Chemistry*, **347**, 195-205.

Vaughan, D.J., and Craig, J.R., 1978, *Mineral Chemistry of Metal Sulfides*, Cambridge University Press.

Walker, G.W., Walters, C.P., and Richardson, P.E., 1986, "Hydrophobic effects of sulfur and xanthate on metal and mineral surfaces," *International Journal of Mineral Processing*, **18**, 119-137.

Woods, R., 1971, "The oxidation of ethyl xanthate on platinum, gold, copper, and galena electrodes. Relation to the mechanism of mineral flotation," *The Journal of Physical Chemistry*, **75**, 354-362.

Woods, R., 1976, "Electrochemistry of sulfide flotation," In: Fuerstenau, M.C., ed., *Flotation*, A.M. Gaudin Memorial Volume, AIME, New York, 298-333.

Yoon, R.H., Lagno, M.L., Luttrell, G.H., and Mielczarski, J.A., 1991, "On the hydrophobicity of coal pyrite," In: Dugan, P.R., Quigley, D.R., and Attia, Y.A., eds., *Processing and Utilization of High-Sulfur Coals IV*, 241-253.

Zhu, X., Li, J., Bodily, D.M., and Wadsworth, M.E., 1992, "Transpassive oxidation of pyrite," In: Woods, R., and Richardson, P.E., eds., *Proceedings of the Third International Symposium on Electrochemistry in Mineral and Metal Processing III*, Proceedings Volume 92-17, The Electrochemical Society, Inc., Pennington, NJ, 391-409.

Vita

Yanqing Li was born on June 25, 1964, in a small town, Hebei province, China, where he lived until graduating from the town middle school in 1978. Two years later, he finished his high school in Gaocheng High School. In the fall of 1980, he enrolled in the Department of Mining and Minerals Engineering at Tangshan Institute of Technology, and graduated with a B.S. degree in 1984. Then he started his graduate study in the Department of Mining and Minerals Engineering at University of Science and Technology Beijing and received his M.S. degree in June 1987. After working as a patent examiner in the Chinese Patent Office for four years, he entered Virginia Polytechnic Institute and State University in the fall, 1991.